Parametric Interaction of Focused Gaussian Light Beams

G. D. Boyd
Bell Telephone Laboratories, Incorporated, Holmdel, New Jersey
AND
D. A. Kleinman
Bell Telephone Laboratories, Incorporated, Murray Hill, New Jersey
(Received 5 February 1968)

A theoretical study is presented on the optimization of second harmonic generation (SHG) and parametric generation (PG) by a laser beam in a uniaxial nonlinear crystal. Numerically computed curves show the dependence of the SHG power, and the reciprocal of the PG threshold power, on the parameter l/b, where l is the optical path length in the crystal and b is the confocal parameter (determined by the focal length of the focusing lens and the minimum radius of the laser beam, assumed to be in the TEM_{00} mode of an optical resonator). The calculations take full account of diffraction and double refraction. In the absence of double refraction, the optimum focusing condition is found to be $l/b=2.84$. For PG the optimization of the crystal length l is also discussed, and curves are given showing the dependence of the threshold on l for the case in which signal and idler have the same losses. It is shown that the computed functions are also relevant to the mixing of two Gaussian beams and to parametric amplification. Pump depletion is neglected. Appendices are provided on (1) the theory of Gaussian extraordinary beams and the extension of the theory to cover both positive and negative birefringent crystals, (2) the general definition of nonlinear coefficients, (3) the effective nonlinear coefficient, and (4) details of the computations. The theory of the PG threshold is applied to tellurium and $LiNbO_3$. On the basis of reasonable assumptions about the losses, a PG threshold of 1.0 W is obtained for a pump at 10.6 μ in Te. The optimum length is found to be $l=0.14$ cm. For $LiNbO_3$ of length $l=1$ cm the threshold is 22 mW at 0.5147 μ. Also calculated is the quantum efficiency for up-conversion in HgS from 10.6 to 0.6729 μ using the 0.6328 μ He–Ne laser.

1. INTRODUCTION

The most familiar nonlinear interaction of light beams is the production of the second harmonic[1,2] from a laser beam through the second-order polarization of the medium

$$\mathcal{P}=\mathbf{d}\cdot\mathbf{EE}, \tag{1.1}$$

where $\mathbf{E}$ is the amplitude of the laser electric field, $\mathcal{P}$ is the amplitude of the polarization at the second harmonic frequency, and d represents a tensor property of the medium. Only a crystalline medium lacking inversion symmetry can have a nonvanishing d in (1.1). The same nonlinear interaction can also mix two light beams to produce a polarization at either the sum or difference frequency, and can cause an interaction of three light beams[3] (the "parametric interaction"), whereby power is continuously transferred from the highest frequency beam ("pump") to the other beams ("signal" and "idler"). The parametric oscillator has been demonstrated in $LiNbO_3$[4] and also KDP[5] using as the pump a second harmonic beam produced by a Q-switched laser. A careful analysis of the threshold for parametric oscillation by Boyd and Ashkin[6] (BA) has indicated that the threshold pump power in $LiNbO_3$, one of the most favorable crystals known at present for operation in the visible region of the spectrum, is about 11 mW in a single Gaussian mode (argon ion laser, $\lambda=0.5147$ μ). This result indicates that the continuous parametric oscillator (or amplifier) is technologically feasible at the present time, but it also indicates that reaching the threshold may require careful attention to the problem of *optimization* of the *parametric generation* (PG). The optimization of *second harmonic generation* (SHG) is also an important problem, since SHG is at present the only practical technique for measuring the nonlinear optical coefficients d, and in some cases may be used for pumping a parametric oscillator.

The optimization of a nonlinear interaction, as we shall use the term in this paper, means the specification of a particular Gaussian laser beam which will transfer the greatest power to the beam or beams to be produced. This is the central problem considered in this paper. In the case of PG, the signal and idler beams will also be specified in the optimization, and all three beams are considered Gaussian beams. In the case of SHG, the laser beam is considered a Gaussian beam, but the harmonic is in general not a Gaussian beam if double refraction is present and the harmonic simply radiates out of the crystal without being contained by mirrors in an optical resonator. On the other hand, by means of a resonator the harmonic can be produced as a Gaussian

[1] P. A. Franken, A. E. Hill, C. W. Peters, and G. W. Weinreich, Phys. Rev. Letters **7**, 118 (1961).
[2] D. A. Kleinman, Phys. Rev. **128**, 1761 (1962).
[3] (ABDP) J. A. Armstrong, N. Bloembergen, J. Ducuing, and P. Pershan, Phys. Rev. **127**, 1918 (1962).
[4] J. A. Giordmaine and R. C. Miller, Phys. Rev. Letters **14**, 973 (1965)
[5] S. Akhmanov, A. Kovrigin, V. Kolosov, A. Piskarskas, V. Fadeev, and R. Khokholv, Zh. Eksper. Teor. Fiz. **3**, 372 (1966). [Sov. Phys.—JETP **3**, 241 (1966)].
[6] (BA) G. D. Boyd and A. Ashkin, Phys. Rev. **146**, 187 (1966). In this paper (2.1) should read $\mathcal{P}_{1Y}{}^{o}=2d_{31}E_{2Y}{}^{o}E_{3Z}{}^{e}$, $\mathcal{P}_{2Y}{}^{o}=2d_{31}E_{1Y}{}^{o}E_{3Z}{}^{e}$ and (4.5) should read $n_1{}^{0}=n_0{}^{0}-\gamma D$.

beam, making the theory of resonant SHG very similar to that of PG. Gaussian beams[7] are specified by the direction of the beam axis, the location of the focus, the confocal parameter, and the frequency and power. Of these, we regard the first three as *optimizable parameters*. The optical properties (linear and nonlinear) of the crystal we regard as fixed parameters of the problem. Of the crystal dimensions, only the length (optical path measured along the beam axis) enters our considerations, the other dimensions being assumed large enough that they do not limit the aperture of the system. Except in certain formulas having very general validity, we neglect absorption in describing the interacting light fields. However, it is necessary to include the effect of losses whenever an optical resonator is used, and this is done here for PG and resonant SHG by requiring the beam amplitudes to satisfy an over-all energy balance. If absorption in the crystal contributes significantly to the losses an *optimum crystal length* can be defined for PG and resonant SHG. This is discussed with particular reference to PG in tellurium using the CO_2 laser. When three Gaussian beams are interacting, as in PG or resonant mixing in which the generated beam is produced in a Gaussian mode of the resonator, the optimization of the focusing really involves three confocal parameters. At first we assume for simplicity that all three are equal; later we return to the general case and show that our results apply to an effective confocal parameter which is a simple function of the parameters of the three beams.

Recently the theory (specifically, for negative birefringent crystals) of SHG by focused Gaussian beams has been described by Kleinman *et al.*[8] (KAB), and strong experimental evidence was presented for the validity of the theory. The treatment applies to the case in which the crystal length l is large compared to the confocal parameter b, which is a measure of the length of the focal region. For this case, $l \gg b$ KAB obtain an expression for the SHG power P_2 in the absence of a resonator. They find that $P_2(\Delta k)$, where Δk is the mismatch in wavevector

$$\Delta k = 2k_1 - k_2 = (2\omega_1/c)(n_1 - n_2), \tag{1.2}$$

has a single maximum which defines an optimum phase-matching (or mismatching) condition, and in general this does not correspond to the ordinary phase-matching condition $\Delta k = 0$. Experimentally this optimum could be achieved by applying an electric field, varying the crystal temperature, or adjusting the direction of the beam axis relative to the crystal axes to get maximum power. KAB do not treat the optimization with respect to confocal parameter because this optimum occurs at a value of (l/b), which is not large enough for their expression for P_2 to be valid. Previously the theory for unfocused laser beams had been described by Boyd *et al.*[9] (BADK) along with experimental evidence confirming the theory. This treatment applies to the case in which the crystal length is small compared to the confocal parameter. For this case, $l \ll b$ BADK obtain an expression for the power which completely accounts for the effects of double refraction, but the expression is not valid when (l/b) is close to optimum. Likewise, Boyd and Ashkin[6] (BA) have assumed $l \ll b$ in their derivation of the PG threshold, but in the resulting expression they have set $(l/b) = 1$ for the purpose of making a quantitative estimate of the threshold. The optimum value of (l/b), however, cannot be determined from the theory of BA. Ashkin *et al.*[10] (ABD) have considered resonant SHG in which the harmonic is produced in the TEM_{00} mode of an optical resonator. If one of the resonator mirrors has a small transmission, the transmitted beam is a Gaussian beam which may be considerably more powerful than the SHG without a resonator. The resonant enhancement depends upon the coupling coefficient to the resonator TEM_{00} mode which ABD compute assuming $l \ll b$.

In the present paper, an exact integral expression for the SHG power is obtained (Chap. 2) which is valid for arbitrary values of the *focusing parameter*

$$\xi = l/b. \tag{1.3}$$

The expression reduces properly when $\xi \ll 1$ to that of BADK, and when $\xi \gg 1$ to that of KAB. It takes diffraction, double refraction, and absorption into account exactly within the paraxial approximation, which is necessary for the validity of Gaussian beams. The theory for P_2 is based on integrating an expression for the intensity distribution far from the crystal. A derivation of this expression is given along the lines of the heuristic theory of BADK. This has the advantage of making the discussion understandable to a reader not having familiarity with BADK or KAB. The formal derivation of the intensity distribution has been given by KAB, but in treating P_2 they considered only the strong focusing limit $\xi \to \infty$. The theory is written for negative uniaxial crystals, but it is shown in Appendix 1 that it also applies to positive uniaxial crystals. Curves are presented showing SHG as a function of ξ with optimum phase matching for a variety of double refraction angles ρ including $\rho = 0$. These curves have a single maximum which allows *the optimum focusing parameter* ξ_m to be determined for each ρ. Double refraction in the theory enters through the parameter

$$B = \rho(lk_1)^{1/2}/2. \tag{1.4}$$

[7] G. D. Boyd and J. P. Gordon, Bell System Tech. J. **40**, 489 (1961).

[8] (KAB) D. A. Kleinman, A. Ashkin, and G. D. Boyd, Phys. Rev. **145**, 338 (1966). On the right side of (A3) τ should be σ.

[9] (BADK) G. D. Boyd, A. Ashkin, J. M. Dziedzic, and D. A. Kleinman, Phys. Rev. **137**, A1305 (1965).

[10] (ABD) A. Ashkin, G. D. Boyd, and J. M. Dziedzic, IEEE J. Quantum Electron. **QE-2**, 109 (1966).

The most important results apply to the case $B=0$, where we find $\xi_m=2.8$.

The theory of PG as given by BA is here (Chap. 3) generalized to arbitrary B and ξ. For the very important case $B=0$ the optimization of PG and SHG are essentially the same problem. We find the PG threshold only 7% lower than the expression given by BA, so their general remarks on the feasibility of continuous PG need no revision. The reciprocal of the PG threshold is obtained in a form quite analogous to that obtained for SHG which exhibits its dependence on the optimizable parameters. Curves are presented for this function as a function of ξ with optimum phase matching for a variety of values of B. As in the case of SHG these curves have a single maximum which allows ξ_m to be determined for each B. Application is made to PG in tellurium and $LiNbO_3$.

Likewise, the theory of resonant SHG of ABD is generalized (Chap. 4) to arbitrary B and ξ. It is shown that resonant SHG is described by the same function of the optimizable parameters as the PG threshold. The power-coupling coefficient is simply the ratio of this function to the function describing nonresonant SHG. Curves of the coupling coefficient are given as a function of ξ for several values of B. The theory does not reduce to that of ABD in the limit $\xi\ll 1$ because ABD assume a nonoptimum arrangement in which the fundamental and harmonic beams intersect (due to double refraction) at the surface, instead of the center of the crystal.

Finally, it is shown (Chap. 5) that the functions defined for SHG and PG also describe the dependence of sum frequency and difference-frequency mixing upon the optimizable parameters. The problem of beams having the same axis and focus but different confocal parameters is considered in the absence of double refraction. The optimum condition is when the confocal parameters are equal. Application is made to up conversion in HgS. It is also shown that the function defined for PG applies to low-gain parametric amplifiers.

The theory of SHG by focused beams has been considered by Bjorkholm,[11] who obtains for the optimum focus $\xi_m=\pi/2$ independent of B. His integral expression for P_2 is exact for the (nonoptimum) case of ordinary phase matching $\Delta k=0$. When B is large ($B>2$), corresponding to the usual situation of reasonably thick crystals ($l>0.2$ cm) and phase matching far from 90° to the optic axis, there is negligible difference between ordinary and optimum phase matching. This is the case for three of the four curves computed by Bjorkholm, and for these cases our computed optimum P_2 is in excellent agreement with his computations and also his measurements. However, when B is small, either because of small ρ or small l, his analysis is no longer valid. His estimate of ξ_m is not exact, but is based on the intersection of asymptotic relations. The erroneous conclusion that ξ_m is independent of B followed from an asymptotic expression for the region of strong focusing ($\xi\gg 1$) that was too small by a factor of four. His recipe for maximum power ($B=0$, $\xi_m=\pi/2$, $\Delta k=0$) gives 54% of the true maximum power which corresponds to ($B=0$, $\xi_m=2.8$, $\Delta k=3.2/l$).

The formal theory of optical PG was given first by ABDP[3] for three interacting plane waves. They obtained analytic solutions describing the interchange of power between the three waves. These solutions are primarily of interest in defining a characteristic length l_p for the transfer of power

$$l_p=(cn/2\pi\omega_3)d^{-1}E_3^{-1} \tag{1.5}$$

between the pump (ω_3, E_3) and the signal and idler waves. Inasmuch as l_p, at least for continuous operation, is apt to be extremely long ($l_p\gg 10^3$ cm), the usual theory which neglects the depletion of the pump through the nonlinear interaction is justified. The plane-wave theory for SHG can be applied to Gaussian beams in the near field ($l\ll b$) in a plausible way,[9] and the resulting theory agrees with the rigorous theory in the limit $l\ll b$. In this near-field theory double refraction is retained but diffraction is neglected, so it can not be used to discuss optimum focusing. Kingston and McWhorter[12] have used a still more restrictive approximation which neglects both diffraction and double refraction. They have given a formal theory of SHG from a mode-coupling point of view for a very thin crystal without assuming at the outset that any of the beams are Gaussian. From an expansion of an arbitrary laser beam in the paraxial modes given by Boyd and Gordon,[7] they obtain a general expression for the SHG power in each paraxial mode. They find that when the laser is in the lowest-order mode (TEM_{00}), which we here call the Gaussian mode, the SHG is also in a Gaussian mode and the greatest transfer of power takes place. Accordingly, they assume for their treatment of PG, as we do, that all three beams are Gaussian. In order to insure the validity of their approximation, they consider a rather thin crystal ($l=0.1$ cm), and thereby obtain a discouragingly high estimate of the pumping threshold for PG (200 kW) in KDP.

We have mentioned that the location of the focus is an optimizable parameter. In the absence of absorption, however, one might expect that the center of the crystal should be the optimum location. The behavior of SHG as a function of focal position for various values of mismatch Δk has been studied by Kleinman and Miller.[13] They find that when Δk has the optimum value,

[11] J. E. Bjorkholm, Phys. Rev. **142**, 126 (1966).

[12] R. H. Kingston and A. L. McWhorter, Proc. IEEE **53**, 4 (1965).

[13] D. A. Kleinman and R. C. Miller, Phys. Rev. **148**, 302 (1966).

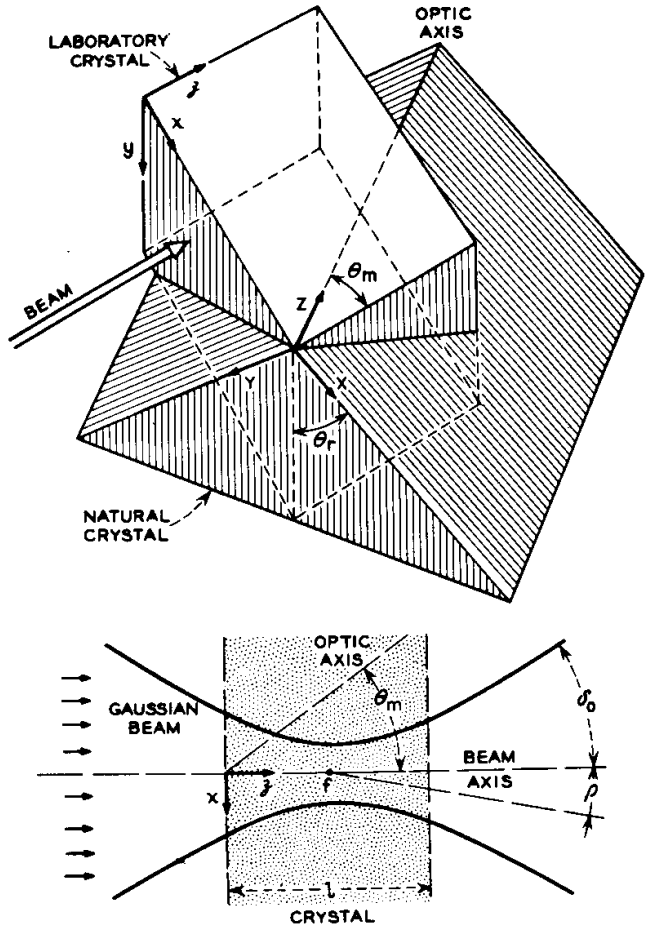

FIG. 1. The crystal is shown as a rectangular solid with the laboratory axes **x**, **y**, **z** parallel to the edges. For the purpose of visualizing the relation between **x**, **y**, **z** and the crystallographic axes **X**, **Y**, **Z**, the latter are shown as the edges of a hypothetical "natural" crystal. The lower diagram shows the Gaussian laser beam focused in the crystal at $x=y=0$, $z=f$. The divergence of the Gaussian beam is greatly exaggerated in the lower diagram. The origin of x, y, z is taken on the beam axis at the incident surface. Phase matching for a uniaxial crystal is determined by the matching angle $\theta_m=\angle(\mathbf{z}, \mathbf{Z})$. Rotation of the crystal about its optic axis is specified by $\theta_r=\angle(\mathbf{y}, \mathbf{Y})$.

the optimum focal position is the center of the crystal. For nonoptimum $\Delta k>0$, structure was observed in P_2 as a function of focal position which was fully in accord with theory.

We have gathered into Appendices material which is primarily of interest to the specialist. Appendix 1 shows that the results derived in the text assuming a negative uniaxial crystal apply also to a positive uniaxial crystal. The first step in the proof is the derivation of the form of a Gaussian beam in the extraordinary wave. Appendix 2 contains a discussion from first principles of the meaning of the various nonlinear coefficients that commonly appear in this paper and the previous literature. This is particularly important for the interpretation of quantitative measurements in terms of numerical values for various nonlinear coefficients, since otherwise discrepancies by factors of two or four can easily sneak into elementary discussions of the various nonlinear effects. Appendix 3 contains complete details on the relation between the effective nonlinear coefficient in an experiment and the tensor components of the second order susceptibility. Appendix 4 contains all relevant details on the computations presented in this paper.

2. OPTIMIZATION OF THE SHG POWER

2.1. Theory of SHG

Consider a negative uniaxial crystal (nonlinear) of length l with parallel faces so oriented that the ordinary matching condition $\Delta k=0$ occurs for propagation approximately normal to the faces. The adjustment in crystal orientation required for optimum phase matching will be very small, and we can regard the beam axis as normal to the faces. The notation will follow that of BADK and KAB; the beam axis is the z direction, the optic axis lies in the xz plane ($y=0$), and the origin $x=y=z=0$ is at the point where the beam axis enters the crystal as shown in the lower diagram of Fig. 1. For pictorial purposes it was necessary to exaggerate the divergence angle of the Gaussian beam. The upper drawing of Fig. 1 is an attempt to show visually the relationship between the laboratory axes **x**, **y**, **z** and the crystallographic axes **X**, **Y**, **Z** (optic axis). The laboratory crystal is the rectangular solid with the laser beam impinging normally on one face. Also shown is a hypothetical "natural" crystal from which the laboratory crystal might be cut. The natural crystal is shown as a right triangular prism with edges along the crystallographic axes **X**, **Y**, **Z** (optic axis). As discussed in Appendix 3, the effective nonlinear coefficient depends upon the relative orientation of the laboratory crystal and "natural" crystal.

The double-refraction direction for extraordinary waves (**E** in the xz plane) is a line of slope $dx/dz=\tan\rho\approx\rho$. The laser beam is a Gaussian beam with focus at $z=f$. The minimum beam radius w_0, confocal parameter b, diffraction half-angle δ_0, and propagation constant (in the medium) k_1 satisfy the relations[7]

$$w_0^2k_1=b$$
$$\delta_0=2w_0/b=2/w_0k_1=2/(bk_1)^{1/2}. \tag{2.1}$$

These parameters describe the beam *in the crystal*; if the crystal were removed the beam would have confocal parameter $=b/n_1$, diffraction angle $=n_1\delta_0$, propagation constant $=k_1/n_1$, beam radius $=w_0$, and focal position $=f/n_1$. The fundamental electric field is [time dependence $\exp(-i\omega_1t)$]

$$\mathbf{E}_1(x', y', z')=\mathbf{E}_0[1/(1+i\tau')]\exp(ik_1z')$$
$$\times\exp[-(x'^2+y'^2)/w_0^2(1+i\tau')]\exp(-\tfrac{1}{2}\alpha_1z')$$
$$\tau'=2(z'-f)/b. \tag{2.2}$$

The harmonic polarization (1.1) may be written

$$\mathcal{P}(x', y', z') = \mathcal{P}_0[1/(1+i\tau')^2] \exp(2ik_1z' - \alpha_1 z') \times \exp[-2(x'^2+y'^2)/w_0^2(1+i\tau')]B(z') \quad (2.3)$$

$$B(z') = 1 \qquad 0 \le z' \le l$$
$$= 0 \qquad z' < 0, z' > l.$$

Here α_1 is the absorption coefficient for the fundamental.

We now compute the harmonic field

$$\mathbf{E}_2(x, y, z) = \mathbf{A}_2(x, y, z) \exp(ik_2 z) \quad (2.4)$$

at a point x, y, z outside the crystal ($z > l$). To eliminate reflective and refractive effects at the surface we imagine the crystal to be embedded in an isotropic medium of refractive index $n_1 \approx n_2$. In the heuristic approach we consider x', y', z' to be a source point radiating to the observer point x, y, z. The source and observer points must lie on the same ray (trajectory of energy flow), and the source point must lie inside the crystal

$$x' = x - \rho(z - z') \qquad (z < l)$$
$$x' = x - \rho(l - z') \qquad (z > l)$$
$$y' = y \qquad 0 \le z' \le l. \quad (2.5)$$

In the heuristic theory we introduce these relations on the basis of physical insight. Consider now a slab of thickness dz'; it can easily be shown from Maxwell's equations for unbounded plane waves [or see BADK (3.3)] that the increment of harmonic amplitude contributed by the slab is

$$dA_2(x', y', z') = (2\pi i\omega_2/cn_2)\mathcal{P}_x(x', y', z') \exp(-ik_2 z')dz'$$
$$= (2\pi i\omega_2/cn_2)[\mathcal{P}_{0x}/(1+i\tau')] \times \exp(i\Delta k z' - \alpha_1 z') \cdot \{[1/(1+i\tau')] \times \exp[-2(x'^2+y'^2)/w_0^2(1+i\tau')]\}dz', \quad (2.6)$$

where (in this case) $\mathcal{P}_{0x}$ is the effective component of $\mathcal{P}$ for radiating the extraordinary wave. This is the incremental amplitude within the slab dz' due to sources within the slab. The increment propagates according to the wave equation and produces an increment at the observer point x, y, z. We have enclosed in brackets in (2.6) that part of $dA_2(x', y', z')$ which has the form of the amplitude of a Gaussian beam of spot size $w_0/\sqrt{2}$, confocal parameter b, and focus in the plane $z = f$. It is the quantity in brackets which propagates, since this is known to be a solution of the wave equation (in the paraxial approximation $\delta_0 \ll 1$). To propagate the bracket expression we substitute for x', y' from (2.5) and replace τ' by

$$\tau = 2(z - f)/b. \quad (2.7)$$

Also we take into account the possible absorption α_2 of the harmonic in propagating from z' to $z > l$. Thus, the incremental harmonic amplitude at x, y, z is

$$dA_2(x, y, z) \underset{(z>l)}{=} (2\pi i\omega_2/cn_2)[\mathcal{P}_{0x}/(1+i\tau')] \times \exp[i\Delta k z' - \alpha_1 z' - \tfrac{1}{2}\alpha_2(l - z')] \cdot [1/(1+i\tau)] \times \exp(-2\{[x - \rho(l-z')]^2 + y^2\}/w_0^2(1+i\tau))dz'. \quad (2.8)$$

We now integrate over all the sources in the crystal to obtain the total harmonic field outside the crystal

$$E_2(x, y, z) \underset{(z>l)}{=} \frac{2\pi i\omega_2 \mathcal{P}_{0x}}{cn_2(1+i\tau)} \exp(-\tfrac{1}{2}\alpha_2 l + 2ik_1 z) \cdot \int_0^l dz' \frac{\exp(-\alpha z' + i\Delta k z')}{1+i\tau'} \times \exp\left(-\frac{2\{[x - \rho(l-z')]^2 + y^2\}}{w_0^2(1+i\tau)}\right), \quad (2.9)$$

where

$$\alpha = \alpha_1 - \tfrac{1}{2}\alpha_2. \quad (2.10)$$

This is the desired result of the heuristic theory. It can also be derived by formal methods that do not directly introduce (2.5) or (2.6) as assumptions [see KAB (4.20)]. In the formal theory a Green's function is derived rigorously for SHG by an arbitrary polarization, and (2.9) is obtained by integrating this Green's function over a Gaussian polarization beam (2.3). It is shown in KAB that this Green's function has the property that energy propagates from the source point to the observer point along the ray, which justifies (2.5). Further justification of (2.5) is given in Appendix 1, where an explicit derivation is given of the form of a Gaussian beam propagating as an extraordinary wave. It is shown there that if (2.6) is regarded as a Gaussian extraordinary beam, (2.8) follows directly from (2.6) without the use of (2.5) as a separate assumption. The justification of (2.6) is the paraxial approximation $\delta_0 \ll 1$. In order to have $\delta_0 \ll 1$, it is necessary that $\mathcal{P}(x, y, z)$ be a slowly varying function of x, y; this same condition then insures that (2.6) is valid. The extension of the theory to positive uniaxial crystals is given in Appendix 1.

We now consider the far field outside the crystal in the limit

$$\tau \to \infty. \quad (2.11)$$

We shall find that in this limit (2.9) is greatly simplified and we can readily obtain a rigorous expression for the SHG power. Notice that (2.11) makes no assumption about the crystal thickness l; it is the plane z in which we observe the field that is assumed to be in the far field. From (2.1) and (2.8)

$$1/w_0^2(1+i\tau) = (1-i\tau)/w_0^2(1+\tau^2)$$
$$= [(1-i\tau)/w_0^2\tau^2](1 - \tau^{-2} + \tau^{-4} + \cdots)$$
$$\to (1-i\tau)/w_0^2\tau^2. \quad (2.12)$$

Let us define the parameters:

$$s=[x-\rho(l-f)]/w_0\tau, \qquad s'=y/w_0\tau, \qquad \beta=\rho/\delta_0, \quad (2.13)$$

so that

$$[x-\rho(l-z')]^2/w_0^2(1+i\tau)=(1-i\tau)[s+\beta(\tau'/\tau)]^2 \times(1-\tau^{-2}+\cdots)\rightarrow s^2(1-i\tau)-2i\beta s\tau'. \quad (2.14)$$

It now follows that (2.9) becomes

$$E_2(x, y, z)\rightarrow(2\pi\omega_2\mathcal{P}_{0x}/cn_2\tau)\exp(-\tfrac{1}{2}\alpha_2 l+2ik_1 z) \cdot\exp[-2(1-i\tau)(s^2+s'^2)]\cdot\int_0^l dz'\frac{\exp(-\alpha z'+i\Delta k z')}{1+i\tau'} \times\exp(4i\beta s\tau'). \quad (2.15)$$

We define the function

$$H(\sigma', \kappa, \xi, \mu)=(2\pi)^{-1}\int_{-\xi(1-\mu)}^{\xi(1+\mu)}\frac{d\tau'}{1+i\tau'}e^{-\kappa\tau'}e^{i\sigma'\tau'}, \quad (2.16)$$

and the parameters

$$\sigma=\tfrac{1}{2}b\Delta k$$
$$\sigma'=\sigma+4\beta s$$
$$\xi=l/b$$
$$\mu=(l-2f)/l$$
$$\kappa=\tfrac{1}{2}\alpha b. \quad (2.17)$$

The effective polarization $\mathcal{P}_{0x}$ may be written in terms of the laser power P_1

$$\mathcal{P}_{0x}=dE_0^2=(16P_1/n_1cw_0^2)d, \quad (2.18)$$

where d is an *effective nonlinear coefficient* related to the **d** tensor of (1.1) as discussed in Appendix 3. The SHG intensity $(n_2c/8\pi)\mid E_2\mid^2$ can now be written

$$S(s, s')=4\pi K(P_1^2k_1^2/\tau^2)\exp[-\alpha' l+\mu\alpha l-4(s^2+s'^2)] \cdot\mid H(\sigma', \kappa, \xi, \mu)\mid^2, \quad (2.19)$$

with

$$K=(128\pi^2\omega_1^2/c^3n_1^2n_2)d^2 \quad (2.20)$$

and

$$\alpha'=\alpha_1+\tfrac{1}{2}\alpha_2. \quad (2.21)$$

The SHG power is obtained by integrating over the intensity distribution

$$P_2=\delta_0^2\tau^2(b/2)^2\iint ds\,ds'S(s, s') =KP_1^2lk_1e^{-\alpha' l}\cdot h(\sigma, \beta, \kappa, \xi, \mu), \quad (2.22)$$

where

$$h(\sigma, \beta, \kappa, \xi, \mu)=(\pi^2/\xi)e^{\mu\alpha l}F(\sigma, \beta, \kappa, \xi, \mu) \quad (2.23)$$

with

$$F(\sigma, \beta, \kappa, \xi, \mu) =(2/\pi^{1/2})\int_{-\infty}^{\infty}ds\mid H(\sigma+4\beta s, \kappa, \xi, \mu)\mid^2e^{-4s^2}. \quad (2.24)$$

The function $h(\sigma, \beta, \kappa, \xi, \mu)$ contains all of the dependence of P_2 upon the *optimizable parameters* σ, μ, ξ representing, respectively, the phase mismatch, focal position, and strength of focusing. In addition, h depends on the double refraction β and absorption κ. From the fact that (2.24) is invariant to changing the sign of β $(\beta\rightarrow-\beta)$, we may infer that our final result (2.22) is valid for both negative and positive uniaxial crystals, and $\beta=\mid\beta\mid$ can always be considered positive. This is shown explicitly in Appendix 1. The far-field approximation (2.15) is simply a convenient method of obtaining P_2, which of course is constant across all planes $z>l$ outside the crystal. The exterior far-field intensity (2.19) is given in KAB (7.31) for the case $\sigma=0$, and the prescription for including the mismatch is given in KAB (6.75). P_2 for the strong focusing case $\xi\gg1$ is given in KAB (8.14), and we show in Sec. 2.3 that (2.22) reduces to that result in the limit $\xi\rightarrow\infty$. Similarly, in the weak focusing limit $\xi\ll1$ it reduces to BADK (3.32). The numerical computation of h is discussed in Appendix 4. We show in Chap. 5 that h is also relevant for the mixing of two Gaussian beams.

Inserting (2.16) into (2.24) and integrating over s gives

$$F(\sigma, \beta, \kappa, \xi, \mu)=(1/4\pi^2)\iint_{-\xi(1-\mu)}^{\xi(1+\mu)}d\tau d\tau' \times\frac{\exp[-\kappa(\tau+\tau')+i\sigma(\tau-\tau')-\beta^2(\tau-\tau')^2]}{(1+i\tau)(1-i\tau')}. \quad (2.25)$$

When $\alpha_1=\alpha_2=0$, $\mu=0$, and $\sigma=0$, and F is expressed in the form (2.25), our result (2.22) agrees with Bjorkholm[11] (31).

2.2. Dependence of SHG upon Focusing

We shall now present the evaluation of the nonlinear interaction for SHG as measured by the function $h(\sigma, \beta, \kappa, \xi, \mu)$ defined in (2.23) optimized with respect to phase matching σ and focal position μ. We immediately set all absorption equal to zero and set the focus in the center of the crystal

$$\kappa=\mu=0. \quad (2.26)$$

As explained in the Introduction, this is the optimum focal position when $\kappa=0$ and σ has its optimum value. Therefore, consider the function $h(\sigma, \beta, 0, \xi, 0)$. We must vary the parameters σ, β, ξ in such a way that ρ and l are held fixed while the confocal parameter b varies. The parameters ξ, β, σ are defined in (2.13) and (2.17). We write

$$\beta=B\xi^{-1/2}, \quad (2.27)$$

where B is defined in (1.4), and define the function

$$h(\sigma, B, \xi)=h(\sigma, B\xi^{-1/2}, 0, \xi, 0), \quad (2.28)$$

in which σ, ξ are optimizable parameters, while B is the constant representing double refraction. For fixed Δk the matching parameter σ depends upon b. This is of no concern, however, because we shall *optimize* (2.28) with respect to σ for each ξ to obtain

$$h_m(B, \xi) = h(\sigma_m, B, \xi) = h[\sigma_m(B, \xi), B\xi^{-1/2}, 0, \xi, 0], \tag{2.29}$$

where $\sigma_m(B, \xi)$ is the optimum σ. The subscript m in (2.29) indicates that an optimization has been performed. Experimentally σ_m would be obtained by a fine adjustment of the crystal orientation or crystal temperature, or by an applied electric field in the crystal, to maximize P_2. The actual value of $\sigma_m(B, \xi)$ is usually not of practical interest, but in Sec. 2.4 we

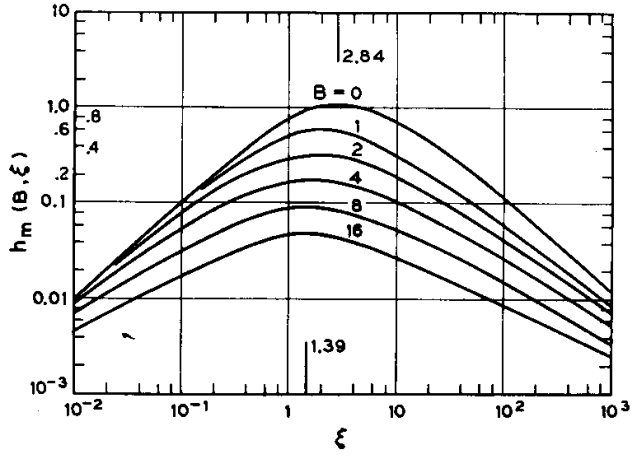

FIG. 2. SHG power (2.22) represented by the function $h_m(B, \xi)$ (2.29) for optimum phase matching as a function of focusing parameter $\xi = l/b$ for several values of double-refraction parameter $B = \rho(lk_1)^{1/2}/2$. Vertical lines indicate optimum focusing in the limits of small and large B.

shall consider the behavior of $\sigma_m(0, \xi)$ as an aid to a better physical understanding of optimum phase matching. In the strong focusing limit $\xi \gg 1$ KAB have measured σ_m and shown that it is in agreement with theory.

Figure 2 shows curves of $h_m(B, \xi)$ as a function of ξ for several values of the double-refraction parameter B defined in (1.4). As an aid in understanding the numerical value of B we give the special formula

$$B = 5.8l^{1/2} \qquad (\text{ADP}, \lambda_1 = 6328\ \text{Å}), \tag{2.30}$$

valid for ADP ($n_1 = 1.5$, $\rho = 0.03$) and the 6328 Å laser when l is in centimeters. Each curve of Fig. 2 has a single maximum which defines the *optimum focusing parameter* $\xi_m(B)$. The optimized SHG represented by

$$h_{mm}(B) = h_m[B, \xi_m(B)] \tag{2.31}$$

is plotted (solid curve) in Fig. 3. The maximum

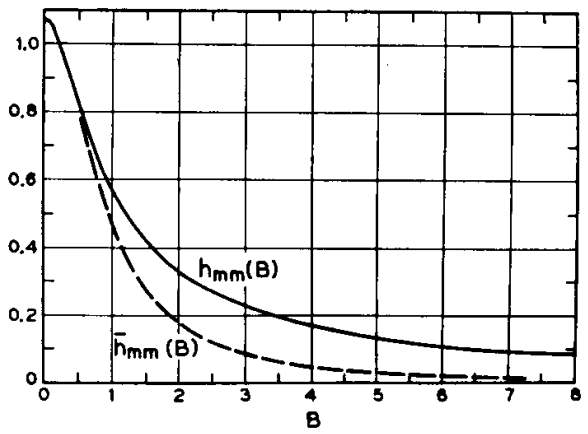

FIG. 3. Optimized SHG (solid) represented by $h_{mm}(B)$ (2.31) and optimized PG (dashed) represented by $\bar{h}_{mm}(B)$ (3.38). The dashed curve approximately satisfies the empirical relation (3.49).

nonlinear interaction is specified by ($B = 0$)

$$h_{mm}(0) = 1.068$$
$$\xi_m(0) = 2.84. \tag{2.32}$$

In Fig. 4, we show $\xi_m(B)$, which lies in the range

$$1.392 \leq \xi_m(B) \leq 2.84. \tag{2.33}$$

We see from Fig. 2 that optimization with respect to ξ is not a very critical adjustment; the sharpest of the peaks ($B = 0$) is within 10% of its maximum over the range $1.52 < \xi < 5.3$. The computations of Figs. 2–4 cover the entire range of interest of ξ and B for which numerical computations are needed. We show in the next section how these results connect with those previously reported by BADK for weak focusing ($\xi \ll 1$) and by KAB for strong focusing ($\xi \gg 1$).

It may be of interest to know how $h(\sigma, \beta, 0, \xi, \mu)$ behaves as the focus is moved away from the center of the crystal $\mu = 0$. Therefore, consider the function

$$h_m(B, \xi, \mu) = h[\sigma_m(B, \xi), B\xi^{-1/2}, 0, \xi, \mu], \tag{2.34}$$

where $\sigma_m(B, \xi)$ has been defined in (2.29) for opti-

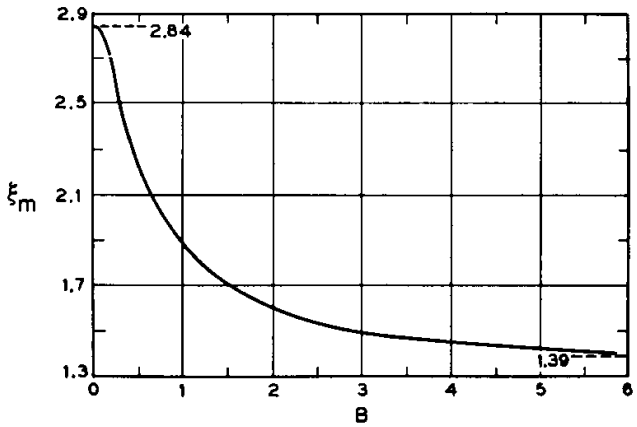

FIG. 4. Optimum focusing parameter $\xi_m(B)$ defined by the maxima of the curves in Fig. 2.

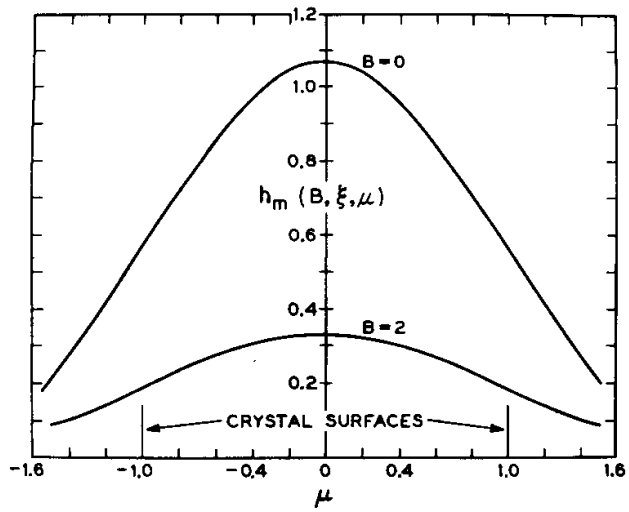

FIG. 5. SHG represented by $h_m(B, \xi, \mu)$ (2.34) as a function of the position μ of the focus for $B=0$, $\xi=2.8$ and $B=2$, $\xi=1.7$.

mization of σ at $\mu=0$. In Fig. 5 we show $h_m(B, \xi, \mu)$ for $B=0$, $\xi=2.8$ and $B=2$, $\xi=1.7$. In doing the computations we observed that a separate optimization of σ at each μ would have given substantially the same results.

2.3. Limiting Cases

We consider first the *weak focusing* limit (near field)

$$\xi \ll 1. \tag{2.35}$$

The denominator in the integral (2.25) becomes unity and we have

$$F(\sigma, \beta, \kappa, \xi, \mu) \underset{(\xi\ll 1)}{\longrightarrow} (8\pi^2\beta^2)^{-1} e^{2\alpha f} \iint_0^t dy\, dy' \times \exp[-2q(y+y') - \tfrac{1}{2}(y-y')^2] \exp[i2\sqrt{2}\epsilon(y+y')] \tag{2.36}$$

after making the transformation $y=\beta\sqrt{2}[\tau+\xi(1-\mu)]$ and introducing the parameters

$$t=2\sqrt{2}\beta\xi=\sqrt{2}\rho l/w_0=2\sqrt{2}B\xi^{1/2}=(2\pi)^{1/2}(l/l_a)$$
$$q=\kappa/(2\sqrt{2}\beta)=w_0\alpha/(2\sqrt{2}\rho)$$
$$\epsilon=\sigma/4\beta=b\Delta k/8\beta. \tag{2.37}$$

For the definition of l_a, see (2.96). The phase-matching parameter ϵ agrees with KAB (8.9). It is shown in KAB that optimum matching in the weak focusing limit (2.35) is given by $\epsilon\to 0$; note that this does not mean $\sigma\to 0$, since the limit (2.35) implies $b\to\infty$, which through (2.1) and (2.13) implies $\beta\to\infty$. Therefore, we set $\epsilon=0$ in (2.36) and replace σ by σ_m to indicate optimum phase matching; the result may be written

$$F(\sigma_m, \beta, \kappa, \xi, \mu) \underset{\xi\ll 1}{\longrightarrow} (\xi^2/\pi^2) e^{2\alpha f} G(t, q) \tag{2.38}$$

with

$$G(t, q) = t^{-2} \iint_0^t dy\, dy' \exp[-2q(y+y') - \tfrac{1}{2}(y-y')^2]. \tag{2.39}$$

It can easily be shown that (2.39) is identical with the function $G(t, q)$ defined in BADK (3.33), and the definitions (2.37) of t, q are identical with BADK (3.19, 3.20). For the important case of zero absorption $q=0$, we have [BADK (3.38)]

$$G(t, 0) \equiv G(t) = (2\pi/t^2)^{1/2} \operatorname{erf}(t/\sqrt{2}) - (2/t^2)(1-e^{-t^2/2})$$
$$= 1 - t^2/12 + t^4/120 \cdots$$
$$= (2\pi)^{1/2} t^{-1} - 2t^{-2} + 2t^{-4} e^{-t^2/2} \cdots. \tag{2.40}$$

We define $\operatorname{erf}(z)$ in (2.52). Plots of $G(t, q)$ against t for several values of q are given in BADK Fig. 7.

From (2.23) and (2.38) we have

$$h(\sigma_m, \beta, \kappa, \xi, \mu) \underset{(\xi\ll 1)}{\longrightarrow} \xi e^{\alpha l} G(t, q), \tag{2.41}$$

and the power (2.22) reduces in the near field to

$$P_2 \underset{(\xi\ll 1)}{\longrightarrow} K P_1^2 l^2 e^{-\alpha_2 l} (1/w_0^2) G(t, q) \tag{2.42}$$

In agreement with BADK (3.32). Of particular interest is the function (2.29) which becomes

$$h_m(B, \xi) \underset{(\xi<0.4)}{\longrightarrow} \xi G(2\sqrt{2}B\xi^{1/2}). \tag{2.43}$$

Here we indicate an *explicit condition* on ξ, whereas up to now we have merely indicated $\xi\ll 1$. We adopt the convention that an explicit condition means that the corresponding approximation has been found empirically (from numerical computations) to hold with an error not exceeding 10%.

Our limiting form (2.43) actually contains two types of behavior corresponding to the asymptotic forms of $G(t)$

$$G(t) \underset{(t>7)}{\longrightarrow} (2\pi)^{1/2}/t$$
$$G(t) \underset{(t<1)}{\longrightarrow} 1. \tag{2.44}$$

It follows that $h_m(B, \xi)$ has the asymptotic behaviors

$$h_m(B, \xi) \to \xi \qquad (\xi<0.4, \xi<1/8B^2), \tag{2.45}$$

and

$$h_m(B, \xi) \to (\pi^{1/2}/2)\xi^{1/2}B^{-1} = (lk_1)^{-1}(ll_a/w_0^2) \qquad (\xi<0.4, \xi>6/B^2). \tag{2.46}$$

The aperture length l_a is defined in (2.96). The case (2.45) corresponds to the thin crystal in which both diffraction and double refraction can be neglected. The second case (2.46) corresponds to a thicker crystal in which diffraction can still be neglected, but SHG is limited by double refraction.

We now consider the *strong focusing limit*

$$\xi \gg 1. \tag{2.47}$$

In addition, as will be fully explained later in (2.90) we must require

$$\beta\xi = B\xi^{1/2} > \pi/4. \tag{2.48}$$

Thus, our present considerations clearly exclude the case $B=0$, which will be treated separately in Sec. 2.4. The condition (2.48) is associated with the validity of using the representation [see (2.82)]

$$|H(\sigma, 0, \xi, 0)|^2 \underset{\xi\to\infty}{\longrightarrow} e^{-2\sigma}[\theta(\sigma)]^2, \tag{2.49}$$

where $\theta(\sigma)$ is the step function

$$\begin{aligned} \theta(\sigma) &= 1 \qquad \sigma > 0 \\ &= \tfrac{1}{2} \qquad \sigma = 0 \\ &= 0 \qquad \sigma < 0. \end{aligned} \tag{2.50}$$

We have written $[\theta(\sigma)]^2$ in (2.49) to make it assume the correct value at $\sigma=0$; for all other $\sigma\neq 0$ we have $[\theta(\sigma)]^2=\theta(\sigma)$. Inserting (2.49) into (2.24) gives immediately

$$\begin{aligned} F(\sigma, \beta, \kappa, \xi, \mu) &\to (2/\pi^{1/2}) \int_{-\infty}^{\infty} ds \\ &\quad \times \exp[-4s^2 - 8\beta(s+\epsilon)]\theta(s+\epsilon) \\ &= \tfrac{1}{2}[1-\operatorname{erf}(2\beta-2\epsilon)]\exp(4\beta^2-8\beta\epsilon) \\ &\equiv F(\epsilon, \beta) \qquad (\xi \gg 1), \end{aligned} \tag{2.51}$$

where ϵ has been defined in (2.37), and

$$\operatorname{erf}(z) = (2/\pi^{1/2}) \int_0^z dr e^{-r^2}. \tag{2.52}$$

The function $F(\epsilon, \beta)$ was previously defined in KAB (8.15). It will be observed that all dependence on κ, ξ, μ in F has dropped out of (2.51), although P_2 and h in (2.22) and (2.23) still contain the essential dependence on these parameters. From (2.23) and (2.51) we have

$$h(\sigma, \beta, \kappa, \xi, \mu) \underset{(\xi\gg 1)}{\longrightarrow} (\pi^2/\xi) e^{\mu\alpha_1 l} F(\epsilon, \beta). \tag{2.53}$$

It now follows that the power (2.22) reduces to

$$P_2 \underset{(\xi\gg 1)}{\longrightarrow} KP_1^2 \exp[-2\alpha_1 f - \alpha_2(l-f)](4\pi^2/\delta_0^2) F(\epsilon, \beta), \tag{2.54}$$

which agrees with KAB (8.14). The optimization of of $F(\epsilon, \beta)$ with respect to ϵ gives $F_m(\beta)$ plotted in KAB (Fig. 31). Thus, we have

$$h_m(B, \xi) \to (\pi^2/\xi) F_m(B\xi^{-1/2}) \qquad (\xi > 10, \xi > \pi^2/16B^2). \tag{2.55}$$

The asymptotic behavior of $F_m(\beta)$ is given by

$$\begin{aligned} F_m(\beta) &\to 1/4\pi^{1/2}\beta \qquad (\beta > \tfrac{1}{2}) \\ F_m(\beta) &\to 1 \qquad (\beta < 0.015). \end{aligned} \tag{2.56}$$

It follows that $h_m(B, \xi)$ has the asymptotic behavior

$$\begin{aligned} h_m(B, \xi) &\to \pi^{3/2}/4B\xi^{1/2} \\ &= (lk_1)^{-1}(l_a l_f / w_0^2) \\ &\qquad (\xi > 10) \qquad (4B^2 > \xi > \pi^2/16B^2) \end{aligned} \tag{2.57}$$

and

$$\begin{aligned} h_m(B, \xi) &\to \pi^2/\xi \\ &\qquad (\xi > 10, \xi > \pi^2/16B^2) \qquad (\xi > 4\times 10^3 B^2). \end{aligned} \tag{2.58}$$

The effective length l_f of the focus is defined in (2.97). The condition $(4B^2 > \xi)$ is simply $(\beta > \frac{1}{2})$ in (2.56); the condition $\xi > 4\times 10^3 B^2$ comes from $\beta < 0.015$. We note that (2.58) eventually becomes valid as ξ increases unless $B=0$. The modification required in the limit $B\to 0$ is given in (2.91).

If B is sufficiently large the transition from weak to strong focusing is described by a simple analytic approximation. Consider the two factors in the integral (2.24). We have seen in (2.49) that $|H|^2$ as a function of $\sigma' = \sigma + 4\beta s$ has a finite range in σ'. It follows that if $\beta \gg 1$ the range of $s = (\sigma' - \sigma)/4\beta$ will be small. On this basis we set $\sigma = \sigma_m$ in $\exp(-4s^2)$ in (2.24) and obtain

$$\begin{aligned} F(\sigma_m, \beta, 0, \xi, \mu) &\underset{\beta\gg 1}{\longrightarrow} (2\pi^{1/2}\beta)^{-1} \int_{-\infty}^{\infty} d\sigma' |H(\sigma', 0, \xi, \mu)|^2 \cdot \\ &\quad \cdot \exp[-(\sigma - \sigma_m)^2/4\beta^2], \end{aligned} \tag{2.59}$$

where the optimum σ_m need not be specified precisely. As noted by KAB, optimum phase matching does not differ significantly from ordinary phase matching for large double refraction. When $\mu=0$ (2.59) becomes

$$F(\sigma_m, \beta, 0, \xi, 0) \underset{\beta\gg 1}{\longrightarrow} (\tan^{-1}\xi)/2\pi^{3/2}\beta \tag{2.60}$$

and from (2.53) and (2.29)

$$\begin{aligned} h_m(B, \xi) &\to (\pi^{1/2}/2B\xi^{1/2}) \tan^{-1}\xi = [(2/\pi)\tan^{-1}\xi] \\ &\quad \times (lk_1)^{-1}(l_a l_f / w_0^2) \\ &\qquad (4B^2 > \xi > 6/B^2). \end{aligned} \tag{2.61}$$

This form satisfies both the near-field and far-field asymptotic limits (2.46) and (2.57), respectively, and is valid also at intermediate ξ providing $B^4 > 6/4 = \frac{3}{2}$. If (2.61) holds in the vicinity of ξ_m we have

$$h_{mm}(B) \underset{(B>2)}{=} (0.714)/B \qquad \xi_m(B) = 1.392. \tag{2.62}$$

Finally, we shall obtain the expansion of $h_{mm}(B)$ for small B. To do this we set $\sigma = \sigma_m(0, \xi_m)$, $\xi = \xi_m(0)$, $\kappa = \mu = 0$ in (2.23). We expand H in powers of $\sigma - \sigma_m$

$$H(\sigma', 0, \xi_m, 0) = H_{mm} + \tfrac{1}{2}(\sigma' - \sigma_m)^2 H_{mm}'' + \cdots, \tag{2.63}$$

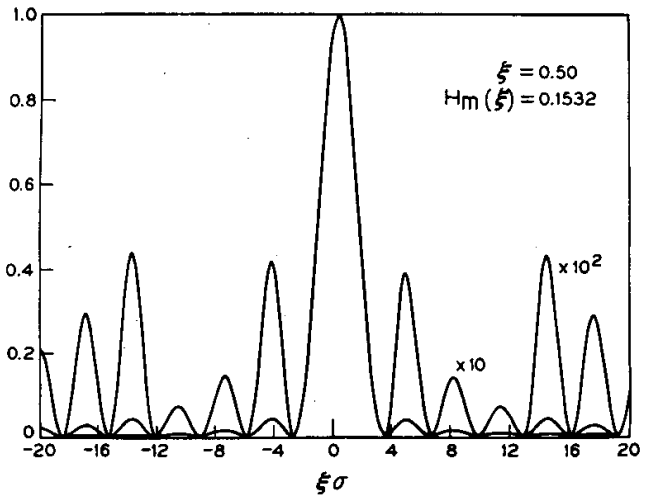

FIG. 6. The function $|H(\sigma, \xi)|^2$ (2.70) normalized to unity for $\xi=50$ as a function of mismatch $\sigma\xi=\frac{1}{2}l\Delta k$. Magnified curves ($\times 10$, $\times 100$) are also shown to better reveal the structure. The maxima and minima represent the coherence length effect.

where $H_{mm}=H(\sigma_m, 0, \xi_m, 0)$ and $H_{mm}''=\partial^2 H(\sigma_m, 0, \xi_m, 0)/\partial\sigma_m^2$. The linear term can be neglected because σ_m maximizes H as well as h when $B=0$. Substituting into (2.24) gives a power series in β^2; the result can be written

$$h_{mm}(B)=h_{mm}(0)[1+2B^2(H_{mm}''/H_{mm}\xi_m)+\cdots] \quad (2.64)$$

It can easily be shown from (2.16) that

$$H_{mm}''=H_{mm}-(\sin\sigma_m\xi_m/\pi\sigma_m)[(1/\sigma_m)+1] + (\xi_m\cos\sigma_m\xi_m/\pi\sigma_m). \quad (2.65)$$

Using $\sigma_m=0.57$, $\xi_m=2.8$, $H_{mm}=0.55$, $H_{mm}''=-0.98$, $h_{mm}(0)=1.068$ we obtain the expansion

$$h_{mm}(B) \underset{(B<0.2)}{\rightarrow} 1.068-1.36B^2, \quad (2.66)$$

where the criterion on B is based on an accuracy of about 10% in $1.068-h_{mm}(B)$.

2.4. SHG without Double Refraction

We give detailed consideration to the case

$$\beta=\kappa=\mu=0 \quad (2.67)$$

and define the simplified functions

$$h(\sigma, \xi)=h(\sigma, 0, 0, \xi, 0)$$
$$H(\sigma, \xi)=H(\sigma, 0, \xi, 0). \quad (2.68)$$

The discussion will also be applicable to PG when $B=0$. From (2.24) and (2.23) it follows that

$$h(\sigma, \xi)=(\pi^2/\xi)\,|H(\sigma, \xi)|^2, \quad (2.69)$$

and from (2.16)

$$H(\sigma, \xi)=(2\pi)^{-1}\int_{-\xi}^{\xi} d\tau[e^{i\sigma\tau}/(1+i\tau)]. \quad (2.70)$$

Evidently $H(\sigma, \xi)$ is real. Let the optimum matching parameter be

$$\sigma_m(\xi)=\sigma_m(0, \xi) \quad (2.71)$$

in the notation of (2.29), and let the optimized functions be written

$$h_m(\xi)=h(\sigma_m(\xi), \xi)=h_m(0, \xi)$$
$$H_m(\xi)=H(\sigma_m(\xi), \xi). \quad (2.72)$$

The curve $B=0$ in Fig. 2 is a plot of $h_m(\xi)$. We have seen in (2.32) that the optimum focusing when $B=0$ is specified by

$$h_{mm}=h_m(\xi_m)=h_{mm}(0)=1.068$$
$$\xi_m=\xi_m(0)=2.84. \quad (2.73)$$

The behavior of $H(\sigma, \xi)^2$ as a function of σ for selected values of ξ covering the entire range of interest is shown in Figs. 6–10. The functions are shown normalized to a maximum value of unity, and the value of $H_m(\xi)$ is indicated numerically in each case. To better show the structure and facilitate comparison of different curves, magnified curves ($X10$, $X100$) are included, and the curves are plotted with $\sigma\xi$ as the abscissa.

In Fig. 6 ($\xi=0.5$), we see the familiar coherence length effect typical of SHG in the near field. The central peak represents phase matching (infinite coherence length), and the successive zeros occur when

$$l_c=l/N \qquad N=1, 2, 3, \cdots, \quad (2.74)$$

where l_c is the coherence length

$$l_c=|\pi l/\sigma\xi|. \quad (2.75)$$

The curve is almost symmetric about its maximum. Figure 7 ($\xi=1.0$) has similar structure but also shows a pronounced asymmetry between the two peaks neighboring the central maximum. In Fig. 8 ($\xi=2.84=\xi_m$) the coherence length structure has become weaker relative to the central region, which now has minima

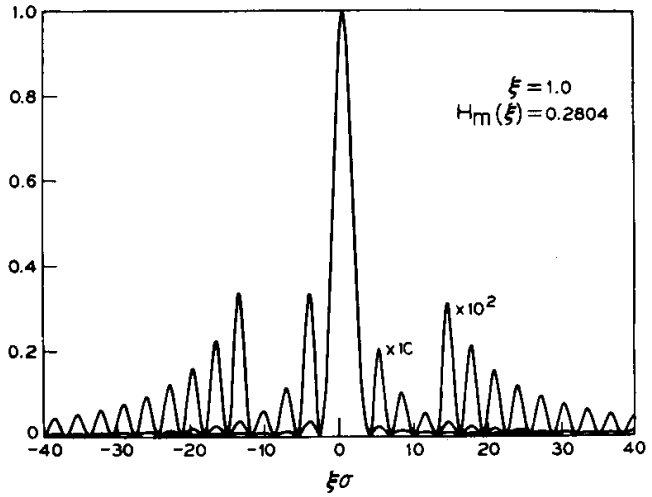

FIG. 7. Similar to Fig. 6 except $\xi=1.0$.

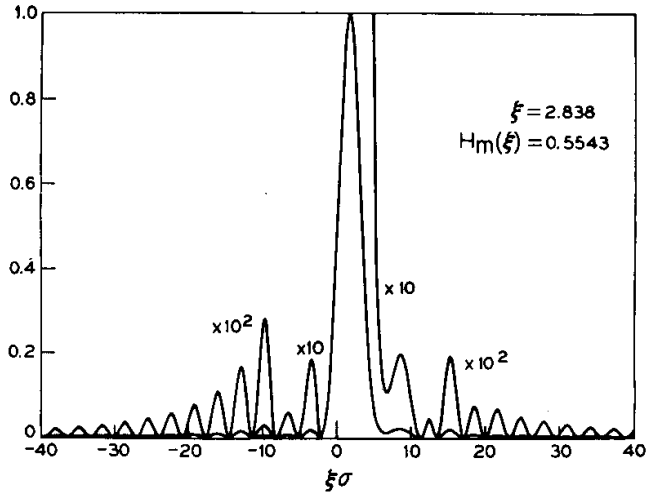

FIG. 8. Similar to Fig. 6 except $\xi=2.84$.

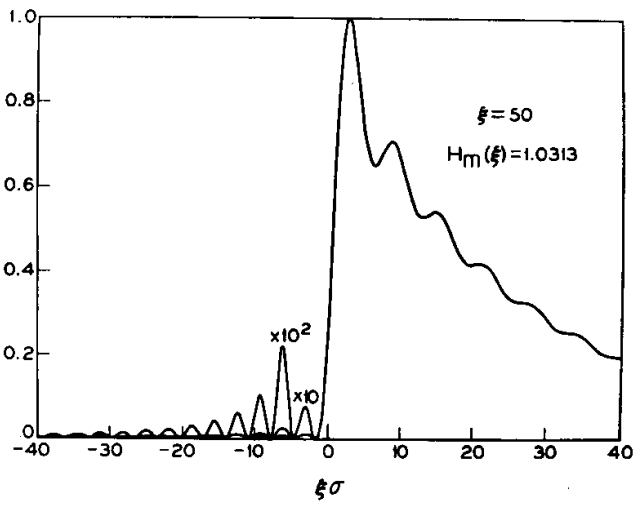

FIG. 10. Similar to Fig. 6 except $\xi=50$. This is the structure characteristic of strong focusing.

at some positions that were maxima in Figs. 6 and 7. In Fig. 9 ($\xi=5$), we see a central pattern emerging which is characteristic of strong focusing and quite distinct from the coherence length pattern, which is now only discernable in the magnified curves. In Fig. 10 ($\xi=50$) the strong focusing pattern is fully developed with its steep rise at $\sigma=0$ and weak fine structure of uniformly spaced maxima superposed on a gradual decay. The spacing of maxima on the side $\sigma>0$ is twice that on the side $\sigma<0$. We see that ordinary phase matching $\sigma=0$ gives much less than the maximum SHG.

Experimental data similar to Figs. 6–10 has been published by Kleinman and Miller,[13] Adams and Barrett,[14] and Labuda and Johnson.[15] It is clear that $H(\sigma, \xi)^2$ has a single main maximum which defines a unique optimum phase-matching parameter $\sigma_m(\xi)$.

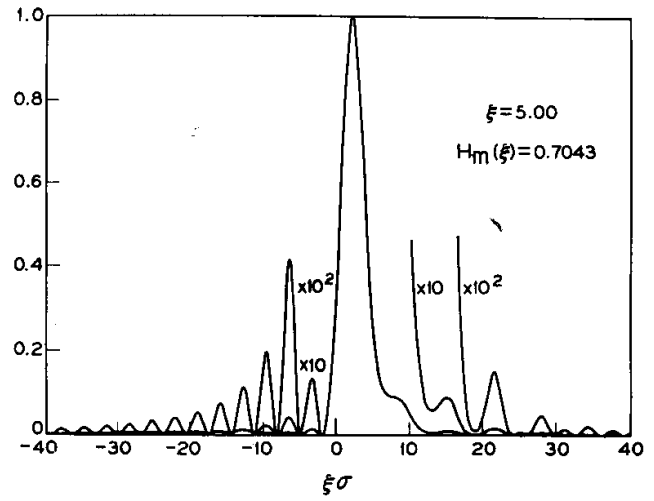

FIG. 9. Similar to Fig. 6 except $\xi=5.0$.

[14] N. I. Adams, III and J. J. Barrett, IEEE J. Quantum Electron. QE-2, 430 (1966).
[15] E. F. Labuda and A. M. Johnson, IEEE J. Quantum Electron. QE-3, 164 (1967).

In Fig. 11 we see $\sigma_m(\xi)$ (solid curve) as a function of ξ. Note that the optimum σ_m corresponds to $\Delta k>0$ for all values of ξ. This can be understood by regarding the laser beam as a diverging pencil of plane waves. When $\Delta k>0$ for the central component of the pencil, there still exist mixing processes for which $\Delta\mathbf{k}=\mathbf{k}_1'+\mathbf{k}_1''-\mathbf{k}_2=0$, but when $\Delta k<0$ matching by mixing is not possible.

The coherence length structure can be described analytically by expanding $H(\sigma, \xi)$ in the form

$$H(\sigma,\xi)=(\xi/\pi)f_1[\xi(\sigma-1)]+(\xi^3/2\pi)f_2[\xi(\sigma-1)]+(\xi^4/3\pi)f_3[\xi(\sigma-1)]+\cdots, \quad (2.76)$$

valid for $\xi<1$ and arbitrary values of σ. Into (2.70) we introduce the expansion

$$(1+i\tau)^{-1}=e^{-i\tau}\{1+[(i\tau)^2/2]-[(i\tau)^3/3]+[3(i\tau)^4/8]+\cdots\} \quad (2.77)$$

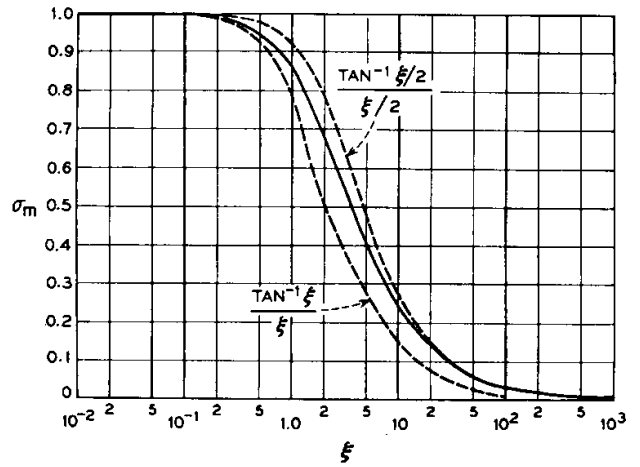

FIG. 11. Optimum phase-matching parameter $\sigma_m(\xi)$ ($\sigma=\frac{1}{2}b\Delta k$). Also shown are two approximations of the general form (2.94).

and immediately obtain (2.76) with

$$f_1(x)=\sin x/x=1-(x^2/6)+(x^4/120)+\cdots$$

$$f_2(x)=[(2/x^2)-1]f_1(x)-(2\cos x/x^2)=-\tfrac{1}{3}+(x^2/10)-(x^4/168)+\cdots$$

$$f_3(x)=(3/x)f_2(x)+(\cos x/x)=-(x/5)+(x^3/42)+\cdots. \quad (2.78)$$

Since the term in ξ^2 is missing in (2.76), the leading term

$$H(\sigma,\xi)\underset{\xi\ll 1}{\rightarrow}(\xi/\pi)\{\sin[\xi(\sigma-1)]/\xi(\sigma-1)\} \quad (2.79)$$

is a good approximation even for $\xi=0.5$ (Fig. 6). Asymmetry about $\sigma=1$ first comes in with increasing ξ through the third term of order ξ^4 in (2.76). From the power-series expansions given in (2.78) we obtain the expansion of $H(\sigma,\xi)$ in powers of $(\sigma-1)$ and ξ

$$H(\sigma,\xi)=(\xi/\pi)\{[1-(\xi^2/6)]-(\xi^4/15)(\sigma-1)+(\xi^2/2)[(\xi^2/10)-\tfrac{1}{3}](\sigma-1)^2+(\xi^4/120)(\sigma-1)^4+\cdots\}. \quad (2.80)$$

The optimum $\sigma_m(\xi)$ according to (2.80) is given by the expansion

$$\sigma_m(\xi)=1-(\xi^2/5)+\cdots \qquad (\xi<0.5). \quad (2.81)$$

The limit indicated for ξ is an empirical one corresponding to a requirement of 10% accuracy for $1-\sigma_m(\xi)$.

The strong focusing pattern is characterized by a steep edge at $\sigma=0$ and a gradual decay for $\sigma>0$. This is described by the limiting form (2.49), which is the leading term of the asymptotic expansion KAB (7.22)

$$H(\sigma,\xi)^2=e^{-2\sigma}\theta(\sigma)-2e^{-\sigma}\theta(\sigma)(\cos\sigma\xi/\pi\sigma\xi)+(1/2\pi^2\sigma^2\xi^2)(1+\cos 2\sigma\xi)+\cdots \quad |\sigma\xi|>1. \quad (2.82)$$

For $\sigma<0$ the first two terms do not contribute and the third term contributes a relatively weak coherence length structure. The second term describes the oscillatory structure superposed on the gradual decay as seen in Fig. 10. The maxima of $H(\sigma,\xi)^2$ occur very nearly at the maxima of $(-\cos\sigma\xi)$; thus, the main peak occurs at

$$\sigma_m(\xi)=\pi/\xi+\cdots \qquad (\xi>20). \quad (2.83)$$

The value of $H_m(\xi)$ when $\xi\gg 1$ is best obtained from [KAB (7.20)]

$$H(\sigma,\xi)=e^{-\sigma}\theta(\sigma)-\tfrac{1}{2}[\theta(\sigma)-\theta(-\sigma)]+(1/\pi)Si(\sigma\xi)+\cdots(\xi>7) \quad (2.84)$$

with

$$Si(x)=\int_0^x\frac{\sin\tau}{\tau}d\tau=\tfrac{1}{2}\pi(x/|x|)-(\cos x/x)+\cdots. \quad (2.85)$$

The form (2.84) gives 10% accuracy for $H_m(\xi)^2$ when $\xi>7$, goes over into (2.82) when $|\sigma\xi|>1$, and gives a continuous representation of $H(\sigma,\xi)$ in the region of the steep rise $\sigma\sim 0$. Since the maximum value of $(2/\pi)Si(x)$ is 1.1790 attained at $x=\pi$, we obtain from (2.84) the simple approximation

$$H_m(\xi)=e^{-\pi/\xi}+0.0895+\cdots \qquad (\xi>7), \quad (2.86)$$

and the limit

$$H_m(\xi)^2\underset{\xi\rightarrow\infty}{\rightarrow}1.187. \quad (2.87)$$

It is important to notice that the main peak of $H(\sigma,\xi)$ is part of the fine structure; if it were not for the fine structure the peak would be a cusp $H^2=1$ at $\sigma=0$ according to the leading term of (2.84). For ordinary phase matching $\sigma=0$ (2.70) reduces to

$$H(0,\xi)=\pi^{-1}\tan^{-1}\xi\underset{\xi\gg 1}{\rightarrow}\tfrac{1}{2}. \quad (2.88)$$

Thus, the ratio of SHG for optimum and ordinary phase matching approaches the limit

$$[H_m(\xi)/H(0,\xi)]^2\underset{\xi\rightarrow\infty}{\rightarrow}4.75. \quad (2.89)$$

For small ξ this ratio approaches unity.

If B is small but not zero, the criterion for the validity of this section may readily be derived from a consideration of the domains of the functions e^{-4s^2} and $|H|^2$ in (2.24). If the oscillatory structure of $|H(\sigma,\xi)|^2$ as a function of σ is to be observed, it is required that the domain of e^{-4s^2} be less than the width in s of the maxima of $|H(\sigma+4\beta s,\xi)|^2$. Taking the domain of e^{-4s^2} as $|s|<1$ and the width of the fine structure as $\Delta\sigma=\pi/\xi$ we obtain the criterion

$$\beta\xi=B\xi^{1/2}<\pi/4 \quad (2.90)$$

for the validity of setting $B=0$. It will be recalled that the opposite of (2.90) was assumed in (2.48) as the condition for the validity of neglecting the fine structure in $|H|^2$ and using (2.49). The theory based on (2.48) led to (2.51), (2.55), and finally the asymptotic form (2.58) of $h_m(B,\xi)$ for $\xi\gg 1$. We now see that there is another asymptotic form of interest when $B\ll 1$ and (2.90) is satisfied. From (2.69), (2.72), and (2.87) we obtain

$$h_m(\xi)=h_m(0,\xi)\rightarrow 1.187\pi^2/\xi=1.187(lk_1)^{-2}(4l_f^2/w_0^2) \qquad (80<\xi<\pi^2/16B^2). \quad (2.91)$$

The range indicated for ξ exists as soon as $B<\frac{1}{12}$.

It is of interest to discuss optimum phase matching from an intuitive point of view. One approach is to consider the phase along the axis for the fundamental and harmonic focused beams. The harmonic beam when $\rho=0$ is a Gaussian beam with spot radius $w_0/\sqrt{2}$ and the same confocal parameter b as the fundamental.

The phases of the fundamental and harmonic fields along the axis relative to the focus are

$$\theta_1=k_1(z-f)-\tan^{-1}(2/b)\,(z-f)$$
$$\theta_2=k_2(z-f)-\tan^{-1}(2/b)\,(z-f). \qquad (2.92)$$

The polarization wave generated in the nonlinear medium has the phase $2\theta_1$. We imagine that there is some effective region of interaction of length l'. It is reasonable to expect $l'<l$ for strongly focused beams ($\xi\gg1$) and $l'\to l$ for weakly focused beams ($\xi\ll1$). We define an effective focusing parameter

$$\xi'=l'/b \qquad (2.93)$$

similar to ξ in (1.3), and define l' as the length over which the change in phase $\Delta\theta_2$ of the harmonic should equal the change in phase $2\Delta\theta_1$ of the polarization wave to maximize the nonlinear interaction. From (2.92), (2.93), and (2.17) we have

$$\begin{aligned}\Delta kl'&=2\tan^{-1}\xi'\\ \sigma_m(\xi')&=(\tan^{-1}\xi')/\xi'\\ &=(\pi/2\xi')+\cdots\\ &=1-(\xi'^2/3)+\cdots.\end{aligned} \qquad (2.94)$$

In Fig. 11 we have indicated two examples of (2.94). The lower dashed curve corresponds to taking $l'=l$, $\xi'=\xi$. Upon comparing (2.94) with (2.83) we see that this model gives only half the correct $\sigma_m(\xi)$ in the limit $\xi\gg1$. The upper dashed curve corresponds to $l'=l/2$, $\xi'=\xi/2$. This model gives the correct behavior for $\xi\gg1$. Neither model gives the correct dependence (2.81) of $1-\sigma_m(\xi)$ in the region $\xi<0.5$. Any model of the form (2.94) correctly predicts the total range of $\sigma_m(\xi)$

$$1\geq\sigma_m(\xi)\geq0$$
$$\sigma_m(0)=1, \qquad \sigma_m(\infty)=0. \qquad (2.95)$$

2.5. Characteristic Lengths in SHG

In this section we present a set of asymptotic relations in terms of four characteristic lengths which are quite helpful in understanding SHG. These relations are helpful for a qualitative discussion of optimization, even though three of the four lengths depend on the focusing parameter ξ. The four lengths are the crystal length l, beam radius w_0 (2.1), the aperture length [BADK (3.41)]

$$l_a=\pi^{1/2}w_0/\rho \qquad (2.96)$$

and the effective length of the focus [KAB (8.37)]

$$l_f=\pi b/2. \qquad (2.97)$$

In terms of B and ξ we have

$$\begin{aligned}w_0&=(l/k_1)^{1/2}\xi^{-1/2}\\ l_a&=(\pi/4)^{1/2}(l/B)\xi^{-1/2}\\ l_f&=(\pi/2)l\xi^{-1}.\end{aligned} \qquad (2.98)$$

The asymptotic forms have already been given in (2.45), (2.46), (2.57), (2.58), and (2.91) together with the appropriate conditions for their validity. All these conditions can easily be rewritten in terms of l, l_f, l_a by means of (2.98). In this way we obtain five asymptotic representations for P_2.

$$P_2=\frac{KP_1^2}{w_0^2}\begin{cases} l^2 & (l_a,\ l_f\gg l) \quad (2.45)\\ ll_a & (l_f\gg l\gg l_a) \quad (2.46)\\ l_fl_a & (l\gg l_f\gg l_a) \quad (2.57)\\ 4l_f^2 & (l\gg l_a\gg l_f) \quad (2.58)\\ 4.75l_f^2 & (l_a\gg l\gg l_f) \quad (2.91)\end{cases} \qquad (2.99)$$

for the case $\alpha=\alpha'=\mu=0$.

These relations are particularly helpful in understanding how P_2 varies with crystal length l. The first four have been given previously in BADK (3.36), BADK (3.39), KAB (8.36), and KAB (8.40), respectively. Also Bjorkholm[11] has used these relations [except for the factor 4 in (2.58)] to estimate ξ_m from the intersection of (2.45) and (2.58). This intersection gives $l=2l_f$ or $\xi=\pi$, reasonably close to the true value $\xi_m(0)=2.84$. For large B, the relevant intersection is that of (2.46) and (2.57), which gives $l=l_f$ or $\xi=\pi/2$, reasonably close to $\xi_m=1.392$ given in (2.62). The last relation has not been given previously.

3. OPTIMIZATION OF THE PG THRESHOLD

3.1. Theory of PG

In a previous paper[6] BA have obtained the parametric generation (PG) threshold for Gaussian beams in the near field neglecting diffraction and double refraction. The approach used was to assume a condition of steady-state oscillation in which signal and idler, frequencies ω_1 and ω_2, were simultaneously resonated while the pump of frequency

$$\omega_3=\omega_1+\omega_2 \qquad (3.1)$$

made a single one-way traversal of the signal-idler resonator. Ordinary collinear phase matching $\Delta k=0$ was assumed, where

$$\Delta k=k_1+k_2-k_3. \qquad (3.2)$$

The PG threshold was determined by equating the one-way power gain per pass in the signal and the idler to the round-trip loss at each frequency within the resonator. In the steady-state condition, the signal mixes with the pump to produce a polarization wave at the idler frequency. This polarization wave then radiates and causes an increase in the electric field which is just canceled by the loss in the idler resonator. A similar argument applies to the signal in the steady state.

Parametric gain takes place only in one direction since the pump is assumed to travel in only one direction. The time average power gain ΔP_2 in the idler is given by (A2.57) which we write as

$$\Delta P_2 = -\mathrm{Im}\left(\tfrac{1}{2}\omega_2 \int \mathbf{E}_2^* \cdot \bar{\mathcal{P}}_2 dx dy dz\right), \qquad (3.3)$$

where the integration is over the transverse beam cross section and over the length of the resonator. $\bar{\mathcal{P}}_2$ represents the polarization wave at frequency ω_2 due to mixing the pump wave at ω_3 with the signal wave at ω_1. E_2 represents the *one-way* electric field amplitude at frequency ω_2 in the resonator mode. The bar in the polarization symbol is used here to indicate that the polarization wave is not necessarily in a single mode of the resonator. According to (A2.16) the polarization is given by

$$\mathcal{P}_2(x, y, z) = \chi : \mathbf{E}_1(x, y, z)^* \mathbf{E}_3(x, y, z)$$
$$\chi = \chi(-\omega_2, -\omega_1, \omega_3). \qquad (3.4)$$

We denote the pump power (in the crystal) by P_3, and the one-way power in the signal and idler modes (i.e., the power impinging on the resonator mirrors) by P_1 and P_2 respectively. The field and polarization Fourier amplitudes are defined in Appendix 2.

In BA the discussion was restricted to PG in negative uniaxial crystals for which it is appropriate that the signal and idler be ordinary waves and the pump an extraordinary wave. $LiNbO_3$ was taken as an example. Phase matching was assumed normal to the optic axis where $\rho=0$ and the effects of double refraction are absent. Diffraction was also neglected in that the analysis was restricted to the near field. In the present treatment both of these effects will be included.

The eigenfunctions or modes of the signal-idler resonator are familiar from Gaussian mode theory.[7] The one-way traveling electric fields in the TEM_{00} mode can be written as in (2.2):

$$E_j(x, y, z) = [E_{j0}/(1+i\tau_j)] \exp(ik_j z) \times \exp[-(x^2+y^2)/w_{j0}^2(1+i\tau_j)]$$
$$\tau_j = 2(z-f)/b_j, \qquad (3.5)$$

where $j=1, 2$ designates the frequency (ω_1 or ω_2), w_{j0} is the Gaussian beam radius, and b_j is the confocal parameter [see (2.1)]. All beams will have their focus at the same point $x=y=0$, $z=f$ and the same axis. As in BA we assume the signal and idler to be ordinary waves while the pump is an extraordinary wave. The theory of Gaussian extraordinary beams is given in Appendix 1. We write the pump as in (A1.10)

$$E_3(x, y, z) = [E_{30}/(1+i\tau_3)] \exp(ik_3 z - i\varphi_3) \cdot \exp\left(-\{[x-\rho(z-f)]^2+y^2\}/w_{30}^2(1+i\tau_3)\right)$$
$$\tau_3 = 2(z-f)/b_3, \qquad (3.6)$$

except for a different choice of origin for x, y so as to put the focus on the line $x=y=0$. Since the signal and idler are reflected and resonated for the TEM_{00} mode (3.5), and higher-order modes are not simultaneously resonant, we can neglect the field in higher-order modes. The amplitudes E_{j0} and E_{30} are real, and the phase φ_3 of the pump relative to the signal and idler is automatically determined when the device oscillates. For the near-field treatment BA mention that $\varphi_3=\pi/2$, as is well known for microwave parametric oscillators. We shall leave it an adjustable parameter to maximize the PG. The beam radii and confocal parameters satisfy

$$w_{10}^2 = b_1 c/n_1\omega_1 = b_1/k_1,$$
$$w_{20}^2 = b_2 c/n_2\omega_2 = b_2/k_2,$$
$$w_{30}^2 = b_3 c/n_3\omega_3 = b_3/k_3. \qquad (3.7)$$

It is convenient to define parameters ω_0, n_0, γ, ζ as follows:

$$2\omega_0 = \omega_1 + \omega_2$$
$$2n_0 = n_1 + n_2$$
$$\omega_1 = \omega_0(1-\gamma), \qquad \omega_2 = \omega_0(1+\gamma)$$
$$n_1 = n_0(1-\zeta), \qquad n_2 = n_0(1+\zeta). \qquad (3.8)$$

Ordinarily ω_1, ω_2 will be close to the degenerate frequency ω_0 so γ, ζ will be small compared with unity. Phase matching $\Delta k=0$ requires

$$n_3\omega_3 = n_1\omega_1 + n_2\omega_2. \qquad (3.9)$$

From (3.8) and (3.9)

$$n_3/n_0 = 1+\gamma\zeta. \qquad (3.10)$$

The case we are treating is equivalent (see Appendix 1) to that of a positive uniaxial crystal in which the pump is an ordinary wave and the signal and idler are extraordinary waves having the same ρ. However, we do not treat the case in which the signal and idler have opposite polarizations. Approximately twice the birefringence is required for phase matching when the signal and idler are of opposite polarization than when they are of the same polarization. It should be noted that recently pulsed PG in KDP was achieved[6] where the signal and idler were ordinary and extraordinary waves instead of both ordinary waves. It is fortunate that one case of interest, that of *equal polarization* for signal and idler, leads to a function (3.32) which is relatively convenient to compute and optimize using programs already developed for treating SHG. The close connection between the computation of (3.32) and (2.23) is brought out in Appendix 4. On the other hand, the case of opposite polarizations for signal and idler leads to formidable computational difficulties.

In the near-field analysis of BA it was shown that the optimum pump radius to minimize the parametric

threshold is given by

$$1/w_{30}^2=(1/w_{10}^2)+(1/w_{20}^2). \tag{3.11}$$

Furthermore, it was assumed for practical reasons that the signal and idler at ω_2 and ω_1 should share the same reflector surfaces and thus have the same surfaces of constant phase throughout the resonator, which requires $b_1=b_2$. This together with (3.11) implies that the confocal parameters should all be equal to some constant b_0

$$b_1=b_2=b_3=b_0, \tag{3.12}$$

so that all three frequencies share the same surfaces of constant phase. We continue to assume (without proof) that (3.11) and (3.12) are appropriate for arbitrary values of l/b_0 and ρ, and seek to find the optimum b_0. It would be very unwieldy to attempt a more general discussion in terms of three different parameters b_1, b_2, b_3 at this time. In Sec. 5.5, however, we shall show that when $\rho=0$ an effective confocal parameter (5.26) can always be defined which plays the role of b_0 in (3.12). Furthermore, we show that (3.12) is actually the optimum condition when $\rho=0$.

In (3.5) and (3.6) we replace τ_j for $j=1, 2, 3$ by the position variable

$$\tau=2(z-f)/b_0. \tag{3.13}$$

The crystal resonator is assumed to extend from $z=0$ to $z=l$ and the position of the minimum mode radius $z=f$ is symmetrically placed between the reflectors at

$$f=l/2. \tag{3.14}$$

Furthermore define, as in (1.3), the focusing parameter

$$\xi=l/b_0, \tag{3.15}$$

and thus the running position variable τ within the resonator extends from $-\xi$ to $+\xi$. It is also convenient to define the spot size parameter

$$w_0^2=b_0c/n_0\omega_0=b_0/k_0 \tag{3.16}$$

by analogy with (3.7).

3.2. PG Threshold Condition

From (3.4), (3.5), and (3.6) one obtains

$$\mathbf{E}_2^*\cdot\overline{\mathcal{P}}_2=E_{20}\mathcal{P}_{20}\exp[-i(\sigma\xi+\varphi_3)]$$
$$[\exp(-i\sigma\tau)/(1+\tau^2)(1-i\tau)]$$
$$\times\exp\{-[2y^2/w_{30}^2(1+\tau^2)]-[x^2/w_{30}^2(1-i\tau)]$$
$$-[x-\rho(z-f)]^2/[w_{30}^2(1+i\tau)]\}, \tag{3.17}$$

where $\sigma=\frac{1}{2}b_0\Delta k$ is defined as in (2.17), and (see Appendix 3)

$$\mathcal{P}_{20}=\chi E_{10}E_{30} \tag{3.18}$$

defines an *effective nonlinear coefficient* χ. The transfer of power from the polarization wave $\mathcal{P}_2$ to the idler mode is obtained from (3.3) and (3.17). The result may be written

$$\Delta P_2=(\pi^2/4)b_0w_{30}^2\omega_2E_{20}\mathcal{P}_{20}\bar{H}(\sigma,\beta,\xi)$$
$$\times\{-\mathrm{Im}\exp[-i(\sigma\xi+\varphi_3)]\}, \tag{3.19}$$

where the real function

$$\bar{H}(\sigma,\beta,\xi)=(2\pi)^{-1}\int_{-\xi}^{+\xi}\frac{\exp(i\sigma\tau-\beta^2\tau^2)}{1+i\tau}\,d\tau \tag{3.20}$$

is closely analogous to the previous H function (2.16). In the above β is defined by

$$\beta=(\rho/\delta_3\sqrt{2})=(\rho/\delta_0)(n_3/n_0)^{1/2}, \tag{3.21}$$

which is analogous to the previous β in (2.13), and δ_0 and δ_3 are far-field diffraction angles [see (2.1)]:

$$\delta_0=2w_0/b_0$$
$$\delta_3=2w_{30}/b_0. \tag{3.22}$$

Similarly, the transfer of power from the polarization wave $\mathcal{P}_1$ to the signal mode can be written

$$\Delta P_1=(\pi^2/4)b_0w_{30}^2\omega_1E_{10}\mathcal{P}_{10}\bar{H}(\sigma,\beta,\xi)$$
$$\times\{-\mathrm{Im}\exp[-i(\sigma\xi+\varphi_3)]\}$$
$$\mathcal{P}_{10}=\chi E_{20}E_{30}. \tag{3.23}$$

In PG as represented by (3.19) or (3.23) the phase φ_3 of the pump will adjust itself automatically to maximize the gain. Consequently, the term in curly brackets will equal $+1$ requiring that

$$\sigma\xi+\varphi_3=\pi/2. \tag{3.24}$$

In near-field operation $\sigma\xi=0$ and the phase of the pump relative to the signal and idler is $\varphi_3=\pi/2$ implying that the pump leads in phase by $\pi/2$ as stated in BA. Obviously from (3.24) when the effects of diffraction are included in PG theory the optimum phase of the pump is no longer $\pi/2$. The inclusion of (3.24) in (3.19) and (3.23) will be assumed throughout the rest of this chapter.

The one-way power in each beam is

$$P_j=(n_jc/16)E_{j0}^2w_{j0}^2, \qquad j=1, 2, 3. \tag{3.25}$$

A little algebra then yields

$$\Delta P_2=(1+\gamma)(\bar{K}P_1P_2P_3)^{1/2}[2l^2/(w_{10}^2+w_{20}^2)]^{1/2}(\pi/\xi)\bar{H}$$
$$\Delta P_1=(1-\gamma)(\bar{K}P_1P_2P_3)^{1/2}[2l^2/(w_{10}^2+w_{20}^2)]^{1/2}(\pi/\xi)\bar{H}, \tag{3.26}$$

where

$$\bar{K}=128\pi^2\omega_0^2\chi^2/n_1n_2n_3c^3. \tag{3.27}$$

Note the similarity in the definitions of $\bar{K}$ for PG in (3.27) and K for SHG in (2.20). Consequently, an experimental measurement of K for SHG is applicable to PG providing the fundamental frequency used is sufficiently close to ω_0, and providing it is permissible to set $\omega_1=\omega_2=\omega_0$ in $\chi(-\omega_3, \omega_1, \omega_2)$. Since the effective

coefficients are related by $\chi=2d$ (see Appendix 3) for PG and SHG, respectively, it follows that

$$\bar{K}(\mathrm{PG})=4K(\mathrm{SHG}). \tag{3.28}$$

This holds only for PG with signal and idler having equal polarizations. For explicit expressions for χ see Appendix 3.

The PG threshold condition (minimum P_3 for oscillation) is dependent upon the resonator losses. Let ϵ_1 and ϵ_2 be the equivalent one-way loss of the signal and idler modes

$$\delta P_1/P_1=-\epsilon_1 \qquad \delta P_2/P_2=-\epsilon_2. \tag{3.29}$$

The pump power threshold condition is obtained by equating the round-trip loss at ω_2 and ω_1 to the one-way power gain (3.26), since the pump traverses the resonator in only one direction. The result is

$$P_3=\frac{4\epsilon_1\epsilon_2}{\bar{K}(1-\gamma^2)(\pi\bar{H}/\xi)^2[2l^2/(w_{10}^2+w_{20}^2)]}\cdot$$

$$=\frac{4\epsilon_1\epsilon_2(1+\gamma\zeta)}{\bar{K}(1-\gamma^2)^2(1-\zeta^2)(\pi\bar{H}/\xi)^2(l^2/w_0^2)}\cdot \tag{3.30}$$

In the near-field limit $\xi\ll 1$ we have

$$(\pi\bar{H}/\xi)\underset{\xi\to 0}{\longrightarrow}1, \tag{3.31}$$

so that (3.30) reduces properly to BA (2.41).

If the effects of double refraction and diffraction are included it is convenient for purposes of optimization to define the function

$$\bar{h}(\sigma,\beta,\xi)=(\pi^2/\xi)\,|\,\bar{H}(\sigma,\beta,\xi)\,|^2. \tag{3.32}$$

We also write

$$(l^2/\xi w_0^2)=lk_0 \qquad k_0=n_0\omega_0/c. \tag{3.33}$$

Then the condition giving the *reciprocal pump threshold* can be written

$$\epsilon_1\epsilon_2/P_3=[(1-\gamma^2)^2(1-\zeta^2)/(1+\gamma\zeta)]\cdot\tfrac{1}{4}\bar{K}lk_0\cdot\bar{h}(\sigma,\beta,\xi)$$

$$\approx\tfrac{1}{4}\bar{K}lk_0\cdot\bar{h}(\sigma,\beta,\xi). \tag{3.34}$$

Here we have assumed nearly degenerate operation $|\gamma|\ll 1$, $|\zeta|\ll 1$. Note the similarity in form between (3.34) and (2.22). The function $\bar{h}(\sigma,\beta,\xi)$, analogous to $h(\sigma,\beta,0,\xi,0)$ for SHG, now contains all of the dependence of P_3 on the optimizable parameters σ, ξ. In view of (3.28), and the fact that we shall establish in the next section that $\bar{h}$ is very similar in its behavior to h, we note that $(\epsilon_1\epsilon_2/P_3)$ is closely analogous to (P_2/P_1^2) for SHG. We note that as $\gamma\to\pm 1$ (i.e., ω_1 or ω_2 vanishes) the threshold becomes infinite.

3.3. Dependence of PG upon Focusing

We now present the evaluation of the nonlinear interaction for PG as measured by the function $\bar{h}(\sigma,\beta,\xi)$ optimized with respect to phase matching σ. In general, $\bar{h}$ would be a function of absorption and focal position [like h in (2.23)], but we are neglecting absorption and setting the focus in the center of the crystal just as we did for SHG in Sec. 2.2. We must vary σ, β, ξ in such a way that ρ and l are held fixed while the confocal parameter b_0 varies. We define a double-refraction parameter

$$B=\rho(lk_0)^{1/2}(n_3/n_0)^{1/2}/2 \tag{3.35}$$

analogous to the previous B of (1.4); for all practical purposes the factor $(n_3/n_0)^{1/2}$ can be omitted. As in (2.37) we write

$$\beta=B\xi^{-1/2} \tag{3.36}$$

and seek to maximize the function $\bar{h}(\sigma, B\xi^{-1/2},\xi)$, with respect to σ and ξ with B held constant. Optimization with respect to σ gives

$$\bar{h}_m(B,\xi)=\bar{h}(\sigma_m(B,\xi), B\xi^{-1/2},\xi), \tag{3.37}$$

where $\sigma_m(B,\xi)$ is the optimum σ.

Figure 12 shows curves of $\bar{h}_m(B,\xi)$ as a function of ξ for several values of B. These curves are qualitatively similar to those of Fig. 2. Each curve has a single maximum which defines the optimum focusing parameter $\bar{\xi}_m(B)$. The optimized PG represented by

$$\bar{h}_{mm}(B)=\bar{h}_m[B,\bar{\xi}_m(B)] \tag{3.38}$$

is plotted (dashed curve) in Fig. 3. Note that as B increases the curves of $\bar{h}_m(B,\xi)$ against ξ become very flat topped. Therefore the exact location of the maximum of these curves giving $\bar{\xi}_m(B)$ is not very significant, and we do not show a curve of $\bar{\xi}_m(B)$ analogous to Fig. 4. It is apparent in Fig. 12, however, that $\bar{\xi}_m(B)$ decreases monotonically to zero as B increases; this is unlike the case of SHG in which $\xi_m(B)$ lies within the

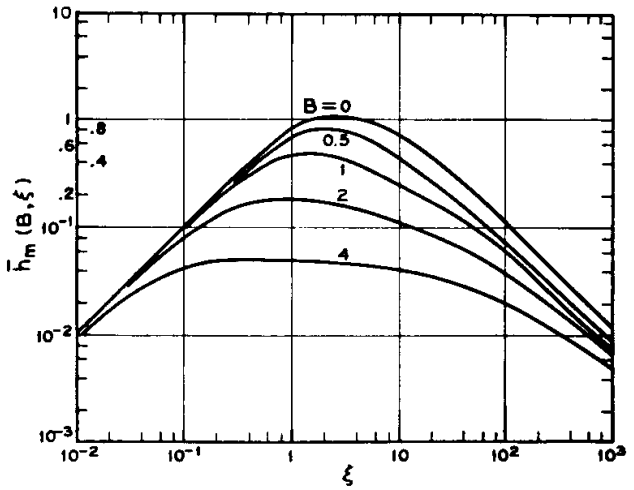

FIG. 12. PG reciprocal threshold (3.34) represented by the function $h_m(B,\xi)$ (3.37) for optimum phase matching as a function of focusing parameter ξ for several values of B. For $B=0$ the curve is the same as that of Fig. 2.

range (2.33). The maximum PG is specified by ($B=0$)

$$\bar{h}_{mm}(0)=1.068$$
$$\bar{\xi}_m(0)=2.84, \tag{3.39}$$

which are exactly the same as (2.32) for SHG. The whole curve for $B=0$ is, in fact, the same as the $B=0$ curve of Fig. 2. The computations are described in Appendix 4.

3.4. Limiting Cases

In the *absence of double refraction*, $B=0$, (3.20) reduces to (2.70)

$$\bar{H}(\sigma, 0, \xi)=H(\sigma, \xi) \tag{3.40}$$

and (3.32) reduces to (2.69)

$$\bar{h}(\sigma, 0, \xi)=h(\sigma, \xi)=h(\sigma, 0, 0, \xi, 0). \tag{3.41}$$

Thus, the curves for $B=0$ in Figs. 2 and 12 are the same. The discussion of Sec. 2.4 therefore applies to PG as well as to SHG. In particular the criterion (2.90) for setting $B=0$ is also valid for PG. To prove this we make use of the general formula

$$\bar{H}(\sigma, \beta, \xi)=(2\beta\pi^{1/2})^{-1}\int_{-\infty}^{\infty} d\sigma' H(\sigma', \xi) \times\exp[-(\sigma-\sigma')^2/4\beta^2], \tag{3.42}$$

which can easily be verified by substituting for $H(\sigma', \xi)$ from (2.70) and carrying out the integration over σ'. The criterion for setting $B=0$ is that the domain of $\exp[-(\sigma-\sigma')^2/4\beta^2]$ in (3.42) must be smaller than the width $\Delta\sigma'=\pi/\xi$ of the fine structure of $H(\sigma', \xi)$. Taking $\Delta\sigma'=4\beta$ as the full width of the exponential immediately gives (2.90). The case $B=0$ was treated by BA in the near-field approximation $\xi\ll 1$; the BA approximation may be written

$$(\pi\bar{H}/\xi)^2(l^2/w_0^2)\underset{\xi\gg 1}{\longrightarrow}\xi l k_0, \tag{3.43}$$

which is to be substituted into (3.30). This indicates that P_3 falls off as ξ^{-1} with increasing ξ, but eventually the theory breaks down because it neglects diffraction. However, BA argued that the effective interaction length should be roughly b_0, and (3.43) should still be roughly correct at $\xi=1$, so they estimated the minimum P_3 from (3.30) and (3.43) with $\xi=1$. From (3.16), (3.32), and (3.33) we can write the exact form of (3.43)

$$(\pi\bar{H}/\xi)^2(l^2/w_0^2)=\bar{h}l k_0. \tag{3.44}$$

It follows that the BA approximation amounts to assuming

$$\bar{h}_{mm}(0)\sim 1 \text{ (BA)}, \tag{3.45}$$

which is only 7% below the accurate value 1.068 given in (3.39). The error in using a near-field approximation appears primarily in the inability of the near-field theory to provide an estimate of the optimum focusing parameter $\bar{\xi}_m(0)$.

For small B we can expand $\bar{h}_{mm}(B)$ in much the same way as we expanded $h_{mm}(B)$ for SHG to obtain (2.66). We set $\sigma=\sigma_m(0, \xi)$, $\xi=\xi_m(0)$ and expand $H(\sigma', \xi)$ as in (2.63), substitute this expansion into (3.42), and obtain a power series in β^2

$$\bar{H}(\sigma_m, \beta, \xi_m)=H_{mm}+\beta^2 H_{mm}''+\cdots, \tag{3.46}$$

where $H_{mm}=H(\sigma_m, \xi_m)$, $H_{mm}''=\partial^2 H(\sigma_m, \xi_m)/\partial\sigma_m^2$ are the same as in (2.63). Substituting (3.46) into (3.32) gives the expansion (2.66) for $\bar{h}_{mm}(B)$.

The case of *large double refraction* can be treated very easily from (3.42). If β is sufficiently large, the exponential can be taken outside the integral and set equal to unity, providing σ is given a suitable value close to the optimum value σ_m; thus (3.42) becomes

$$\bar{H}(\sigma_m, \beta, \xi)\underset{\beta\gg 1}{\longrightarrow}(2\beta\pi^{1/2})^{-1}\int_{-\infty}^{\infty} d\sigma' H(\sigma', \xi), \tag{3.47}$$

which may be compared with our previous result (2.59) for SHG. The integral gives unity for all ξ, so we obtain

$$\bar{h}_m(B, \xi)\rightarrow\bar{h}_{mm}(B)\rightarrow\pi/4B^2 \quad (B^2/4>\xi>2/B^2). \tag{3.48}$$

The criterion for the validity of (3.48) is based on an accuracy of 10%. Note that (3.48) differs from the corresponding limit (2.61) for SHG; in particular, $\bar{h}_m(B, \xi)$ is independent of ξ over the range of validity of (3.48), thereby explaining the flatness of the curves for $B=2$ and $B=4$ in Fig. 12.

The limiting forms (2.66) and (3.48) suggest that an empirical approximation of the form

$$\bar{h}_{mm}(B)\approx\bar{h}_{mm}(0)/[1+(4B^2/\pi)\bar{h}_{mm}(0)] \tag{3.49}$$

might represent $\bar{h}_{mm}(B)$ with satisfactory accuracy over the entire range of B. This is in fact the case, and (3.49) is good to better than 10% for all B and satisfies the limiting form (3.48) exactly.

In the limit $\xi\ll 1$ corresponding to the *near field* $\bar{H}(\sigma, \beta, \xi)$ can be treated by means of the expansion (2.77); retaining only the first term of this expansion in (3.20) gives

$$\bar{H}(\sigma, \beta, \xi)\underset{\xi\ll 1}{\longrightarrow}(2\pi)^{-1}\int_{-\xi}^{\xi} d\tau \exp[i(\sigma-1)\tau-\beta^2\tau^2].$$

The optimum σ is obviously $\sigma_m=1$, which gives

$$\bar{H}_m(\beta, \xi)\underset{\xi\ll 1}{\longrightarrow}\operatorname{erf}(\beta\xi)/2\pi^{1/2}\beta, \tag{3.50}$$

where $\operatorname{erf}(z)$ is defined in (2.52). It follows that

$$\bar{h}_m(B, \xi)\underset{(\xi<0.4)}{\longrightarrow}(\pi/4B^2)[\operatorname{erf}(B\sqrt{\xi})]^2, \tag{3.51}$$

which is analogous to the near-field limit (2.43) for SHG. The asymptotic behavior is given by

$$\bar{h}_m(B, \xi)\rightarrow\xi \quad (\xi<0.4, \xi<1/6B^2) \tag{3.52}$$

analogous to (2.43). When $\xi>2/B^2$, (3.51) reduces to (3.48). The aperture length for parametric effects can be defined as

$$l_a=(2\pi)^{1/2}w_{30}/\rho$$
$$=(\pi^{1/2}w_0/\rho)(n_0/n_3)^{1/2}, \quad (3.53)$$

similar to (2.96). We also define the variable

$$t=2\sqrt{2}\beta\xi=2\sqrt{2}B\xi^{1/2}=(2\pi)^{1/2}(l/l_a) \quad (3.54)$$

as in (2.37). The function

$$\bar{G}(t)=(2\pi/t^2)[\mathrm{erf}(t/2\sqrt{2})]^2$$
$$=1-t^2/12+(7/1440)t^4\cdots$$
$$=2\pi t^{-2}-8(2\pi)^{1/2}t^{-3}e^{-t^2/8}+\cdots \quad (3.55)$$

plays the same role in near-field PG as $G(t)$ defined in (2.40) plays in near-field SHG. Thus (3.51) can be written

$$\bar{h}_m(B,\xi)\underset{(\xi<0.4)}{\longrightarrow}\xi\bar{G}(2\sqrt{2}B\xi^{1/2}) \quad (3.56)$$

in the same form as (2.43). We also have

$$[\pi\bar{H}_m(B,\xi)/\xi]^2\underset{(\xi<0.4)}{\longrightarrow}\bar{G}(t)\underset{(t<1)}{\longrightarrow}1, \quad (3.57)$$

which insures that (3.30) reduces properly to BA (2.41).

In the *far-field* limit $\xi\gg1$ we use (3.42) and represent $H(\sigma'\xi)$ by the leading term of (2.84); the result is $(B\neq0)$

$$\bar{H}(\sigma,\beta,\xi)\underset{(\xi\gg1)}{\longrightarrow}(2\beta\pi^{1/2})^{-1}$$
$$\times\int_0^\infty\exp[-\sigma'-(\sigma-\sigma')^2/4\beta^2]d\sigma'$$
$$=\tfrac{1}{2}\{1-\mathrm{erf}[\beta-(\sigma/2\beta)]\}e^{\beta^2}e^{-\sigma}. \quad (3.58)$$

Let us define the function

$$\bar{F}(\epsilon,\beta)\equiv\tfrac{1}{4}[1-\mathrm{erf}(\beta-2\epsilon)]^2\exp(2\beta^2-8\beta\epsilon), \quad (3.59)$$

which is very similar $F(\epsilon,\beta)$ defined in (2.51). Then if $\epsilon=\sigma/4\beta$, as in (2.37), we have

$$|\bar{H}(\sigma,\beta,\xi)|^2\underset{(\xi\gg1)}{\longrightarrow}\bar{F}(\epsilon,\beta) \quad (3.60)$$

$$\bar{h}(\sigma,\beta,\xi)\underset{(\xi\gg1)}{\longrightarrow}(\pi^2/\xi)\bar{F}(\epsilon,\beta), \quad (3.61)$$

and

$$\bar{h}_m(B,\xi)\rightarrow(\pi^2/\xi)\bar{F}_m(B\xi^{-1/2}),\qquad(\xi>10,\ \xi>\pi^2/16B^2), \quad (3.62)$$

where $\bar{F}_m(\beta)$ is $\bar{F}(\epsilon,\beta)$ maximized with respect to ϵ. It follows from (3.59) that

$$\bar{F}_m(\beta)=(4\pi\beta^2)^{-1}\exp(-8\bar{\epsilon}_m^2), \quad (3.63)$$

where $\bar{\epsilon}_m(\beta)$ is the optimum value of ϵ. For $\beta>1$ we can neglect $\bar{\epsilon}_m$ and write

$$\bar{F}_m(\beta)\underset{(\beta>1)}{\longrightarrow}(4\pi\beta^2)^{-1}. \quad (3.64)$$

It follows that (3.62) reduces to (3.48) when $\xi<B^2$. In the limit $\beta\rightarrow0$(3.59) gives

$$\bar{F}_m(0)=1. \quad (3.65)$$

Therefore, the asymptotic form of (3.62) is

$$\bar{h}_m(B,\xi)\rightarrow\pi^2/\xi$$
$$(\xi>10,\ \xi>\pi^2/16B^2)\qquad(\xi>4\times10^3B^2). \quad (3.66)$$

The conditions for the validity of (3.66) are the same as those for the analogous relation (2.58). When $B=0$ (3.58) is not valid as explained following (2.48) and (2.90). In view of (3.41) and (2.91) we have

$$\bar{h}_m(0,\xi)\rightarrow1.187\pi^2/\xi$$
$$(80<\xi<\pi^2/16B^2). \quad (3.67)$$

3.5. Optimization of Crystal Length

We have up to now regarded the crystal length l as a given parameter and have sought to optimize only the phase matching σ and focusing ξ. In the case of SHG treated in Chap. 2 there is no possibility of optimizing l as long as absorption is neglected; we see from (2.22) that P_2 is proportional to l, so the crystal should be as long as possible. The close analogy between PG and SHG, exemplified by the similarity between (3.34) and (2.22), holds as long as l and ϵ_1, ϵ_2 are regarded as given parameters. However, it is reasonable to suppose that the fractional losses ϵ_1, ϵ_2 depend upon l as follows

$$\epsilon_1=1-r_1+\alpha_1 l$$
$$\epsilon_2=1-r_2+\alpha_2 l, \quad (3.68)$$

where r_1, r_2 are the power-reflection coefficients of the mirror for signal and idler. More precisely, if the two mirrors are not the same r_1 is the geometric mean of the reflection coefficients. We include in $1-r_1$ losses at the mirrors due to scattering and transmission. The quantity $\epsilon_1\epsilon_2/l$ now has a minimum at

$$l_0=(1-r_1)^{1/2}(1-r_2)^{1/2}(\alpha_1\alpha_2)^{-1/2}. \quad (3.69)$$

Let us assume that σ and ξ are optimized for any given l; then (3.34) can be written

$$P_3=(4/k_0\bar{K})(\epsilon_1\epsilon_2/l)[1/\bar{h}_{mm}(B)], \quad (3.70)$$

where B depends on l according to (3.35). We see that PG differs from nonresonant SHG in that an optimum $l=l_m$ can be defined by requiring that (3.70) should be a minimum.

In the absence of double refraction the optimum is $l_m=l_0$. In general, however, we have $l_m<l_0$ due to the rapid drop-off of $\bar{h}_{mm}(B)$ as shown in Fig. 3. By means of the empirical formula (3.49), which we may write

in the form

$$1/\bar{h}_{mm}(B)\approx[1/\bar{h}_{mm}(0)]+(\rho^2k_0/\pi)l, \quad (3.71)$$

the general expression for l_m can be obtained as the solution of a cubic equation in l. This result is too cumbersome to be displayed here, so we consider only the case of *large double refraction*. If we may neglect $\alpha_1\alpha_2l^2$ in $\epsilon_1\epsilon_2$ it is easy to minimize P_3 with respect to l and obtain the *optimum crystal length*

$$l_m=l_0/C, \quad (3.72)$$

where

$$C^2=[\rho^2k_0\bar{h}_{mm}(0)/\pi][(1-r_1)/\alpha_1+(1-r_2)/\alpha_2]. \quad (3.73)$$

The condition for the validity of (3.72) is simply

$$C^2\gg1.$$

The theory is somewhat simplified if we may assume

$$\epsilon_1=\epsilon_2=\epsilon=\epsilon_0+\alpha_0l, \quad (3.74)$$

where ϵ_0 is independent of l. The threshold (3.70) can now be written [using (3.71)]

$$P_3=[16\epsilon_0^2/k_0\bar{K}l_0\bar{h}_{mm}(0)]\cdot f(\Gamma, x), \quad (3.75)$$

where

$$x=l/l_0$$

$$l_0=\epsilon_0/\alpha_0$$

$$\Gamma=\bar{h}_{mm}(0)\rho^2k_0l_0/\pi \quad (3.76)$$

and

$$f(\Gamma, x)\equiv[(1+x)^2/4x](1+\Gamma x). \quad (3.77)$$

The crystal length l is now represented by the normalized variable x, and optimization of l consists in minimizing $f(\Gamma, x)$ with respect to x for a given value of Γ. The optimum value x_m satisfies the cubic equation

$$2\Gamma x_m^3+(1+2\Gamma)x_m^2-1=0. \quad (3.78)$$

If $\Gamma\gg1$ this reduces to

$$x_m \underset{\Gamma\gg1}{\longrightarrow} (2\Gamma)^{-1/2}, \quad (3.79)$$

which agrees with (3.72) since $C^2=2\Gamma$ when $\epsilon_1=\epsilon_2$. Figure 13 shows curves of $f(\Gamma, x)$ as a function of x for several values of Γ. From these curves the optimum l can be determined for most practical cases.

3.6. Application to PG in Tellurium

Recently it has been demonstrated that phase matching can be obtained in a crystal of tellurium for both SHG[16] and PG[17] using the CO_2 laser[18] at 10.6 μ. Tellurium is a positive uniaxial crystal of class $32(D_3)$ which is reasonably transparent in the infrared from 5 μ to beyond 25 μ. The combination of tellurium and the CO_2 laser is particularly interesting because of the extremely large value of the nonlinear coefficient[16]

$$d_{11}(T_e)=(1.27\pm0.2)\times10^{-5}\text{esu} \quad (3.80)$$

and the high power (>100 W) available continuously from the CO_2 laser at 10.6 μ. The relevant optical properties of tellurium for PG are summarized below[19]:

$$n_3^o=n_1^e=n_2^e=4.795$$

$$\theta_m=7.2°$$

$$\rho=2.9°=0.051 \text{ rad}$$

$$\alpha_1=\alpha_2=0.1 \text{ cm}^{-1}. \quad (3.81)$$

Here we have assumed $\omega_1=\omega_2$ and the pump ω_3 corresponds to 10.6 μ (in air). The angles θ_m and ρ for positive birefringent crystals can be calculated from BADK (2.9, 3.1) (written for negative crystals) after making the replacements $n_2^o\rightarrow n_1^e$, $n_2^e\rightarrow n_1^o$, $n_1^o\rightarrow n_2^o$. Since the crystal is positive uniaxial we consider the case in which signal and idler are extraordinary waves and the pump is an ordinary wave. From Table I we find that the effective nonlinear coefficient for PG is

$$\chi=2d_{11}\cos^2\theta_m. \quad (3.82)$$

As discussed in Appendix 1 our principal result (3.34), or its optimized form (3.70), is valid for positive as well as negative uniaxial crystals. The constant $\bar{K}$ defined in (3.27) has the value

$$\bar{K}=3.35\times10^{-2}\chi^2$$

$$=2.09\times10^{-12}\text{esu}. \quad (3.83)$$

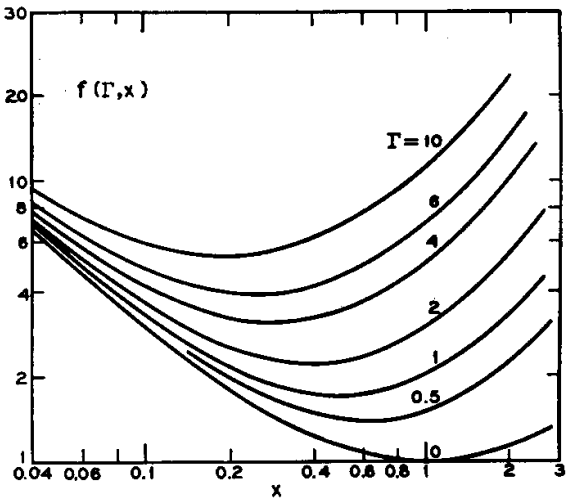

FIG. 13. The PG threshold (3.75) represented by the function $f(\Gamma, x)$ (3.77) for optimum phase matching and focusing as a function of the normalized crystal length x defined in (3.76) for several values of Γ.

[16] C. K. N. Patel, Phys. Rev. Letters **15**, 1027 (1965).
[17] C. K. N. Patel, Appl. Phys. Letters **9**, 332 (1966).
[18] C. K. N. Patel, P. K. Tien, and J. H. McFee, Appl. Phys. Letters **7**, 290 (1965); D. Moeller and J. D. Rigden, Appl. Phys. Letters **7**, 276 (1965).
[19] Calculated by C. K. N. Patel from data of R. S. Caldwell and H. Y. Fan, Phys. Rev. **114**, 664 (1959), and unpublished transmission data by Patel.

TABLE I. Columns 1–4 list, respectively, the uniaxial crystal classes [except $3(C_3)$], the nonvanishing components d_{ij}, the form of the effective nonlinear coefficients defined in (A3.8) as functions of the angles θ_r, θ_m in Fig. 1, and the squared coefficients optimized with respect to crystal orientation. $(\pm)$ refer to $(+)$ positive and $(-)$ negative birefringence. For class $32(D_3)$, $(d_m^+)^2$ has been simplified by invoking the symmetry (A2.46). Coefficients d_{ij} enclosed in brackets vanish according to this symmetry. Fields have been assumed transverse; except relations are obtained by replacing θ_m with $\theta_m+\rho$ for $(-)$ or $\theta_m-\rho$ for $(+)$ birefringence.

Class	$d_{il}\neq 0$	$d(\theta_r,\theta_m)^{\pm}$	$(d_m^{\pm})^2$
$\bar{4}3m(T)$ $23(T_d)$	$d_{14}=d_{25}$ $=d_{36}$	$d^+=d_{14}\cos 2\theta_r \sin 2\theta_m$ $d^-=-d_{14}\sin 2\theta_r \sin\theta_m$	d_{14}^2
$\bar{4}2m(D_{2d})$	$d_{14}=d_{25}$, d_{36}	$d^+=d_{14}\cos 2\theta_r \sin 2\theta_m$ $d^-=-d_{36}\sin 2\theta_r \sin\theta_m$	$d_{14}^2 \sin^2 2\theta_m$ $d_{36}^2 \sin^2\theta_m$
$\bar{6}m2(D_{3h})$	$d_{11}=-d_{12}$ $=-d_{26}$	$d^+=-d_{11}\cos 3\theta_r \cos^2\theta_m$ $d^-=d_{11}\sin 3\theta_r \cos\theta_m$	$d_{11}^2 \cos^4\theta_m$ $d_{11}^2 \cos^2\theta_m$
$\bar{6}(C_{3h})$	$d_{11}=-d_{12}$ $=-d_{26}$, $d_{22}=-d_{21}$ $=-d_{16}$	$d^+=(d_{22}\sin 3\theta_r-d_{11}\cos 3\theta_r)\cos^2\theta_m$ $d^-=(d_{22}\cos 3\theta_r+d_{11}\sin 3\theta_r)\cos\theta_m$	$(d_{22}^2+d_{11}^2)\cos^4\theta_m$ $(d_{22}^2+d_{11}^2)\cos^2\theta_m$
$32(D_3)$	$d_{11}=-d_{12}$ $=-d_{26}$, $(d_{14}=-d_{25})$	$d^+=d_{14}\sin 2\theta_m-d_{11}\cos 3\theta_r \cos^2\theta_m$ $d^-=d_{11}\sin 3\theta_r \cos\theta_m$	$\sim d_{11}^2 \cos^4\theta_m$ $d_{11}^2 \cos^2\theta_m$
$4mm(C_{4v})$ $6mm(C_{6v})$	$d_{31}=d_{32}$, d_{33}, $d_{15}=d_{24}$	$d^+=0$ $d^-=-d_{31}\sin^2\theta_m$	0 $d_{31}^2 \sin^2\theta_m$
$6(C_6)$ $4(C_4)$	$d_{31}=d_{32}$, d_{33} $d_{15}=d_{24}$, $(d_{14}=-d_{25})$	$d^+=d_{14}\sin 2\theta_m$ $d^-=d_{31}\sin\theta_m$	$d_{14}^2 \sin^2 2\theta_m$ $d_{31}^2 \sin^2\theta_m$
$3m(C_{3v})$	$d_{22}=-d_{21}$ $=-d_{16}$, d_{33}, $d_{31}=d_{32}$ $d_{15}=d_{24}$	$d^+=d_{22}\sin 3\theta_r \cos^2\theta_m$ $d^-=d_{22}\cos 3\theta_r \cos\theta_m-d_{31}\sin\theta_m$	$d_{22}^2 \cos^4\theta_m$ $(\lvert d_{22}\rvert \cos\theta_m+\lvert d_{31}\rvert \sin\theta_m)^2$
$\bar{4}(S_4)$	$d_{31}=-d_{32}$ d_{36}, $d_{14}=d_{25}$ $d_{15}=-d_{24}$	$d^+=(d_{14}\cos 2\theta_r-d_{15}\sin 2\theta_r)\sin 2\theta_m$ $d^-=-(d_{31}\cos 2\theta_r+d_{36}\sin 2\theta_r)\sin\theta_m$	$(d_{14}^2+d_{15}^2)\sin^2 2\theta_m$ $(d_{31}^2+d_{36}^2)\sin^2\theta_m$

With P_3 in watts and l in centimeters (3.70) becomes

$$P_3=13.5\cdot(\epsilon_1\epsilon_2/l)\cdot[1/\bar{h}_{mm}(B)] \tag{3.84}$$

and

$$B=3.0l^{1/2}. \tag{3.85}$$

To obtain explicit numerical results, it is most convenient to assume signal and idler have the same loss ϵ given in (3.74). Reasonable numerical values are

$$\epsilon_0=1-r=0.05$$

$$\alpha_0=0.1\ \text{cm}^{-1} \tag{3.86}$$

and from (3.76)

$$\Gamma=6.3$$

$$l_0=0.5\ \text{cm}. \tag{3.87}$$

It follows from Fig. 13 or (3.79) that the optimum crystal length is given by

$$x_m=0.28$$

$$l_m=0.14\ \text{cm}. \tag{3.88}$$

Inserting the appropriate numerical values into (3.75) gives the threshold in watts

$$P_3=0.25f(6.3, x) \tag{3.89}$$

as a function of x. The dependence on x is very close to that of the curve for $\Gamma=6$ in Fig. 13. Inserting $x=x_m=0.28$ gives finally the threshold

$$P_3=1.0\ \text{W} \tag{3.90}$$

optimized with respect to phase matching, focusing, and crystal length. At $l=l_m$ we have from (3.85) $B_m=1.1$, so the dependence on focusing is rather closely represented by the curve for $B=1$ in Fig. 12. We see from this curve that $\bar{\xi}_m=1.5$, which determines the required confocal parameter b_0.

3.7. Application to PG in Lithium Niobate

At the moment one of the most promising materials for PG utilizing a visible pump is $LiNbO_3$. Giordmaine and Miller[4] have observed pulsed PG in $LiNbO_3$. Previously BA[6] have predicted a threshold on the basis of the numbers[20] d_{31} ($LiNbO_3$) $=11\times d_{36}$ (KDP) and[21] $d_{36}(\text{KDP})=(2.1\pm 0.7)\times 10^{-9}$ esu. Recently Francois[22] has reported an improved measurement for ADP

$$d_{36}(\text{ADP})=(1.36\pm 0.16)\times 10^{-9}\ \text{esu}. \tag{3.91}$$

[20] G. D. Boyd, R. C. Miller, K. Nassau, W. L. Bond, and A. Savage, Appl. Phys. Letters **5**, 234 (1964).
[21] A. Ashkin, G. D. Boyd, J. M. Dziedzic, Phys. Rev. Letters **11**, 14 (1963).
[22] G. E. Francois, Phys. Rev. **143**, 597 (1966).

Comparative measurements by Miller[23] indicate that $d_{36}(\text{ADP})=d_{36}(\text{KDP})$. Thus we here adopt the value

$$d_{31}(\text{LiNbO}_3)=1.5\times10^{-8}\text{ esu} \tag{3.92}$$

and give a revised threshold estimate assuming as in BA an argon laser pump (extraordinary wave) at 0.5147 μ, degenerate signal and idler (ordinary waves) at 1.0294 μ, and phase matching normal to the optic axis $\theta_m=\pi/2$, $\rho=0$. From (A3.7) and Table I for crystal symmetry $3m$ $(C_{3v})(-)$ we find that the effective nonlinear coefficient for PG is $\chi=2d_{31}$. From (3.27) one obtains

$$\bar{K}=1.25\times10^{-14}\text{ esu} \tag{3.93}$$

assuming the refractive index[24] $n_1=n_2=n_3=2.239$. From (3.34) and (3.39) one obtains

$$P_3=220\cdot(\epsilon_1\epsilon_2/l) \tag{3.94}$$

with P_3 in watts, l in centimeters. For the case $l=1$ cm, $\epsilon_1=\epsilon_2=0.01$, this gives $P_3=22$ mW. The optimum focusing $\xi=\xi_m=2.84$ requires mirrors on the surface of the crystal having radius of curvature 0.562 cm for $l=1$ cm. For $\xi=1$, which for $l=1$ would require a radius of curvature of 1 cm, the threshold would increase 34% to 30 mW. It is obvious that these reasonably low[25] thresholds are critically dependent upon low-loss resonators and the absence of optically induced inhomogenities[26] in the $LiNbO_3$.

As another example of a potentially useful parametric oscillator consider the use of the room-temperature YAG:Nd laser[27] at 1.0648 μ. At this pumping wavelength $LiNbO_3$ appears[26] to be less susceptible to optically induced damage than at 0.5147 μ. However, a disadvantage of pumping at 1.0648 μ is that phase matching normal to the optic axis would require a temperature[28] of about 740°C. For room-temperature operation one calculates from the refractive index data[24]:

$$\theta_m=43.2$$
$$\rho=0.0374. \tag{3.93}$$

From Table I the effective nonlinear coefficient is

$$\chi=2(d_{22}\cos\theta_m+d_{31}\sin\theta_m)$$
$$=3.0\times10^{-8}\text{ esu} \tag{3.94}$$

using[20] $d_{22}/d_{31}=5.1/10.6$, and from (3.27)

$$\bar{K}=3.1\times10^{-15}\text{ esu} \tag{3.95}$$

using[24] $n_1=n_2=n_3=2.198$. From (3.35)

$$B=4.7l^{1/2} \tag{3.96}$$

with l in centimeters, and (3.34) becomes (P_3 in watts)

$$P_3=2.0\times10^3\cdot(\epsilon_1\epsilon_2/l)[1/\bar{h}_{mm}(B)]. \tag{3.97}$$

In the absence of measurements of the relative importance of bulk losses and reflection losses in $LiNbO_3$, we cannot determine the optimum length discussed in Sec. 3.5.

From (3.35) one may write

$$lk_0=(4B^2/\rho^2)(n_0/n_3) \tag{3.98}$$

and thus from (3.70) (setting $n_0/n_3=1$)

$$P_3=(\epsilon_1\epsilon_2\rho^2/\bar{K})[B^2\bar{h}_{mm}(B)]^{-1}. \tag{3.99}$$

The crystal length l is now contained in the parameter B, and the dependence of P_3 on l in the presence of double refraction (with $\epsilon_1\epsilon_2$ independent of l) is governed by the function $B^2\bar{h}_{mm}(B)$. From (3.49)

$$B^2\bar{h}_{mm}(B)\approx B^2\bar{h}_{mm}(0)/[1+(4B^2/\pi)\bar{h}_{mm}(0)]\underset{(B>3)}{\rightarrow}\tfrac{1}{4}\pi. \tag{3.100}$$

The condition $B>3$ insures that $B^2\bar{h}_{mm}(B)$ differs from its asymptotic upper limit by less than 10%. In the present example it follows from (3.96) that a crystal length $l=0.4$ cm would be adequate, and essentially nothing would be gained by using a longer crystal.

Using $B^2\bar{h}_{mm}(B)=\pi/4$ (3.99) becomes

$$P_3=(\epsilon_1\epsilon_2\rho^2/\bar{K})(\pi/4)$$
$$=4.5\times10^4\,\epsilon_1\epsilon_2\text{ W}. \tag{3.101}$$

For $\epsilon_1=\epsilon_2=0.01$ we obtain $P_3=4.5$ W. We see that double refraction has proved very costly in terms of required threshold power. If we take the case $l=0.33$ cm ($B=2.7$), we see from Fig. 3 that $\bar{h}_{mm}(2.7)=0.1$. It follows now from (3.97) that the threshold without double refraction would have been a factor of ten lower.

4. OPTIMIZATION OF RESONANT SHG

4.1. Theory of Resonant SHG

It has been demonstrated by Ashkin *et al.*[10] (ABD) that SHG can be enhanced by providing a high-Q resonant optical cavity for the harmonic or the fundamental. The theory of this enhancement was given based on the near-field treatment of BADK and the concept of coupling coefficients as described by Kogelkik.[29] Here we generalize the theory of ABD to take into account diffraction and double refraction for arbitrary focusing parameter ξ. We shall be primarily interested in the case of resonance of the harmonic. Resonance of only the fundamental is already covered by the theory of Chap. 2 if P_1 is interpreted as the

[23] R. C. Miller, Appl. Phys. Letters **5**, 17 (1964).
[24] G. D. Boyd, W. L. Bond, and H. L. Carter, J. Appl. Phys. **38**, 1941 (1967).
[25] L. M. Osterink and R. Targ, Appl. Phys. Letters **10**, 115 (1967).
[26] A. Ashkin, G. D. Boyd, J. M. Dziedzic, R. G. Smith, A. A. Ballman, J. J. Levinstein, and K. Nassau, Appl. Phys. Letters **9**, 72 (1966).
[27] J. E. Geusic, H. M. Marcos, and L. G. Van Uitert, Appl. Phys. Letters **4**, 182 (1964).
[28] R. C. Miller, G. D. Boyd, and A. Savage, Appl. Phys. Letters **6**, 77 (1965).

enhanced one-way power in the resonator in the TEM_{00} (Gaussian) mode. The design of the resonator and the enhancement to be obtained are fully discussed by ABD. We find that the case of resonance of the harmonic is closely related to PG discussed in Chap. 3.

We consider a negative uniaxial crystal of length l and a fundamental (laser) beam $E_1(x, y, z)$ at ω_1 propagating normal to the crystal faces along the z direction as shown in Fig. 1.

$$E_1(x, y, z) = E_{10}[1/(1+i\tau)] \exp(ik_1 z) \times \exp[-(x^2+y^2)/w_0^2(1+i\tau)]$$
$$\tau = 2(z-f)/b. \tag{4.1}$$

The focus is at $x=y=0$, $z=f$, and the spot radius w_0, confocal parameter b, and diffraction angle δ_0 of this beam are related by (2.1). Later we place the focus at $f=l/2$. We imagine that the crystal is placed in an optical cavity formed by mirrors which are transparent to the fundamental beam but highly reflecting to the harmonic. Furthermore, let the cavity have the same confocal parameter b as the fundamental beam and the same focus f. The field in the TEM_{00} mode of the cavity may be written as in (3.6)

$$E_2'(x, y, z) = E_{20}'[1/(1+i\tau)] \exp(ik_2 z - i\varphi) \times \exp(-2\{[x-\rho(z-f)]^2+y^2\}/w_0^2(1+i\tau)). \tag{4.2}$$

We shall neglect absorption in writing the fields, but take it into account later in writing the energy balance for the cavity; this is the same method used to derive the PG threshold (3.30). We also neglect the difference between n_1, n_2 except in Δk.

Following ABD, let r_2 be the power-reflection coefficient of the right mirror as seen just inside the exit surface of the crystal, and let r_1 be the power-reflection coefficient of the left mirror as seen just inside the incident surface of the crystal. If the transmission of the right mirror is t_2 we have

$$r_2 + t_2 + a_2 = 1, \tag{4.3}$$

where a_2 includes the losses due to absorption in the mirror and scattering at the mirror and crystal surfaces. Define the cavity parameter

$$r = (r_1 r_2)^{1/2} \exp(-\alpha_2 l) < 1 \qquad 1-r \ll 1 \tag{4.4}$$

so that the average one-way power loss in the TEM_{00} cavity mode is

$$\delta P_2'/P_2' = \tfrac{1}{2}(1-r^2) \approx (1-r). \tag{4.5}$$

We see that $(1-r)$ is analogous to ϵ_1, ϵ_2 for the signal and idler in (3.29).

The power gain is given by (A2.57):

$$\Delta P_2' = -\mathrm{Im}\left(\tfrac{1}{2}\omega_2 \int \mathbf{E}_2'^* \cdot \mathcal{P}_2' dx\, dy\, dz\right). \tag{4.6}$$

We are using primes to distinguish the resonant case from the nonresonant case treated in Chap. 2. The fundamental is an ordinary wave ($\mathbf{E}_1$ in the y direction) and the harmonic an extraordinary wave ($\mathbf{E}_2$ in the x direction). The polarization is given by (A2.23)

$$\mathcal{P}_2'(x, y, z) = \mathbf{d}(-2\omega_1, \omega_1, \omega_1) \cdot \mathbf{E}_1(x, y, z)\mathbf{E}_1(x, y, z). \tag{4.7}$$

Thus, assuming $f=l/2$, we have

$$\mathbf{E}_2'^* \cdot \mathcal{P}_2' = E_{20}'\mathcal{P}_{20}' \exp(i\sigma\xi + i\varphi)[e^{i\sigma\tau}/(1+i\tau)^2(1-i\tau)] \cdot \exp(-2(x^2+y^2)/w_0^2(1+i\tau) - 2\{[x-\rho(z-f)]^2+y^2\}/w_0^2(1-i\tau)), \tag{4.8}$$

where $\sigma = \frac{1}{2}b\Delta k$, $\xi = l/b$ are defined as in (2.17), and (see Appendix 3)

$$\mathcal{P}_{20}' = dE_{10}^2 \tag{4.9}$$

defines an *effective nonlinear coefficient* d as in (2.18). The phase φ of the cavity should be chosen to maximize $\Delta P_2'$. The evaluation of (4.6) gives

$$\Delta P_2' = (\pi^2/4) b w_0^2 \omega_1 E_{20}' \mathcal{P}_{20}' \bar{H}(\sigma, \beta, \xi), \tag{4.10}$$

where $\beta = \rho/\delta_0$ as in (2.13), and $\bar{H}(\sigma, \beta, \xi)$ has been defined previously in (3.20). Note the identical forms of (4.10) and (3.19) showing the intimate connection between PG and resonant SHG. We have assumed the focus is located at the center of the crystal $f=l/2$.

We obtain the one-way SHG power P_2' in the cavity from (4.10) by equating the power gain $\Delta P_2'$ to the round-trip power loss $2\delta P_2'$. The relation between powers and Gaussian field amplitudes is

$$P_1 = (nc/16) w_0^2 E_{10}^2$$
$$P_2' = (nc/16) \tfrac{1}{2} w_0^2 E_{20}'^2, \tag{4.11}$$

and the steady-state condition is

$$\Delta P_2' = 2\delta P_2' = 2(1-r) P_2' = (1-r)(nc/16) w_0^2 E_{20}'^2. \tag{4.12}$$

Solving (4.10) and (4.12) for P_2' gives

$$(1-r)^2 P_2' = K P_1^2 l k_1 \cdot \bar{h}(\sigma, \beta, \xi), \tag{4.13}$$

where K has been defined in (2.20) (where we now set $n_1^2 n_2 = n^3$) and $\bar{h}(\sigma, \beta, \xi)$ is the function (3.32). This shows that optimization of PG is equivalent to optimization of resonant SHG. (4.13) is also valid for positive uniaxial crystals as shown in Appendix 1. Upon comparing (4.13) with (3.34) we see a strong analogy between $(1-r)^2 P_2'/P_1^2$ and $\epsilon_1\epsilon_2/P_3$. There will be an *optimum crystal length* in (4.13) just as for PG as discussed in Sec. 3.5.

4.2. Resonant Enhancement

We have written the one-way SHG power P_2' in order to distinguish it from the power P_2 given by (2.22) which would have been produced without the

cavity. The transmitted power P_t through the right mirror is

$$P_t=t_2P_2'=[t_2/(1-r)^2]\cdot KP_1^2lk_1\cdot\bar{h}_m(B,\xi), \quad (4.14)$$

where $B=\rho(lk_1)^{1/2}/2$ as in (1.4), and the function $\bar{h}_m(B,\xi)$ defined in (3.37) is $\bar{h}(\sigma,\beta,\xi)$ optimized with respect to σ. If the right mirror were taken away we should obtain the power P_2 given by (2.22). Thus, the *enhancement ratio* due to resonating the harmonic is

$$P_t/P_2=[t_2/(1-r)^2]\cdot\bar{h}_m(B,\xi)/h_m(B,\xi), \quad (4.15)$$

where $h_m(B,\xi)$ defined in (2.29) is $h(\sigma,\beta,\xi)$ optimized with respect to σ. The enhancement ratio is readily measured experimentally as shown by ABD, who report achieving an enhancement $P_t/P_2=9.0$ with $1-r=0.05$ and $t_2=0.03$. Let us define

$$\kappa(B,\xi)\equiv\bar{h}_m(B,\xi)/h_m(B,\xi)$$

$$\kappa(0,\xi)\equiv 1. \quad (4.16)$$

This function represents the effect of double refraction in reducing the coupling between the harmonic TEM_{00} mode and the nonlinear polarization (4.7). In Fig. 14 $\kappa(B,\xi)$ is plotted against ξ for several values of B.

From (3.56) and (2.43) the near-field limit is

$$\kappa(B,\xi)\underset{(\xi<0.4)}{\longrightarrow}\bar{G}(t)/G(t)$$

$$t=2\sqrt{2}B\xi^{1/2}. \quad (4.17)$$

It follows from (2.40) and (3.55) that $\kappa(B,\xi)$ has the near-field asymptotic form

$$\kappa(B,\xi)\underset{(B^2\xi<0.5)}{\longrightarrow}1-0.22B^4\xi^2+\cdots. \quad (4.18)$$

From (2.55) and (3.62) the far-field limit is

$$\kappa(B,\xi)\rightarrow\bar{F}_m(B\xi^{-1/2})/F_m(B\xi^{-1/2}). \quad (4.19)$$

It is difficult to deduce the asymptotic form of (4.19) as $\xi\rightarrow\infty$, but the general behavior is shown in Fig. 14. Even though

$$\kappa(B,\xi)<1, \qquad (B\neq 0), \quad (4.20)$$

(4.15) shows that resonance of the harmonic still leads to a significant enhancement in the SHG power if $t_2\sim 1-r\ll 1$.

4.3. Coupling Coefficients

Our result (4.15) agrees in form with ABD (27) if we interpret $\kappa(B,\xi)$ as the power *coupling coefficient*. Our derivation based on (4.6), with E_2' the field of the TEM_{00} mode of the cavity, automatically includes the correct coupling to the resonant mode. It is not necessary then to introduce coupling coefficients separately. Equivalent results can be obtained, however, by the method of ABD. The basic equation in this method is

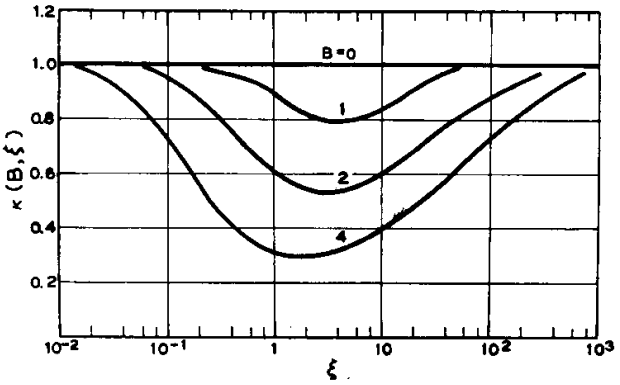

FIG. 14. The power coupling coefficient $\kappa(B,\xi)$ (4.16) as a function of ξ for several values of B.

the self-consistency relation for the cavity field ABD (21), which at cavity resonance can be written

$$E_2'=rE_2'+c_{a0}E_2. \quad (4.21)$$

Here E_2' stands for the amplitude of the one-way TEM_{00} electric field and E_2 the amplitude of the field generated by the nonlinear polarization. The *coupling coefficient*[29] to the TEM_{00} mode is defined by

$$c_{a0}=(N')^{-1/2}(N)^{-1/2}\iint E_2'(x,y,l)^*E_2(x,y,l)\,dxdy \quad (4.22)$$

with

$$N=\iint|E_2(x,y,l)|^2dxdy$$

$$N'=\iint|E_2'(x,y,l)|^2dxdy. \quad (4.23)$$

Higher-order coupling coefficients to higher-order transverse modes of the resonator are defined in a similar way with E_2' replaced by the appropriate eigenfunction. ABD consider explicitly the coupling to TEM_{10} in the near-field approximation. It is clear that the coefficients c_{ai} $(i=0, 1, 2, \cdots)$ are the coefficients in an expansion of the source field $E_2(x,y,z)$ in the orthogonal eigenfunctions of the resonator. In (4.21) E_2 is identified with the field (2.9) at $z=l$ that would have been produced without a resonator; this field corresponds to the power P_2 in (2.22). It then follows immediately from (4.21) that the enhancement ratio is [ABD (27)]

$$P_t/P_2=[t_2/(1-r)^2]\kappa, \quad (4.24)$$

where

$$\kappa=|c_{a0}|^2 \quad (4.25)$$

is the power coupling coefficient [ABD (25)].

The evaluation of (4.22), (4.23), and (4.25) using (2.9) for $E_2(x,y,l)$ and (4.2) for $E_2'(x,y,l)$ leads to

[29] H. W. Kogelnik, *Proceedings of the Symposium on Quantum Optics* (Polytechnic Press, Brooklyn, New York, 1964), Vol. 14, p. 333.

the results (assuming $\alpha_1=\alpha_2=0, f=l/2$)

$$N=(8\pi/nc)Kk_1lP_1^2h(\sigma,\beta,0,\xi,0)$$

$$N'=(\pi w_0^2/4)\mid E_{20}'\mid^2$$

$$\iint E_2'(x,y,l)^*E_2(x,y,l)\,dxdy$$

$$=d(16\pi^3/c^2n^2)b\omega_1P_1E_{20}'^*\bar{H}(\bar{\sigma},\beta,\xi), \quad (4.26)$$

where $h(\sigma,\beta,0,\xi,0)$ is defined in (2.23) and $\bar{H}(\bar{\sigma},\beta,\xi)$ in (3.20). The phase φ in (4.2) has been chosen so as to make the integral real. We have written two mismatch parameters σ and $\bar{\sigma}$ because we wish to choose σ to maximize $h(\sigma,\beta,0,\xi,0)$ and $\bar{\sigma}$ to maximize $\bar{H}(\bar{\sigma},\beta,\xi)$. This corresponds to the separate optimizations of crystal orientation the experimenter would normally make (with and without the resonator mirror) in determining P_t/P_2. It then follows from (4.22) and (4.26) that

$$\kappa=\mid c_{a0}\mid^2=\bar{h}_m(B,\xi)/h_m(B,\xi) \quad (4.27)$$

in agreement with (4.16).

In the near-field approximation (4.17) we can write (4.25) in the form

$$c_{a0}(t)=\{2/t[G(t)]^{1/2}\}(\pi/2)^{1/2}\,\mathrm{erf}(t/2\sqrt{2}). \quad (4.28)$$

We point out that this is not in agreement with the result of ABD (41), who give

$$c_{a0}(t)\,(\mathrm{ABD})=\{1/t[G(t)]^{1/2}\}(\pi/2)^{1/2}\,\mathrm{erf}(t/\sqrt{2}). \quad (4.29)$$

The discrepancy is due to a difference in beam geometry between ABD and the present treatment. The resonator mode assumed in ABD (35) is a Gaussian extraordinary beam centered on the ρ line through the point $z=0$. In the present treatment this would correspond to placing the common focus at $f=0$ instead of at $f=l/2$. The generalization of (4.13) to an arbitrary value of $\mu=(l-2f)/l$ simply replaces $\bar{h}(\sigma,\beta,\xi)$ with the function

$$\bar{h}(\sigma,\beta,0,\xi,\mu)$$

$$=(\pi^2/\xi)\left|(2\pi)^{-1}\int_{-\xi(1-\mu)}^{\xi(1+\mu)}\frac{d\tau}{1+i\tau}\exp(i\sigma\tau-\beta^2\tau^2)\right|^2 \quad (4.30)$$

analogous to $h(\sigma,\beta,0,\xi,\mu)$ defined in (2.23). In the near-field limit after optimization of σ, (4.30) becomes

$$\bar{h}_m(B,\xi,\mu)\to(\pi/16B^2)\{\mathrm{erf}[(1+\mu)B\xi^{1/2}]$$
$$+\mathrm{erf}[(1-\mu)B\xi^{1/2}]\}^2, \quad (4.31)$$

which agrees with (3.51) when $\mu=0$:

$$\bar{h}_m(B,\xi,0)=\bar{h}_m(B,\xi). \quad (4.32)$$

Putting $\mu=\pm1$, corresponding to the focus on one of the crystal surfaces, gives

$$\bar{h}_m(B,\xi,\pm1)\to(\pi/16B^2)[\mathrm{erf}(2B\xi^{1/2})]^2. \quad (4.33)$$

According to (2.38) the near-field limit for nonresonant SHG is independent of μ

$$h_m(B,\xi,\mu)\to\xi G(t). \quad (4.34)$$

Thus, the power coupling coefficient for arbitrary focal position μ

$$\kappa(B,\xi,\mu)\equiv\bar{h}_m(B,\xi,\mu)/h_m(B,\xi,\mu) \quad (4.35)$$

has the near-field limit

$$\kappa(B,\xi,\pm1)\to[\pi/2t^2G(t)][\mathrm{erf}(t/\sqrt{2})]^2 \quad (4.36)$$

when ($\mu=\pm1$) the focus is at one of the surfaces of the crystal. We see that (4.36) agrees with the coupling coefficient (4.29) of ABD.

Experimentally, ABD found an enhancement of $P_t/P_2=9.0$ under conditions such that

$$t(ABD)=(2\pi)^{1/2}(l/l_a)=2.18. \quad (4.37)$$

It follows from (2.40) and (4.36) that

$$G(t)=0.73$$

$$\kappa(B,\xi,\pm1)=0.43, \quad (4.38)$$

which is the calculated value quoted by ABD. On the other hand, with the focus at the center of the crystal, 4.(17) and (3.55) give

$$\bar{G}(t)=0.69$$

$$\kappa(B,\xi)=0.95. \quad (4.39)$$

Using $t_2=0.03$, $(1-r)=0.05$, $P_t/P_2=9.0$, (4.24) gives

$$\kappa(\mathrm{ABD})=0.75 \quad (4.40)$$

for the measured coupling coefficient. This is an upper limit because the resonator beam may have contained a small but unknown amount of the TEM_{10} mode. Nevertheless, it is very difficult to account for the difference between (4.40) and (4.38) on this basis. From the observed full width (135 MHz) of the harmonic resonance and the observed frequency splitting (200 MHz) between the TEM_{10} and TEM_{00} modes of the resonator, combined with the calculated ratio (0.45) of the respective power coupling coefficients as given by ABD (41, 47), we estimate that the TEM_{10} component of P_t could amount to no more than 5%. It is quite reasonable to believe, however, that the point of intersection of the fundamental and resonator beams (i.e., the focus in the terminology of the present treatment) occurred inside the crystal rather that at the surface. We would then expect κ(ABD) to lie somewhere between 0.43 and 0.95 in agreement with observation.

5. MIXING, UP-CONVERSION, AND PARAMETRIC GAIN

Mixing is the process in which two beams from external sources are introduced into a crystal and produce a third beam. In this section, we consider the

optimization of mixing just as we have considered the optimization of SHG in Sec. 2, PG in Sec. 3, and resonant SHG in Sec. 4. We shall find that mixing can be treated in terms of the functions previously defined in (2.23) and (3.32). The problem of the optimization of mixing has therefore already been solved by the computations presented in Figs. 2 and 12. We shall assume (until Sec. 5.5) that both source beams introduced from external sources are Gaussian beams having the same axis, focus, and confocal parameter b_0. If the generated beam is resonated by reflecting mirrors it too will be assumed to be a Gaussian beam with the same axis, focus, and confocal parameter as the source beams. As explained following (3.11) the condition of equal confocal parameters for all the beams is believed to be an optimum condition, although a completely general proof can not be given here. The same may be said about the assumption of a common axis and common focus. In addition, we limit ourselves as in Sec. 3 to the case in which the two lower frequency fields (ω_1, ω_2) have the same polarization direction (ordinary waves in negative uniaxial crystals) and the highest frequency field ($\omega_3=\omega_1+\omega_2$) has the other polarization (extraordinary wave in negative uniaxial crystals). The reasons for this are discussed following (3.10).

The interaction responsible for mixing is the second order polarization introduced in (1.1) and fully discussed in Appendix 2. The general definition of this nonlinear interaction is (A2.10). The interaction of three monochromatic fields $\mathbf{E}_1(\mathbf{r})$, $\mathbf{E}_2(\mathbf{r})$, and $\mathbf{E}_3(\mathbf{r})$ is described by (A2.15) and (A2.16). As shown in (A2.18), SHG may be considered as a special case of mixing in which $\mathbf{E}_1(\mathbf{r})$ mixes with itself to produce $\mathbf{E}_2(\mathbf{r})$ at $\omega_2=2\omega_1$. Therefore, *sum-mixing* in which $\mathbf{E}_1(\mathbf{r})$ and $\mathbf{E}_2(\mathbf{r})$ are the source beams which produce $\mathbf{E}_3(\mathbf{r})$ in the crystal is quite analogous to SHG. Let us suppose that $\mathbf{E}_3(\mathbf{r})$ is one of the source beams, and call the other source beam $\mathbf{E}_1(\mathbf{r})$. These beams mix to produce $\mathbf{E}_2(\mathbf{r})$ at $\omega_2=\omega_3-\omega_1$ which we may call *difference-mixing*. The process may also be considered parametric amplification[6] with $\mathbf{E}_3(\mathbf{r})$, $\mathbf{E}_1(\mathbf{r})$, and $\mathbf{E}_2(\mathbf{r})$ representing the conventional pump, signal, and idler, respectively. As $\mathbf{E}_2(\mathbf{r})$ is generated in the crystal there is an amplification of the signal $\mathbf{E}_1(\mathbf{r})$ and an attenuation of the pump $\mathbf{E}_3(\mathbf{r})$. We assume that these are very small effects on the source beams, which may be assumed to be prescribed Gaussian beams for the purpose of computing the generated beam $\mathbf{E}_2(\mathbf{r})$. Under this assumption it follows that $P_2 \ll P_1$ where P_1 is the incoming signal power and P_2 is the mixing power. Similarly, in sum-mixing with P_1 and P_2 the incoming powers we must have $P_3 \ll P_1$, where P_3 is now the mixing power. Even though the mixing power is less than the signal power, it may still be true that P_2 or P_3 can be detected with higher signal-to-noise ratio than P_1 and with faster detectors. We shall use the term *up-conversion* to mean a mixing process which generates a higher frequency than the signal frequency ω_1 whether by sum-mixing or difference-mixing.

5.1. Sum-Mixing

The theory of Sec. 2.1 can readily be generalized to the sum-mixing of two Gaussian beams in the ordinary wave

$$E_1(x', y', z') = E_{10}[1/(1+i\tau')] \exp(ik_1 z') \times \exp[-(x'^2+y'^2)/w_{10}^2(1+i\tau')] \exp(-\tfrac{1}{2}\alpha_1 z')$$
$$E_2(x', y', z') = E_{20}[1/(1+i\tau')] \exp(ik_2 z') \times \exp[-(x'^2+y'^2)/w_{20}^2(1+i\tau')] \exp(-\tfrac{1}{2}\alpha_2 z') \quad (5.1)$$

to produce the mixing field

$$E_3(x, y, z) = A_3(x, y, z) \exp(ik_3 z) \quad (5.2)$$

in the extraordinary wave in a negative uniaxial crystal. We see that (5.1) is analogous to (2.2) and (5.2) is analogous to (2.4). The polarization at ω_3, according to (3.11) and the above, is

$$\mathcal{P}_3(x', y', z') = \mathcal{P}_{30}[1/(1+i\tau')^2] \times \exp[i(k_1+k_2)z' - \tfrac{1}{2}(\alpha_1+\alpha_2)z'] \times \exp[-(x'^2+y'^2)/w_{30}^2(1+i\tau')] B(z'), \quad (5.3)$$

where

$$\mathcal{P}_{30} = \chi E_{10} E_{20} \quad (5.4)$$

and χ is the same *effective nonlinear coefficient* as previously introduced in (3.18). As shown in (A3.6), the same χ applies for three interacting fields regardless of which pair of fields is mixed to obtain the other (generated) field. If dispersion in χ is sufficiently small we have

$$\chi = 2d, \quad (5.5)$$

where d is the effective nonlinear coefficient for SHG introduced in (2.18).

Since (5.3) is in the form (2.3) there is no difficulty in carrying out the heuristic approach of Sec. 2.1. In order to use our previous treatment we define a fictitious beam analogous to the fundamental beam in SHG; let the spot size and diffraction angle of this beam be defined by

$$w_0^2 = 2w_{30}^2$$
$$\delta_0 = 2w_0/b_0. \quad (5.6)$$

We replace (1.4), (2.10), and (2.21) by the definitions

$$\Delta k = k_1+k_2-k_3$$
$$\alpha = \tfrac{1}{2}(\alpha_1+\alpha_2-\alpha_3)$$
$$\alpha' = \tfrac{1}{2}(\alpha_1+\alpha_2+\alpha_3). \quad (5.7)$$

Then we obtain for the intensity a result equivalent to (2.19)

$$S(s, s') = 4\pi \bar{K}(P_1 P_2 k_1 k_2/\tau^2) \exp(-\alpha' l + \mu\alpha l) \times \exp[-4(s^2+s'^2)] \cdot |H(\sigma', \kappa, \xi, \mu)|^2, \quad (5.8)$$

where P_1, P_2 are the powers of the source beams and $\tilde{K}$ is given by (3.27). As observed in (3.28), dispersion will ordinarily be small enough in χ that we can write $\tilde{K}=4K$, where K defined in (2.20) is computed for a fundamental frequency $\omega_0=\frac{1}{2}(\omega_1+\omega_2)$. The arguments σ', κ, ξ, μ are still defined by (2.17). The double refraction parameter β is defined in (2.13), which is also equivalent to the definition (3.21). Note, however, that (3.16) does not hold with our present definition of w_0 in (5.6).

The mixing power is obtained from (5.8) by integrating over s, s' as in (2.22) to obtain

$$P_3=\tilde{K}P_1P_2lk_0e^{-\alpha' l}\cdot[(1-\zeta^2)(1-\gamma^2)/(1+\gamma\zeta)]\cdot h(\sigma,\beta,\kappa,\xi,\mu), \quad (5.9)$$

where $k_0=n_0\omega_0/c$ is a parameter previously defined in (3.33), h is the same function as appears in (2.22), and the parameters ζ, γ, n_0, and ω_0 are those defined in (3.8). We see that sum-mixing is formally identical to SHG when the corresponding parameters are appropriately defined. Therefore, Figs. 2–11 and the entire discussion of Sec. 2 apply equally well to sum-mixing. We have treated the case of a negative uniaxial crystal, but it is shown in Appendix 1 that (5.9) applies also to positive uniaxial crystals in which two extraordinary source beams are mixed to generate an ordinary wave. In this case one should use for ρ the value appropriate for the larger of ω_1, ω_2.

5.2. Difference-Mixing

Consider difference-mixing in a negative uniaxial crystal. The source beams are the ordinary field $E_1(x', y', z')$ given in (5.1) and the extraordinary field (see Appendix 1)

$$E_3(x', y', z')=E_{30}[1/(1+i\tau')]\exp(ik_3z')\times\exp\left(-\{[x'-\rho(z'-f)]^2+y'^2\}/w_{30}^2(1+i\tau')\right)\times\exp(-\tfrac{1}{2}\alpha_3z'). \quad (5.10)$$

The polarization at $\omega_2=\omega_3-\omega_1$ is

$$\mathcal{P}_2(x', y', z')=\mathcal{P}_{20}[1/(1-i\tau')(1+i\tau')]\times\exp[i(k_3-k_1)z'-\tfrac{1}{2}(\alpha_1+\alpha_3)z']\cdot\exp\left(-(x'^2+y'^2)/w_{10}^2(1-i\tau')-\{[x'-\rho(z'-f)]^2+y'^2\}/w_{30}^2(1+i\tau')\right)B(z') \quad (5.11)$$

with

$$\mathcal{P}_{20}=\chi E_{10}^*E_{30}. \quad (5.12)$$

Since $\mathcal{P}_2(x', y', z')$ is not in the form (2.3) we can not carry out the heuristic method; more specifically, we can not obtain an equation like (2.6) in which all the x', y' dependence is contained in a factor which we recognize as the amplitude of a Gaussian beam. A formal integral for the mixing field $E_2(x, y, z)$ can be obtained from the Green's function formula KAB (3.21) using (5.11) as the polarization. This leads to a rather complicated result which will not be given here.

In many applications of difference-mixing, such as up-conversion from the infrared to the visible, we can assume [see (3.7)]:

$$\omega_1\ll\omega_3, \qquad w_{10}^2\gg w_{30}^2. \quad (5.13)$$
$$\pi w_{10}^2/\rho^2\gg b_0^2$$

Under this assumption we may neglect the term containing w_{10}^2 in the exponent in (5.11). The heuristic method can then be carried out as in (A1.18), and we obtain a result very similar to (A1.20)

$$E_2(x, y, z)=[2\pi i\omega_2\mathcal{P}_{20}/cn_2(1+i\tau)]\exp(-\tfrac{1}{2}\alpha_2 l+ik_2z)\cdot\int_0^l dz'\,\frac{\exp(-\alpha''z'-i\Delta kz')}{1-i\tau'}\times\exp\left[-\frac{(x-\rho(z'-f))^2+y^2}{w_{30}^2(1+i\tau)}\right], \quad (5.14)$$

where

$$\alpha''=\tfrac{1}{2}(\alpha_1+\alpha_3-\alpha_2). \quad (5.15)$$

The intensity can be written

$$S(s, s')=4\pi\tilde{K}(P_1P_3k_1k_3/\tau^2)\exp(-\alpha' l+\mu\alpha'' l)\times\exp[-4(s^2+s'^2)]\cdot|H(\sigma-4\beta s,\kappa'',\xi,\mu)|^2, \quad (5.16)$$

where $\kappa''=\frac{1}{2}\alpha''b$. The mixing power becomes

$$P_2=\tilde{K}P_1P_2 2lk_1e^{-\alpha' l}\cdot h(\sigma,\beta,\kappa'',\xi,\mu), \quad (5.17)$$

where α is to be replaced by α'' in the definition (2.23) of h.

We see that difference-mixing is formally similar to SHG within the approximation (5.13). Our results apply to positive uniaxial crystals with E_1, E_2 extraordinary waves and E_3 an ordinary wave. It is obvious that ρ in this case refers to ω_2. Note that (5.13) requires $l<\xi l_a$, where l_a defined in (2.96) refers to ω_1. For $l>\xi l_a$, P_2 does not increase with l.

5.3. Resonant Sum-Mixing

The theory of resonant SHG of Sec. 4, in which the harmonic is resonated with the fundamental making only one pass, can readily be generalized to resonant sum-mixing. We suppose that instead of a single fundamental beam (4.1) we introduce two source fields E_1 and E_2 defined in (5.1). These are Gaussian ordinary beams as required for sum-mixing in a negative uniaxial crystal. The generated beam in a Gaussian mode of the optical cavity will be completely analogous to (4.2); the one-way traveling electric field can be written as in (5.10). We shall write the field and power in the resonant case E_3' and P_3' to distinguish them from the nonresonant case. Following the method of Sec. 4.1 we obtain P_3' by equating the

cavity loss to the mixing power; thus, from (A2.56)

$$\Delta P_3' = -\mathrm{Im}\left(\tfrac{1}{2}\omega_3 \int \mathbf{E}_3'^* \cdot \mathcal{P}_3 dx\, dy\, dz\right) = 2(1-r)P_3', \tag{5.18}$$

where $\mathcal{P}_3(x, y, z)$ is given in (5.3) and the cavity parameter r is defined in (4.4) (with α_3 replacing α_2). We shall neglect absorption in E_3' and $\mathcal{P}_3$. The integrand in (5.18) has the same form as (4.8) so we obtain a result very similar to (4.10)

$$\Delta P_3' = (\pi^2/4) b_0 w_0^2 \omega_0 E_{30}' \mathcal{P}_{30} \bar{H}(\sigma, \beta, \xi), \tag{5.19}$$

where w_0 is defined in (5.6), $\omega_0 = \frac{1}{2}(\omega_1+\omega_2)$, $\bar{H}$ is defined in (3.20), β is defined in (2.13), and σ, ξ are defined in (2.17).

The fields E_1, E_2, E_3 are the same fields considered in Sec. 3, where E_3 was the pump and E_1, E_2 the signal and idler. In the theory of the PG threshold in Sec. 3.2 we have computed the mixing powers ΔP_1, ΔP_2. It follows from the energy-conservation theorem (A2.59) that we can obtain $\Delta P_3'$ by adding ΔP_1 and ΔP_2, all quantities being considered positive. Thus, from (3.26) we obtain the alternative form

$$\Delta P_3' = 2(\bar{K} P_1 P_2 P_3)^{1/2} [2l^2/(w_{10}^2+w_{20}^2)]^{1/2} (\pi/\xi) \bar{H}. \tag{5.20}$$

The equivalence of (5.19) and (5.20) follows easily from the relations (3.25), (3.27), and (3.11).

The enhanced mixing power P_3' is now obtained from (5.18) and (5.20) in a form very similar to (4.13)

$$(1-r)^2 P_3' = \bar{K} P_1 P_2 l k_0 \cdot [(1-\gamma^2)(1-\zeta^2)/(1+\gamma\zeta)] \cdot \bar{h}(\sigma, \beta, \xi), \tag{5.21}$$

where k_0 is defined in (3.33), γ and ζ in (3.8), and $\bar{h}$ is the function (3.32). The optimization of resonant sum-mixing is entirely equivalent to the optimization of resonant SHG. The extension of the theory to positive uniaxial crystals is straightforward as shown in Appendix 1.

5.4. Resonant Difference-Mixing

Consider resonant difference-mixing in which the source beams are E_1 and E_3 given by (5.1) and (5.10), respectively. These are Gaussian ordinary and extraordinary beams as required for difference-mixing in a negative uniaxial crystal. The generated beam has the one-way traveling field E_2' of the form (5.2). The enhanced mixing power P_2' will be obtained by equating (4.6) to the cavity loss. The evaluation of (4.6) has already been carried out in (3.26), which gives

$$\Delta P_2' = (1+\gamma)(\bar{K} P_1 P_2' P_3)^{1/2} [2l^2/(w_{10}^2+w_{20}^2)]^{1/2} (\pi/\xi) \bar{H} = 2(1-r) P_2'. \tag{5.22}$$

Solving for P_2' gives a result similar to (4.13)

$$(1-r)^2 P_2' = \bar{K} P_1 P_3 l k_0 \cdot [(1+\gamma)^2 (1-\gamma^2)(1-\zeta^2)/4(1+\gamma\zeta)] \cdot \bar{h}(\sigma, \beta, \xi). \tag{5.23}$$

Thus, resonant difference-mixing is equivalent to resonant SHG with regard to optimization.

5.5. Generalization to Unequal Confocal Parameters

We have argued in Sec. 3.1 that in PG the signal and idler modes should have the same confocal parameter in order that they may be modes of the same optical resonator. It then follows from the optimum condition (3.11) found by BA from their near-field analysis that all three confocal parameters should be equal as assumed in (3.12). BA have argued that this should remain an optimum condition for arbitrary focusing. Up to now we have assumed (3.12) in our discussion of mixing. In the case of mixing, however, there is no compelling practical reason for desiring two of the confocal parameters to be equal if only one beam is to be resonated. It may, in fact, be quite inconvenient to arrange for all the confocal parameters to be equal. In up-conversion when (5.13) holds, it is clear that the beams E_2 and E_3 spatially overlap only a small part of the beam E_1. This might suggest that greater mixing power could be obtained by making the spot sizes more nearly equal, which would raise the intensity of the E_1 beam in the region of interaction. For these reasons, we now discuss the more general case of mixing with arbitrary confocal parameters b_1, b_2, b_3.

We consider specifically the case of resonant difference-mixing *without double refraction*. The relations between spot sizes and confocal parameters are given in (3.7) and the fields are all of the form (3.5). The mixing power is

$$\Delta P_2' = -\mathrm{Im}\left\{\tfrac{1}{2}\omega_2 E_{20} \mathcal{P}_{20} \int \frac{\exp(-i\Delta k z)\, dx dy dz}{(1-i\tau_1)(1-i\tau_2)(1+i\tau_3)} \cdot \exp\left[-\frac{x^2+y^2}{w_{10}^2(1-i\tau_1)} - \frac{x^2+y^2}{w_{20}^2(1-i\tau_2)} - \frac{x^2+y^2}{w_{30}^2(1+i\tau_3)}\right]\right\}, \tag{5.24}$$

with $\mathcal{P}_{20}$ defined in (5.12) and Δk in (5.7). The integrals over x, y can be carried out to give

$$\Delta P_2' = (\omega_2/2a) b \pi^2 E_{20} \mathcal{P}_{20} H(\sigma, \xi), \tag{5.25}$$

where $H(\sigma, \xi)$ is the function (2.70) and

$$\sigma = \tfrac{1}{2} b \Delta k, \qquad \xi = l/b$$
$$b = (k_1 b_2 b_3 + k_2 b_1 b_3 + k_3 b_1 b_2)/(k_1 b_1 + k_2 b_2 + k_3 b_3) \tag{5.26}$$
$$a = (k_1/b_1) + (k_2/b_2) + (k_3/b_3).$$

Here b is the *effective confocal parameter*.

It is convenient to express b_1, b_2, b_3 in terms of b as follows:

$$b_j = \beta_j b, \qquad j = 1, 2, 3. \tag{5.27}$$

From these definitions the ratios β_1, β_2, β_3 are not independent but satisfy

$$k_1\beta_2\beta_3 + k_2\beta_1\beta_3 + k_3\beta_1\beta_2 = k_1\beta_1 + k_2\beta_2 + k_3\beta_3. \tag{5.28}$$

Eliminating $k_2=k_3-k_1$ and solving for β_2 gives

$$\beta_2=[(\beta_3+1)m-\beta_3(\beta_1-1)]/[(\beta_3+1)m+\beta_1-1]$$

$$m=k_1/k_3=(1-\gamma)(1-\zeta)/2(1+\gamma\zeta). \tag{5.29}$$

The condition $0<\beta_2<\infty$ gives the allowable range for β_1:

$$\beta_1>0, \qquad 1-(\beta_3+1)m<\beta_1<1+[(\beta_3+1)/\beta_3]m. \tag{5.30}$$

There are three kinds of solutions permitted by (5.29)

$$\beta_1=\beta_2=1$$

$$\beta_1>1, \qquad \beta_2<1$$

$$\beta_1<1, \qquad \beta_2>1. \tag{5.31}$$

Within the range (5.30) β_1 and β_3 are independent.

It follows from equating (5.25) to the cavity loss $2(1-r)P_2'$ that the enhanced mixing power is given by

$$(1-r)^2P_2'=\bar{K}P_1P_3lk_0$$

$$\times[(1+\gamma)^2(1-\gamma^2)(1-\zeta^2)/4(1+\gamma\zeta)]F(\beta_1,\beta_3)\cdot h(\sigma,\xi) \tag{5.32}$$

where $h(\sigma, \xi)$ is defined in (2.69). For a given effective confocal parameter b, the beams are described by the parameters β_1, β_3 which enter through the factor

$$F(\beta_1,\beta_3)\equiv 4\beta_1\beta_2\beta_3(\beta_3+1)^2/(\beta_1+\beta_3)^2(\beta_2+\beta_3)^2. \tag{5.33}$$

Substituting for β_2 from (5.29) gives

$$F(\beta_1,\beta_3)\equiv[4\beta_1\beta_3/(\beta_1+\beta_3)^2]$$

$$\times\{1-[(\beta_1-1)(\beta_3-1)/(\beta_3+1)m]$$

$$-(\beta_3/m^2)[(\beta_1-1)^2/(\beta_3+1)^2]\}. \tag{5.34}$$

Our previous assumption (3.12) corresponds to the special case

$$\beta_1=\beta_2=\beta_3=1$$

$$F(1,1)=1. \tag{5.35}$$

For this case (5.32) agrees with our previous result (5.23) with $\beta=0$ (see (3.41)). The function $h(\sigma, \xi)$ has been discussed in Sec. 2.4, and optimized with respect to σ it appears as a function of ξ in the $B=0$ curves of Fig. 2 and Fig. 12. Thus, we can optimize resonant difference-mixing with respect to the effective confocal parameter b even in the general case of unequal confocal parameters for the beams. There remains the separate problem of optimizing the beam parameters β_1, β_3 by maximizing $F(\beta_1, \beta_3)$.

We can now quickly generalize the treatment of resonant sum-mixing in Sec. 5.3. With arbitrary confocal parameters b_1, b_2, b_3 (5.18) becomes

$$\Delta P_3'=-\mathrm{Im}\left(\tfrac{1}{2}\omega_3E_{30}\wp_{30}\int\frac{e^{i\Delta kz}dxdydz}{(1+i\tau_1)(1+i\tau_2)(1-i\tau_3)}\right.$$

$$\cdot\exp\left\{-\frac{x^2+y^2}{w_{10}^2(1+i\tau_1)}-\frac{x^2+y^2}{w_{20}^2(1+i\tau_2)}\right.$$

$$\left.\left.-\frac{[x-\rho(z-f)]^2+y^2}{w_{30}^2(1-i\tau_3)}\right\}\right). \tag{5.36}$$

With $\rho=0$ the integral is just the complex conjugate of that appearing in (5.24). It follows from (5.25) and (5.18) that

$$\Delta P_3'=(\omega_3/2a)b\pi^2E_{30}\wp_{30}H(\sigma,\xi)=2(1-r)P_3'. \tag{5.37}$$

Solving for P_3' gives

$$(1-r)^2P_3'=\bar{K}P_1P_2lk_0\cdot[(1-\gamma^2)(1-\zeta^2)/(1+\gamma\zeta)]$$

$$\cdot F(\beta_1,\beta_3)\cdot h(\sigma,\xi). \tag{5.38}$$

This reduces to (5.21) when $\beta=0$ and (5.35) holds.

We have now shown for the resonant case without double refraction that unequal confocal parameters leads to an extra factor $F(\beta_1, \beta_3)$ in the mixing power. We have investigated this function carefully and we believe that (5.35) (equal confocal parameters) is the optimum condition which maximizes $F(\beta_1, \beta_3)$. It is tedious but elementary to show that $F(\beta_1, \beta_3)$ decreases for any infinitessimal variation $\delta\beta_1$, $\delta\beta_3$ from the point $\beta_1=\beta_3=1$. Therefore, set $\beta_3=1$ and consider

$$F(\beta_1,1)=[4\beta_1/(1+\beta_1)^2][1-(\beta_1-1)^2/4m^2]. \tag{5.39}$$

This function vanishes at $\beta_1=1\pm 2m$, which are the extreme points in the range (5.30), and within the range of interest has only one maximum at $\beta_1=1$. Next, set $\beta_1=1$; it follows from (5.31) that this requires $\beta_1=\beta_2=1$. This is the case considered by BA in a near-field approximation. Setting $\beta_1=1$ in (5.34) gives

$$F(1,\beta_3)=4\beta_3/(1+\beta_3)^2, \tag{5.40}$$

which has only one maximum $\beta_3=1$. This confirms the assertion of BA that $\beta_3=1$ remains the optimum condition (when $\beta_1=\beta_2=1$) even when diffraction is taken into account. It may also be noted that $F(\beta_1, \beta_3)$ vanishes when β_1 equals one of the limits in (5.30). We believe that between these limits there is only the one maximum (5.35), although a rigorous proof of this has not been obtained.

The analysis of this section can readily be applied to the PG threshold when $\beta=0$. If E_1 is resonated the enhanced mixing power is analogous to (5.32) except that $(1+\gamma)^2$ must be replaced by $(1-\gamma)^2$

$$\epsilon_1^2P_1'=\bar{K}P_2P_3lk_0\cdot[(1-\gamma)^2(1-\gamma^2)(1-\zeta^2)/4(1+\gamma\zeta)]$$

$$\cdot F(\beta_1,\beta_3)\cdot h(\sigma,\xi). \tag{5.41}$$

We shall let ϵ_1 and $1-r=\epsilon_2$ be the one-way fractional losses as in the notation of Sec. 3. Eliminating P_1' and P_2' from (5.32), (5.41) gives the threshold condition in the form (3.34)

$$\epsilon_1\epsilon_2/P_3=[(1-\gamma^2)^2(1-\zeta^2)/(1+\gamma\zeta)]\cdot\tfrac{1}{4}\bar{K}lk_0\cdot F(\beta_1,\beta_3)\cdot h(\sigma,\xi). \quad (5.42)$$

Thus, the condition (5.35) optimizes the reciprocal PG threshold.

5.6. Application to Up-Conversion from 10.6 to 0.6729 μ using Cinnabar

It has been suggested by ABDP[3] that up-conversion may be a practical means of infrared detection. Takatsuji[30] has discussed the problem and Midwinter and Warner[31] have demonstrated a pulsed up-converter from 1.7 μ to the green using the ruby laser and $LiNbO_3$. Up-conversion has been observed using the 6328 Å He–Ne laser by Boyd *et al.*[32] and by Miller and Nordland.[33] A basic discussion of the noise characteristics and detectable powers for up-conversion will be published in a separate paper.[34] Here we shall be content to discuss the quantum efficiency for up-conversion.

Up-conversion is inherently frequency selective due to the practical necessity of phase matching. Consequently we visualize a communication system at some specified infrared wavelength. We consider only continuous operation, although the discussion could readily be applied to triggered or phase-sensitive pulsed systems. Because of the 10.6 μ CO_2 laser,[18] there is considerable interest in the detection of signals at 10.6 μ. Several crystals are now known which could be used for the up-conversion of signals at 10.6 μ to the visible or near ir photomultiplier region. It is known that phase matching can be achieved in cinnabar[35] (HgS), selenium[36] (Se), proustite[37] (Ag_3AsS_3), and pyrargyrite[37] (Ag_3SbS_3), using the 1.06 μ YAG:Nd laser.[27] The sum-frequency would be 0.964 μ, which is within the usable range of infrared photomultipliers. Cinnabar and proustite can also be used with the 0.6328 μ He–Ne laser to produce the difference-frequency at 0.6729 μ, and proustite could be used to produce the sum-frequency at 0.5972 μ. All these crystals have large birefringence. Cinnabar and selenium have the disadvantage, as shown in Table I for symmetry class $32(D_3)$, that the effective nonlinear coefficient vanishes for phase matching normal to the optic axis ($\theta_m=\pi/2$). At this writing we do not know whether phase matching at $\theta_m=\pi/2$ could be achieved in proustite or pyrargyrite; if not, double refraction will be about equally serious in all these crystals.

In this paper, we consider the case of difference-mixing in HgS with the signal at 10.6 μ, the pump at 0.6328 μ, and the output at 0.6729 μ. Difference-mixing must be used because HgS becomes strongly absorbing for $\lambda<0.62$ μ. The refractive index at room temperature has recently been measured.[35,38] From Table I (class $32(D_3)$, positive birefringence) the effective nonlinear coefficient for mixing ($\chi=2d$) is

$$\chi=2d_{11}\cos^2\theta_m. \quad (5.43)$$

The signal (ω_1) at 10.6 μ and the output (ω_2) at 0.6729 μ will be extraordinary waves, while the pump (ω_3) at 0.6328 μ will be an ordinary wave. The frequencies ω_1, ω_3 satisfy (5.13). The relevant optical quantities are[38]:

$$n_1^o=2.596 \qquad n_1^e=2.847$$
$$n_2^o=2.844 \qquad n_2^e=3.178$$
$$n_3^o=2.885 \qquad n_3^e=3.232$$
$$\left.\begin{aligned} n_1&=2.641\\ n_2&=2.902\end{aligned}\right\} \text{ at } \theta_m=26.1^\circ$$
$$n_3=2.885$$
$$\rho=\rho_2=0.082 \text{ rad} \quad \rho_1=0.069 \text{ rad}. \quad (5.44)$$

It also follows that the parameters γ, ζ of (3.8) are

$$\gamma=0.881, \qquad \zeta=0.047$$
$$(1+\gamma)^2(1-\gamma^2)(1-\zeta^2)/4(1+\gamma\zeta)=0.192 \quad (5.45)$$

and

$$k_0=1.37\times10^5 \text{ cm}^{-1}$$
$$k_1=1.55\times10^4. \quad (5.46)$$

The nonlinear coefficient d_{11} can be estimated with considerable confidence from Miller's rule,[23] which, in the present case, is

$$d_{11}=[(n_1^o)^2-1][(n_2^o)^2-1][(n_3^o)^2-1]\Delta_{11}, \quad (5.47)$$

where Δ_{11} is approximately constant for different crystals of the same symmetry. The following values of Δ_{11} have been reported for various crystals of class $32(D_3)$: quartz[23] 0.44×10^{-9} esu, tellurium[36] 0.99×10^{-9}, selenium[36] 0.51×10^{-9}, and cinnabar[39] 0.77×10^{-9}. For our estimate we use the recently measured value[32]:

$$\Delta_{11}(\text{HgS})=0.62\times10^{-9} \text{ esu},$$

so that (5.47) becomes

$$d_{11}(\text{HgS})=1.8\times10^{-7} \text{ esu} \quad (5.48)$$

[30] Masamoto Takatsuji, Japan. J. Appl. Phys. **5**, 389 (1966).
[31] J. E. Midwinter and J. Warner, J. Appl. Phys. **38**, 519 (1967).
[32] G. D. Boyd, T. J. Bridges, and E. G. Burkhardt, IEEE J. Quantum Electron. (to be published).
[33] R. C. Miller and W. A. Nordland, IEEE J. Quant. Electron. **QE-3**, 642 (1967).
[34] G. D. Boyd and D. A. Kleinman, (unpublished).
[35] M. D. Martin and E. L. Thomas, IEEE **QE-2**, 196 (1966).
[36] C. K. N. Patel, Phys. Rev. Letters **16**, 613 (1966).
[37] K. Hulme, O. Jones, P. Davies, and M. Hobden, Appl Phys Letters **10**, 133 (1967).
[38] W. L. Bond, G. D. Boyd, H. L. Carter, Jr., J. Appl. Phys. **38**, 4090 (1967).
[39] J. Jerphagnon, E. Batifol, G. Tsoucaris, M. Sourbe, C. R. Acad. Sci. Paris **265B**, 495 (1967).

and (5.43) becomes

$$\chi(\mathrm{HgS})=3.0\times10^{-7}\ \text{esu}. \tag{5.49}$$

It now follows that the nonlinear constant (3.27) is

$$\bar{K}=4.2\times10^{-13}\ \text{esu}. \tag{5.50}$$

The double-refraction parameter (3.35) is

$$B=15.5l^{1/2} \qquad (l \text{ in centimeters}). \tag{5.51}$$

The mixing power (5.17) with absorption neglected and phase matching optimized is (P in watts, l in centimeters):

$$P_2=0.13lP_1P_3h_m(B,\xi), \tag{5.52}$$

where $h_m(B,\xi)$ is defined in (2.29) and plotted in Fig. 2. We are here assuming the source beams E_1, E_3 have equal confocal parameters. The resonant mixing power (5.23) with phase matching optimized is

$$(1-r)^2P_2'=0.11\ lP_1P_3\bar{h}_m(B,\xi), \tag{5.53}$$

where $\bar{h}_m(B,\xi)$ is defined in (3.37) and plotted in Fig. 12. Again we have assumed equal confocal parameters. This formula (5.53) applies to the resonance of E_2 with a cavity parameter r defined in (4.4). If E_1 is also resonated, it still applies with P_1 the one-way signal power in the cavity. As discussed in Sec. 4.2, resonance can be expected to give an enhancement in the mixing power. In the resonant case there would be an optimum crystal length l as discussed in Sec. 3.5.

Without knowledge of the absorption coefficient at ω_2 we can not discuss at this time either the enhancement or the optimum length. Therefore, we limit consideration to the nonresonant (single-pass) case (5.52). It is clear from (5.51) that for crystals of reasonable length ($l>0.1$ cm) the large double-refraction approximation (2.62) is valid. Thus, with optimum focusing $\xi=\xi_m$ (5.52) becomes (P in watts, l in centimeters)

$$\begin{aligned}P_2&=0.13lP_1P_3h_{mm}(B)\\&=6.0\times10^{-3}l^{1/2}P_1P_3.\end{aligned} \tag{5.54}$$

We choose reasonable values for the crystal length l and the power P_3 of the He–Ne (6328) laser[40]:

$$\begin{aligned}l&=0.058\ \text{cm}\\P_3&=0.1\ \text{W}\end{aligned} \tag{5.55}$$

and obtain finally

$$P_2=1.4\times10^{-4}P_1. \tag{5.56}$$

Our choice satisfies $l=\xi l_a$ with optimum focusing ($\xi=1.4$); larger l would violate (5.13) and not give much more mixing power.

Let us write

$$\begin{aligned}P_1&=N_1\hbar\omega_1,\\P_2&=N_2\hbar\omega_2,\end{aligned} \tag{5.57}$$

where N_1, N_2 are the number of photons per unit time at frequencies ω_1, ω_2, respectively. The *quantum efficiency* for up-conversion is defined as

$$\eta_{12}=N_2/N_1=(\omega_1/\omega_2)(P_2/P_1). \tag{5.58}$$

In the present example (5.56) gives

$$\eta_{12}=9\times10^{-6}. \tag{5.59}$$

The significance of the quantum efficiency in limiting the noise performance of a detection system has been discussed by Gordon.[41] Essentially the same value would be obtained for sum-mixing with the same crystal and pump power.

It should be pointed out that up-conversion by difference-mixing is subject to noise which is not present in sum-mixing. This noise[42] is due to the spontaneous decay of pump photons ω_3 into photons ω_1, ω_2. These processes produce a background radiation which increases the shot noise in the detected signal. Noise due to these processes is also present in parametric amplifiers[43] and oscillators.

It is of interest to consider the effect of double refraction on the size of η_{12}. Suppose we had a crystal with the same value of $\bar{K}$ as obtained in (5.50), but which could be phase matched at $\theta_m=\pi/2$. A glance at Table I shows that there are a number of such cases allowed by crystal symmetry. The mixing power would be given by (5.54) with $h_{mm}(0)$ instead of $h_{mm}(B)$. It follows that η_{12} would increase by the ratio

$$h_{mm}(0)/h_{mm}(3.7)=5.5. \tag{5.60}$$

5.7. Parametric Gain

Consider again the arrangement of Sec. 5.4. Gaussian beams E_1 and E_3 are mixed and E_2' is generated in a Gaussian mode of a cavity resonant at ω_2. We have obtained the enhanced mixing power (5.23). Accompanying the mixing power is power gain in beam E_1 (and power loss in E_3). From (3.26) and (5.22) we can write

$$\begin{aligned}\Delta P_1&=P_1P_3[(1-\gamma^2)^2(1-\zeta^2)/(1+\gamma\zeta)]\\&\quad\cdot[\bar{K}lk_0/2(1-r)]\bar{h}(\sigma,\beta,\xi)\\&\equiv GP_1,\end{aligned} \tag{5.61}$$

where the parametric gain G is defined by (5.61). If α_1 is the absorption coefficient, the effective gain of the *nonregenerative* parametric amplifier is

$$\text{gain}=G-\alpha_1 l. \tag{5.62}$$

Since G depends on $\bar{h}(\sigma,\beta,\xi)$ defined in (3.32) the problem of optimizing parametric gain has been solved by the computations presented in Figs. 2 and 12. The

[40] A. D. White, E. I. Gordon, and J. D. Ridgen, Appl. Phys. Letters **2**, 93 (1963).

[41] J. P. Gordon, Proc. IRE **50**, 1898 (1962).

[42] S. E. Harris, M. K. Oshman, and R. L. Byer, Phys. Rev. Letters **18**, 732 (1967).

[43] W. H. Louisell, A. Yariv, and A. E. Siegman, Phys. Rev. **124**, 1646 (1961).

theory is only valid for small gain $\ll 1$, since we have not taken the gain into account in evaluating the integral (3.3).

Consider now the arrangement of Sec. 3.1 in which both signal and idler are resonated. Above the threshold (3.34) the signal and idler are unstable and build up to high values until the pump is depleted to threshold at $z=l$. Below threshold steady-state solutions exist for the signal and idler which are nonvanishing if a signal is fed into the signal mode. The one-way idler power is then given by (5.23), with P_1 the one-way signal power in the resonator. Suppose that the first mirror has a transmission t_1 at ω_1 and a reflection $1-t_1$ while the second mirror has essentially perfect reflection. We also suppose it is possible to separate a *signal input* beam $P_1(\text{in})$ propagating in the $(+z)$ direction toward the resonator from the signal output beam $P_1(\text{out})$ leaving the resonator in the $(-z)$ direction. The parameters ϵ_1, ϵ_2 in the notation of (3.29) are

$$\epsilon_1=\alpha_1 l+\tfrac{1}{2}t_1$$
$$\epsilon_2=1-r, \tag{5.63}$$

where r is defined in (4.4) and refers here to the idler mode ω_2. It can easily be shown that

$$P_1=t_1P_1(\text{in})/(2\epsilon_1-G) \tag{5.64}$$

and

$$P_1(\text{out})=t_1P_1+(1-t_1)P_1(\text{in}) \tag{5.65}$$

with P_1 the average one-way power in the resonator. It follows that the effective gain of the *regenerative* parametric amplifier is

$$\text{gain}\equiv[P_1(\text{out})-P_1(\text{in})]/P_1(\text{in})$$
$$=t_1(G-2\alpha_1 l)/(2\epsilon_1-G). \tag{5.66}$$

The gain becomes infinite when $G=2\epsilon_1$ which is equivalent to the PG threshold condition (3.34). The optimization of the regenerative (resonant) parametric amplifier for a given crystal length is equivalent to the optimization of $\bar{h}(\sigma, \beta, \xi)$. One could also optimize (5.66) with respect to crystal length l along the lines described in Sec. 3.5.

6. SUMMARY

In this paper we have discussed the dependence of the SHG power P_2 and the PG threshold power P_3 on the parameters describing a focused laser beam in a nonlinear uniaxial crystal. The beam is assumed to be a Gaussian beam with beam radius, confocal parameter, and diffraction angle satisfying (2.1). Depletion of the laser beam is neglected. The optimizable parameters of the beam are the mismatch σ, the focal position μ, and the strength of the focusing ξ, all defined explicitly in (2.17). A self-contained derivation is given of the harmonic field (2.9) and the SHG power (2.22) which takes full account of diffraction, double refraction, and absorption. The dependence of P_2 upon the parameters σ, μ, ξ is entirely contained in the function $h(\sigma, \beta, \kappa, \xi, \mu)$. Numerical computations are given for the case of no absorption ($\kappa=0$), focus in center of crystal ($\mu=0$), and σ optimized (at each β, ξ) for maximum power. The relevant function is then $h_m(B, \xi)$ defined in (2.29) and plotted in Fig. 2. For each value of the double refraction parameter B defined in (1.4), $h_m(B, \xi)$ has a single maximum $h_{mm}(B)$ which defines the optimum focusing $\xi_m(B)$. At $B=0$ the optimum focusing turns out to be (2.32) $\xi_m(0)=2.84$.

It is shown in (2.42) that the theory given here reduces properly in the near field $\xi\ll 1$ to that of BADK.[9] In (2.54) it is shown that it reduces properly in the far field $\xi\gg 1$ to that of KAB.[8] For large B a simple analytic form (2.61) for $h_m(B, \xi)$ holds for intermediate values of ξ including the region of the optimum $\xi_m(B)$. The dependence of h upon σ is discussed for the important special case of no double refraction ($B=0$), and the entire range of behaviors is illustrated in Figs. 6–10.

A derivation is given of the PG threshold P_3 following the treatment of BA,[6] which is based upon a steady-state energy balance in the signal and idler modes between the losses and the power transferred from the pump. The result is given in (3.30), which reduces to the result of BA in the near-field $\xi\ll 1$. For the discussion of optimization this result is rewritten in (3.34) giving the reciprocal threshold P_3^{-1} in terms of a function $\bar{h}(\sigma, \beta, \xi)$. It is pointed out that $\epsilon_1\epsilon_2/P_3$, where ϵ_1 and ϵ_2 are the fractional losses for the signal and idler per (one-way) pass, is analogous to P_2/P_1^2 in SHG. The function $\bar{h}(\sigma, \beta, \xi)$ defined in (3.32) is also quite analogous to the SHG function $h(\sigma, \beta, 0, \xi, 0)$. Numerical computations are given in Fig. 12 for $\bar{h}_m(B, \xi)$ defined in (3.37), and the optimum values $\bar{h}_{mm}(B)$ are plotted in Fig. 3 along with the corresponding $h_{mm}(B)$. For the case $B=0$, the PG and SHG functions are identical. The optimum value is $\bar{h}_{mm}(0)=1.068$, which causes the approximate treatment of BA equivalent to assuming $\bar{h}_{mm}(0)=1$ to be 7% high in estimating P_3. The qualitative conclusions of BA need no revision.

For PG it is possible to define an optimum crystal length l for a minimum P_3. This is because l enters the fractional losses ϵ_1 and ϵ_2 through the absorption coefficients α_1, α_2 as in (3.68). For the special case in which $\epsilon_1=\epsilon_2$ the dependence of P_3 upon crystal length is entirely contained in the simple function $f(\Gamma, x)$ defined in (3.77). The normalized length x and double refraction parameter Γ are defined in (3.76). Figure 13 shows $f(\Gamma, x)$ for several values of Γ. For large double refraction in the general case $\epsilon_1\neq\epsilon_2$ the optimum length is given by (3.72).

The results are applied to PG in tellurium using the CO_2 laser at 10.6 μ. For arbitrary losses ϵ_1, ϵ_2 and crystal l the threshold is given by (3.84) and (3.85). Assuming $\epsilon_1=\epsilon_2$ the optimum length is (3.88) $l_m=0.14$ cm. For arbitrary crystal length P_3 is given by

(3.89) and the minimum threshold is found to be (3.90) $P_3=1.0$ W.

Application is also made to PG in $LiNbO_3$. For the case of an argon laser (0.5147 μ) pump and no double refraction, the threshold is given by (3.94); specifically a crystal of length $l=1$ cm and one-way power losses $\epsilon_1=\epsilon_2=0.01$ would have a threshold $P_3=22$ mW. For the nonoptimum focusing $\xi=1$ this would go up to 30 mW. Also considered is the case of the YAG:Nd laser (1.0648 μ) with double refraction corresponding to $LiNbO_3$ at room temperature. Threshold is given by (3.101) which is independent of crystal length; specifically $P_3=4.5$ W when $\epsilon_1=\epsilon_2=0.01$.

Resonant SHG, in which the pump makes only one pass but the harmonic is contained in a single Gaussian mode of an optical resonator, is treated by a steady-state energy balance in the harmonic mode between losses and the power transferred from the fundamental. The one-way harmonic power P_2' is given by (4.13) in terms of the PG function $\bar{h}(\sigma, \beta, \xi)$. The optimum crystal length is determined in exactly the same way as for PG. The resonant enhancement is given by (4.15). The theory is reexamined from the point of view of coupling coefficients, and it is shown in (4.27) that the general expression for the coupling coefficient is simply the ratio of $\bar{h}_m(B, \xi)$ to $h_m(B, \xi)$. In taking the near-field limit $\xi \ll 1$ it is shown that it is important to have the harmonic and fundamental beam axes cross in the center of the crystal rather than at one face. This leads to improved agreement between theory and certain experimental results of ABD.[10]

It is shown that the theory of the sum-frequency mixing of two Gaussian beams of the same confocal parameter is formally identical with the theory of SHG; the mixing power is given in (5.9). Difference-mixing is also formally equivalent to SHG in the limit (5.13) where one of the frequencies is very small; the result is given in (5.17). In the resonant case both sum-mixing (5.21) and difference-mixing (5.23) are equivalent to resonant SHG (4.13). The case of unequal confocal parameters in the resonant case without double refraction has been treated in detail. It is shown that there exists an effective confocal parameter b (5.26) in terms of which optimum focusing can be defined. In addition it is shown that for maximum mixing power all the confocal parameters should equal b. The parametric gain defined in (5.61) is proportional to $\bar{h}(\sigma, B, \xi)$. The gain of nonregenerative and regenerative parametric amplifiers are given by (5.62) and (5.65), respectively.

Application is made to the problem of upconversion from 10.6 to 0.6729 μ in cinnabar (HgS) using the 0.6328 μ He–Ne laser. This calculation can serve as a beginning for a discussion of infrared detection by means of parametric upconversion. The quantum efficiency is found (5.59) to be 9×10^{-6} for the single pass (nonresonant) case with reasonable assumptions (5.55) about the crystal and laser beam.

ACKNOWLEDGMENTS

We acknowledge with pleasure our many stimulating and fruitful discussions with J. P. Gordon and A. Ashkin, and the encouragement we have received from the continued interest of several colleagues especially E. F. Labuda, R. G. Smith, and J. E. Bjorkholm. We also thank Mrs. C. A. Lambert for programming the calculations presented in Figs. 6–11, and for suggesting the Chebyshev approximation (A4.45). Finally we wish to acknowledge that A. Ashkin was involved in the early phases of the work reported in Sec. 5.6. We have benefited from discussions on HgS with W. L. Bond and T. J. Bridges.

APPENDIX 1: EXTENSION TO POSITIVE UNIAXIAL CRYSTALS

The theory of Gaussian beams in isotropic media[7] applies without modification to the ordinary wave in birefringent uniaxial crystals. Here we consider a Gaussian beam in the *extraordinary* wave. We imagine that the birefringent medium occupies $0\leq z\leq l$ with the refractive index given by

$$n(\theta)^{-2}=(n^e)^{-2}\sin^2\theta+(n^o)^{-2}\cos^2\theta, \qquad \text{(A1.1)}$$

where θ is the angle between the optic axis and the propagation direction. Let n_1 be a matching index such that

$$n(\theta)=n_1, \qquad \text{(A1.2)}$$

when propagation is normal to the surface $z=0$. We imagine that a fictitious isotropic medium with index n_1 occupies the region $z<0$. We now introduce a Gaussian beam into the birefringent medium by assuming that the isotropic medium contains the Gaussian beam

$$\mathbf{E}(\mathbf{r}) \underset{(z<0)}{=} \mathbf{E}_0(1+i\tau)^{-1}e^{ikz}\exp\left[-\frac{x^2+y^2}{w_0^2(1+i\tau)}\right] \qquad \text{(A1.3)}$$

with

$$\tau=2(z-f)/b$$

$$b=w_0^2k. \qquad \text{(A1.4)}$$

The direction of $\mathbf{E}_0$ is such as to produce only the extraordinary wave in $0\leq z\leq l$. The beam may be written

$$E(\mathbf{r})=\int E_K\exp(i\mathbf{K}\cdot\mathbf{r})\,d\mathbf{K} \qquad (z<0) \quad \text{(A1.5)}$$

$$E_K=(2\pi)^{-3}\int E(\mathbf{r})\exp(-i\mathbf{K}\cdot\mathbf{r})\,d\mathbf{r}. \qquad \text{(A1.6)}$$

In (A1.6) we may assume that (A1.3) holds for all $\mathbf{r}$, but (A1.5) will only hold for $z<0$. Carrying out the

integration (A1.6) gives

$$E_K = E_0(w_0^2/4\pi)\delta[k-K_z-(K_x^2+K_y^2)/2k] \cdot\exp[-(w_0^2/4)[1-2i(f/b)](K_x^2+K_y^2)]. \quad \text{(A1.7)}$$

As a result of the δ function we have

$$K_x^2+K_y^2+K_z^2=K^2=k^2+(K_x^2+K_y^2)^2/4k^2. \quad \text{(A1.8)}$$

The Gaussian beam (A1.3) is a solution of the wave equation only within the paraxial approximation, which is equivalent to neglecting the second term on the right of (A1.8). Thus, $K^2=k^2$, which means that all the plane waves in (A1.5) are ordinary light waves of the isotropic medium.

Now let each plane wave of (A1.5) impinge on the surface $z=0$ and propagate into the birefringent medium as an extraordinary wave. Upon crossing the surface the normal component of $i\mathbf{K}$ is changed by the amount $-i\rho K_x$ where ρ is the double refraction angle. Thus, the waves are changed at $z=0$

$$\exp(i\mathbf{K}\cdot\mathbf{r})\rightarrow\exp(i\mathbf{K}\cdot\mathbf{r})\exp(-i\rho z K_x) \quad \text{(A1.9)}$$
$$(z<0) \qquad (0\leq z\leq l)$$

and the beam (A1.5) becomes

$$E(\mathbf{r}) \underset{(0\leq z\leq l)}{=} \int E_K \exp(i\mathbf{K}\cdot\mathbf{r})\exp(-i\rho z K_x)\,d\mathbf{K}. \quad \text{(A1.10)}$$

Carrying out the integration gives

$$E(\mathbf{r}) \underset{(0\leq z\leq l)}{=} E_0(1+i\tau)^{-1}e^{ikz} \times\exp\{-[(x-\rho z)^2+y^2]/w_0^2(1+i\tau)\}. \quad \text{(A1.10)}$$

At the surface $z=l$ we have another change in the waves similar to (A1.9)

$$\exp(i\mathbf{K}\cdot\mathbf{r})\exp(-i\rho z K_x)\rightarrow\exp(i\mathbf{K}\cdot\mathbf{r})\exp(-i\rho l K_x), \quad \text{(A1.11)}$$
$$(z<l) \qquad (z>l)$$

which gives for the exterior region $z>l$

$$E(\mathbf{r}) \underset{(z>l)}{=} E_0(1+i\tau)^{-1}e^{ikz}\exp\left[-\frac{(x-\rho l)^2+y^2}{w_0^2(1+i\tau)}\right]. \quad \text{(A1.12)}$$

In (A1.3), (A1.10), and (A1.12) we have a complete description of a beam which approaches the crystal like a Gaussian beam along the axis $x=y=0$, propagates in the crystal like an extraordinary Gaussian beam (A1.10), and emerges from the crystal like an ordinary Gaussian beam along the displaced axis $x=\rho l$, $y=0$. Within the crystal the axis of energy flow (ray axis) is along the line $x=\rho z$, and the maximum intensity is at the focal point $x=\rho f$, $y=0$, $z=f$.

In the heuristic method of Sec. 2.1 we obtained the increment (2.6) of harmonic field amplitude in a slab dz' due to the harmonic polarization in a negative uniaxial crystal. We know that the incremental field will propagate as an extraordinary Gaussian beam of the form (A1.10).

Let the field amplitude be defined as in (2.4) and consider the amplitude

$$dA(x,y,z) \underset{(0\leq z\leq l)}{=} dA_0(1+i\tau)^{-1} \times\exp\left(-\frac{2\{[x-\rho(z-z')]^2+y^2\}}{w_0^2(1+i\tau)}\right)$$

$$dA(x,y,z) \underset{(z>l)}{=} dA_0(1+i\tau)^{-1} \times\exp\left(-\frac{2\{[x-\rho(l-z')]^2+y^2\}}{w_0^2(1+i\tau)}\right). \quad \text{(A1.13)}$$

This is an extraordinary Gaussian beam in the crystal having beam size $w_0/\sqrt{2}$ and focus at $x=\rho(z-z')$, $y=0$, $z=f$. At a point x', y', z' (A1.13) becomes identical to $dA_2(x',y',z')$ in (2.6) if we identify

$$dA_0(z') = (2\pi i\omega_2/cn_2)[\mathcal{P}_{0x}/(1+i\tau')] \times\exp(i\Delta k z'-\alpha_1 z')\,dz'. \quad \text{(A1.14)}$$

With this identification (A1.13) immediately gives (2.8) and integration over dz' gives the field (2.9) outside the crystal. Thus by making use of the extraordinary Gaussian beam we have carried out the heuristic derivation without assuming (2.5).

We now consider the modifications required in the theory of SHG and PG when the crystal is *positive* instead of negative uniaxial. For SHG the fundamental is an extraordinary Gaussian beam. Thus instead of (2.2) we have

$$\mathbf{E}_1(x',y',z') = \mathbf{E}_0[1/(1+i\tau')]\exp(ik_1 z') \times\exp(-\{[x'-\rho(z'-f)]^2+y'^2\}/w_0^2(1+i\tau'))\times\exp(-\tfrac{1}{2}\alpha_1 z'), \quad \text{(A1.15)}$$

where $\mathbf{E}_0$ may be considered to lie along the x direction (see Fig. 1). The polarization beam is

$$\mathcal{P}(x',y',z') = \mathcal{P}_0[1/(1+i\tau')^2]\exp(2ik_1 z'-\alpha_1 z') \times\exp(-2\{[x'-\rho(z'-f)]^2+y'^2\}/w_0^2(1+i\tau'))B(z'), \quad \text{(A1.16)}$$

where $B(z')$ is defined in (2.3). The relations analogous to (2.5) between source point x', y', z' and observer point x, y, z are

$$x'=x, \qquad y'=y, \qquad 0\leq z'\leq l. \quad \text{(A1.17)}$$

As in (2.6) we have the increment in harmonic field

amplitude produced in the slab dz'

$$dA_2(x', y', z') = (2\pi i\omega_2/cn_2)\mathcal{P}_y(x', y', z')\exp(-ik_2z')dz'$$
$$= (2\pi i\omega_2/cn_2)[\mathcal{P}_{0y}/(1+i\tau')]$$
$$\times\exp(i\Delta kz'-\alpha_1z')\cdot\left[(1+i\tau')^{-1}\right.$$
$$\left.\times\exp\left(-\frac{2\{[x'-\rho(z'-f)]^2+y'^2\}}{w_0^2(1+i\tau')}\right)\right]dz'. \quad \text{(A1.18)}$$

An ordinary Gaussian beam reducing to the form (A1.18) at x', y', z' is

$$dA(x, y, z) \underset{(0\leq z'\leq l)}{=} dA_0(1+i\tau)^{-1}$$
$$\times\exp\left(-\frac{2\{[x-\rho(z'-f)]^2+y^2\}}{w_0^2(1+i\tau)}\right) \quad \text{(A1.19)}$$
$$dA_0(z') = (2\pi i\omega_2/cn_2)[\mathcal{P}_{0y}/(1+i\tau')]$$
$$\times\exp(i\Delta kz'-\alpha_1z')dz'.$$

Note that (A1.17) is obeyed, although we do not need to introduce it as a separate assumption. Integrating over dz' gives for the positive uniaxial crystal

$$E_2(x, y, z)_+ \underset{(z>l)}{=} \frac{2\pi i\omega_2\mathcal{P}_{0y}}{cn_2(1+i\tau)}\exp(-\tfrac{1}{2}\alpha_2l+2ik_1z)$$
$$\cdot\int_0^l dz'\frac{\exp(-\alpha z'+i\Delta kz')}{1+i\tau'}$$
$$\times\exp\left(-\frac{2\{[x-\rho(z'-f)]^2+y^2\}}{w_0^2(1+i\tau)}\right). \quad \text{(A1.20)}$$

Upon comparing (A1.20) with (2.9) we see that

$$E_2(x, y, z)_+ = E_2(\bar{x}, y, z)_-$$
$$\bar{x} = \rho(l-f)-x, \quad \text{(A1.21)}$$

where the harmonic field $E_2(x, y, z)_-$ for negative uniaxial crystals is given by (2.9). Obviously the SHG power (2.22) is unaffected by the transformation from x to $\bar{x}$, so the theory of the optimization of SHG based on the function (2.23) applies equally well to positive and negative uniaxial crystals.

For PG in positive uniaxial crystals we consider the case in which the pump (ω_3) is an ordinary Gaussian beam and the signal (ω_1) and idler (ω_2) are both extraordinary Gaussian TEM_{00} modes. Following (3.12), we assume all three beams have the same confocal parameter, and the spot sizes are related by (3.11). The theory of the PG threshold based on (3.3) goes through exactly as in Sec. 3.2; instead of (3.17) we have

$$\mathbf{E}_2^*\cdot\bar{\mathcal{P}}_2 = E_{20}\mathcal{P}_{20}\exp[-i(\sigma\xi+\varphi_3)]\frac{e^{-i\sigma\tau}}{(1+\tau^2)(1-i\tau)}$$
$$\cdot\exp\left[-\frac{2y^2}{w_{30}^2(1+\tau^2)}-\frac{x^2}{w_{30}^2(1+i\tau)}\right.$$
$$\left.-\frac{[x-\rho(z-f)]^2}{w_{30}^2(1-i\tau)}\right] \quad \text{(A1.22)}$$

assuming the same ρ for the signal and idler. Carrying out the integrations in (3.3) leads to (3.19) just as for negative uniaxial crystals.

For resonant SHG in positive uniaxial crystals the fundamental is an extraordinary Gaussian beam and the harmonic is an ordinary Gaussian TEM_{00} mode. The theory based on (4.6) goes through as in Sec. 4.1. Instead of (4.8) we have

$$\mathbf{E}_2'^*\cdot\mathcal{P}_2' = E_{20}'\mathcal{P}_{20}'\exp(i\sigma\xi+i\varphi)[e^{i\sigma\tau}/(1+i\tau)^2(1-i\tau)]$$
$$\cdot\exp(-2[(x^2+y^2)/w_0^2(1-i\tau)]$$
$$-2\{[x-\rho(z-f)]^2+y^2\}/w_0^2(1+i\tau)). \quad \text{(A1.23)}$$

Carrying out the integrations in (4.6) leads to (4.10), just as for negative uniaxial crystals.

For mixing in positive uniaxial crystals (5.9), (5.17), (5.21), and (5.23) remain valid providing the extraordinary beams (ω_1, ω_2) can be assigned the same double refraction angle ρ. This introduces no significant error when $\omega_1\sim\omega_2$, but when (5.13) is satisfied the appropriate values ρ_1, ρ_2 may be quite different. In the approximation based on (5.13) we see that ρ_1 would occur in the term in the exponent of (5.11) which we ultimately neglect. Thus, the rule is to use for ρ the value appropriate to the higher-frequency extraordinary beam.

APPENDIX 2: DEFINITION OF NONLINEAR COEFFICIENTS

We present here a general discussion of nonlinear processes arising from the second-order electric polarization of a crystalline medium. Let an arbitrary electric field be written as a Fourier integral over frequency

$$\mathbf{E}(\mathbf{r}, t) = \int_{-\infty}^{\infty}\mathbf{E}(\mathbf{r}, \omega)e^{-i\omega t}d\omega$$
$$\mathbf{E}(\mathbf{r}, \omega) = \mathbf{E}(\mathbf{r}, -\omega)^* \qquad \lim_{\omega\to 0}\mathbf{E}(\mathbf{r}, \omega) \text{ real.} \quad \text{(A2.1)}$$

A special case is the *monochromatic field*:

$$\mathbf{E}_1(\mathbf{r}, \omega) = \tfrac{1}{2}\mathbf{E}_1(\mathbf{r})\delta(\omega_1-\omega)+\tfrac{1}{2}\mathbf{E}_1(\mathbf{r})^*\delta(\omega_1+\omega) \quad \text{(A2.2)}$$
$$\mathbf{E}_1(\mathbf{r}, t) = \mathrm{Re}[\mathbf{E}_1(\mathbf{r})\exp(-i\omega_1t)]. \quad \text{(A2.3)}$$

We call $\mathbf{E}_1(\mathbf{r})$ the (spatially dependent) Fourier

amplitude of $\mathbf{E}_1(\mathbf{r}, t)$. For a plane wave we have

$$\mathbf{E}_1(\mathbf{r}) = \mathbf{E}_1 \exp(i\mathbf{k}_1 \cdot \mathbf{r}), \tag{A2.4}$$

and we call $\mathbf{E}_1$ the plane-wave amplitude. The intensity of the wave (A2.4) is

$$S_1 = (n_1 c/8\pi) \mid \mathbf{E}_1 \mid^2, \tag{A2.5}$$

where n_1 is the refractive index. If $\mathbf{E}_1(\mathbf{r})$ represents a Gaussian beam the intensity (axial component of the Poynting vector) is [see BADK (A.9)]:

$$S_1(\mathbf{r}) = (n_1 c/8\pi) \mid \mathbf{E}_1(\mathbf{r}) \mid^2. \tag{A2.6}$$

This establishes what we mean by $\mathbf{E}_1(\mathbf{r})$.

Write the polarization in the form

$$\mathcal{P}(\mathbf{r}, t) = \int_{-\infty}^{\infty} \mathcal{P}(\mathbf{r}, \omega) e^{-i\omega t} d\omega$$

$$\mathcal{P}(\mathbf{r}, \omega) = \mathcal{P}(\mathbf{r}, -\omega)^* \qquad \lim_{\omega \to 0} \mathcal{P}(\mathbf{r}, \omega) \text{ real.} \tag{A2.7}$$

A monochromatic polarization is specified by

$$\mathcal{P}_3(\mathbf{r}, \omega) = \tfrac{1}{2}\mathcal{P}_3(\mathbf{r})\delta(\omega_3 - \omega) + \tfrac{1}{2}\mathcal{P}_3(\mathbf{r})^*\delta(\omega_3 + \omega) \tag{A2.8}$$

$$\mathcal{P}_3(\mathbf{r}, t) = \mathrm{Re}[\mathcal{P}_3(\mathbf{r}) \exp(-i\omega_3 t)]. \tag{A2.9}$$

Now let the polarization arise from a second-order response of the medium to an arbitrary electric field. The most general second-order polarization can be written

$$\mathcal{P}(\mathbf{r}, \omega)_i = \sum_{jk} \int_{-\infty}^{\infty} d\omega' \chi(-\omega, \omega', \omega - \omega')_{ijk} E(\mathbf{r}, \omega')_j E(\mathbf{r}, \omega - \omega')_k, \tag{A2.10}$$

where the indices ijk refer to crystallographic axes X, Y, Z and χ is a third-rank tensor satisfying the *permutation symmetry* [ABDP[3] (2.16)]

$$\begin{aligned} \chi(-\omega, \omega', \omega - \omega')_{ijk} &= \chi(\omega', -\omega, \omega - \omega')_{jik} \\ &= \chi(\omega - \omega', \omega', -\omega)_{kji} \\ &= \chi(-\omega, \omega - \omega', \omega')_{ikj}. \end{aligned} \tag{A2.11}$$

The implication of this symmetry is discussed later. Also (A2.1) and (A2.7) require

$$\chi(-\omega, \omega', \omega - \omega')_{ijk} = \chi(\omega, -\omega', \omega' - \omega)_{ijk}^*, \tag{A2.12}$$

which insures that $\mathbf{E}(\mathbf{r}, t)$ and $\mathcal{P}(\mathbf{r}, t)$ are real. Observe that $\mathcal{P}(\mathbf{r}, \omega)$ and $\mathbf{E}(\mathbf{r}, \omega)$ are defined for positive and negative frequencies and the sum over ω' runs over the whole (positive and negative) frequency range. Therefore (A2.10) includes sum ($0 \leq \omega' \leq \omega$) and difference ($\omega' < 0$ or $\omega' > \omega$) mixing as well as harmonic generation ($2\omega' = \omega$), optical rectification ($\omega = 0$), and the electro-optic effect ($\omega' \approx 0$).

We shall show that χ is identical with the tensor defined originally in ABDP (3.12) by applying (A2.10) to the case of sum-mixing

$$\omega_3 = \omega_1 + \omega_2 \tag{A2.13}$$

of two monochromatic fields ω_1, ω_2. Write

$$\mathbf{E}(\mathbf{r}, \omega') = \mathbf{E}_1(\mathbf{r}, \omega') + \mathbf{E}_2(\mathbf{r}, \omega') \tag{A2.14}$$

and a similar relation for frequency $\omega - \omega'$. Inasmuch as $\mathbf{E}(\mathbf{r}, \omega')$ and $\mathbf{E}(\mathbf{r}, \omega - \omega')$ in (A2.10) each contains four terms, the complete expansion of (A2.10) would contain 16 terms, only eight of which are distinct because of the symmetry $jk \to kj$ in (A2.11). We see from (A2.8) that $\frac{1}{2}\mathcal{P}_3(\mathbf{r})$ is the coefficient of $\delta(\omega_1 + \omega_2 - \omega)$ in this expansion, which gives

$$\mathcal{P}_3(\mathbf{r}) = \chi(-\omega_3, \omega_1, \omega_2) : \mathbf{E}_1(\mathbf{r})\mathbf{E}_2(\mathbf{r}). \tag{A2.15}$$

The tensor notation here is defined by referring to (A2.10). In the same way we can treat difference mixing $\omega_2 = \omega_3 - \omega_1$ and $\omega_1 = \omega_3 - \omega_2$ to obtain

$$\begin{aligned} \mathcal{P}_2(\mathbf{r}) &= \chi(-\omega_2, -\omega_1, \omega_3) : \mathbf{E}_1(\mathbf{r})^* \mathbf{E}_3(\mathbf{r}) \\ \mathcal{P}_1(\mathbf{r}) &= \chi(-\omega_1, -\omega_2, \omega_3) : \mathbf{E}_2(\mathbf{r})^* \mathbf{E}_3(\mathbf{r}). \end{aligned} \tag{A2.16}$$

From (A2.11) and (A2.12) we have

$$\begin{aligned} \chi(-\omega_2, -\omega_1, \omega_3)_{kji} &= \chi(-\omega_1, -\omega_2, \omega_3)_{jki} \\ &= \chi(-\omega_3, \omega_1, \omega_2)_{ijk}^* \end{aligned} \tag{A2.17}$$

in agreement with the permutation symmetry relations as given by Pershan[44] (3.8). Ordinarily it is permissible to assume[3,44] χ is real. Our definition of the field and polarization amplitudes in (A2.3) and (A2.9) agrees with the notation of ABDP, and (A2.15) is identical with ABDP (3.12), which establishes the identity of $\chi(-\omega, \omega', \omega - \omega')$ with the χ tensor of ABDP.

We now specialize (A2.10) to SHG by the monochromatic field (A2.2). According to (A2.8), $\frac{1}{2}\mathcal{P}_2(\mathbf{r})$ is the coefficient of $\delta(2\omega_1 - \omega)$ in (A2.10) when $\mathbf{E}(\mathbf{r}, \omega) = \mathbf{E}_1(\mathbf{r}, \omega)$ and $\omega_2 = 2\omega_1$; thus, we obtain

$$\begin{aligned} \mathcal{P}_2(\mathbf{r}) &= \tfrac{1}{2}\chi(-\omega_2, \omega_1, \omega_1) : \mathbf{E}_1(\mathbf{r})\mathbf{E}_1(\mathbf{r}) \\ &= \mathbf{d}(-2\omega_1, \omega_1, \omega_1) : \mathbf{E}_1(\mathbf{r})\mathbf{E}_1(\mathbf{r}), \end{aligned} \tag{A2.18}$$

where $d(-2\omega, \omega, \omega)_{ijk}$ is the SHG tensor. Miller[23] has reported quantitative measurements of SHG for a number of crystals in terms of the components d_{ijk}, and Francois[22] has given the value

$$d(-2\omega, \omega, \omega)_{312} = 1.36 \times 10^{-9} (\pm 12\%) \text{ esu (ADP)}. \tag{A2.19}$$

According to (A2.11) $\chi(-\omega_2, \omega_1, \omega_1)_{ijk}$ is symmetric in jk, and $\mathbf{E}_1(\mathbf{r})\mathbf{E}_1(\mathbf{r})$ can be regarded as a symmetric second-rank tensor with components $E_1(\mathbf{r})_j E_1(\mathbf{r})_k$. The indices jk then can be written as a single index

[44] P. S. Pershan, Phys. Rev. **130**, 919 (1963).

$l(jk)=1, \cdots, 6$ according to the scheme

$$l(jk)=1(11), 2(22), 3(33), 4(23), 5(13), 6(12). \tag{A2.20}$$

This leads to the *condensed notation*

$$d_{il}=d_{il(jk)}=d_{ijk}=d_{ikj}. \tag{A2.21}$$

The 3×6 matrix d_{il} operates on the column vector $(\mathbf{EE})_l$ where

$$(\mathbf{EE})_1=E_X^2, \quad (\mathbf{EE})_2=E_Y^2, \quad (\mathbf{EE})_3=E_Z^2$$
$$(\mathbf{EE})_4=2E_YE_Z, \quad (\mathbf{EE})_5=2E_XE_Z,$$
$$(\mathbf{EE})_6=2E_XE_Y. \tag{A2.22}$$

In condensed notation (A2.18) becomes

$$\mathcal{P}_2(\mathbf{r})=\mathbf{d}(-2\omega_1, \omega_1, \omega_1)\cdot\mathbf{E}_1(\mathbf{r})\mathbf{E}_1(\mathbf{r})$$
$$\mathcal{P}_{2i}=\sum_{l=1}^{6} d_{il}(\mathbf{E}_1\mathbf{E}_1)_l, \tag{A2.23}$$

with

$$2d(-2\omega, \omega, \omega)_{il}=\chi(-2\omega, \omega, \omega)_{ijk} \quad l=l(jk). \tag{A2.24}$$

A single dot as in (A2.23) henceforth indicates condensed notation. This is the tensor appearing in (1.1). It should be noted that another condensed notation is in common use for piezoelectric matrices[45] in which the factor 2 in (A2.22) is instead put into the definitions of d_{i4}, d_{i5}, d_{i6}. The disadvantage of this notation is that it destroys the simplicity and elegance of (A2.21) and (A2.24).

The SHG tensor $\mathbf{d}(-2\omega, \omega, \omega)$ can be used to describe sum mixing $\omega_1+\omega_2=\omega_3$ providing it is permissible to set

$$\chi(-\omega_3, \omega_1, \omega_2)=\chi(-\omega_3, \omega_0, \omega_0)$$
$$2\omega_0=\omega_1+\omega_2=\omega_3. \tag{A2.25}$$

Then (A2.15) can be written

$$\mathcal{P}_3(\mathbf{r}) \underset{(\omega_1\sim\omega_2\sim\frac{1}{2}\omega_3)}{=} 2\mathbf{d}(-\omega_3, \omega_0, \omega_0)\cdot\mathbf{E}_1(\mathbf{r})\mathbf{E}_2(\mathbf{r}), \tag{A2.26}$$

where the column vector $(\mathbf{E}_1\mathbf{E}_2)$ has the components

$$(\mathbf{E}_1\mathbf{E}_2)_l=(E_{1j}E_{2k}+E_{1k}E_{2j})(1-\tfrac{1}{2}\delta_{jk}) \qquad l=l(jk). \tag{A2.27}$$

We can also write the companion relations (difference mixing) (A2.16), but they assume a more complicated form (which in general cannot be written in our condensed notation)

$$\mathcal{P}_2(\mathbf{r})_i=2\sum_k E_1(\mathbf{r})_k{}^*\Big[\sum_j d(-\omega_3, \omega_0, \omega_0)_{jl}{}^*E_3(\mathbf{r})_j\Big]$$
$$\mathcal{P}_1(\mathbf{r})_i=2\sum_k E_2(\mathbf{r})_k{}^*\Big[\sum_j d(-\omega_3, \omega_0, \omega_0)_{jl}{}^*E_3(\mathbf{r})_j\Big],$$
$$l=l(ik). \tag{A2.28}$$

Thus the parametric interaction of three fields is completely described by the SHG tensor when $\omega_1\sim\omega_2\sim\frac{1}{2}\omega_3$.

The treatment of optical rectification based upon (A2.10) is completely analogous to the treatment of SHG. When we substitute $\mathbf{E}_1(\mathbf{r}, \omega)$ for $\mathbf{E}(\mathbf{r}, \omega)$ we obtain a zero frequency term

$$\mathcal{P}_0(\mathbf{r}, \omega)=\mathcal{P}_0(\mathbf{r})\delta(\omega), \tag{A2.29}$$

where

$$\mathcal{P}_0(\mathbf{r})=\tfrac{1}{2}\chi(0, \omega_1, -\omega_1):\mathbf{E}_1(\mathbf{r})\mathbf{E}_1(\mathbf{r})^*$$
$$=d(0, \omega, -\omega):\mathbf{E}_1(\mathbf{r})\mathbf{E}_1(\mathbf{r})^*. \tag{A2.30}$$

Here $d(0, \omega, -\omega)_{ijk}$ is the optical rectification tensor which is required by (A2.11), (A2.12) to be real and symmetric in jk. There is no loss in generality in assuming that $\mathbf{E}_1(\mathbf{r})$ is real. The measurements of Bass *et al.*[46] are reported in terms of a tensor $X_{ijk}{}^0$ identical with $d(0, \omega, -\omega)_{ijk}$. Ward[47] gives

$$2d(0, \omega, -\omega)_{123}=(1.32\pm0.18)\times10^{-7}\ \text{esu(ADP)}. \tag{A2.31}$$

If desired, condensed notation can be employed in (A2.29) using the scheme (A2.24) and (A2.22).

The optical rectification tensor can be used to describe difference mixing $\omega_2=\omega_3-\omega_1$ providing it is permissible to set

$$\chi(-\omega_2, -\omega_1, \omega_3)=\chi(0, -\omega_3, \omega_3). \tag{A2.32}$$

In this case, the first relation (A2.16) becomes in condensed notation

$$\mathcal{P}_2(\mathbf{r}) \underset{(\omega_2\sim0)}{=} 2\mathbf{d}(0, \omega_3, -\omega_3)\cdot\mathbf{E}_1(\mathbf{r})^*\mathbf{E}_3(\mathbf{r}), \tag{A2.33}$$

where the column vector $(\mathbf{E}_1{}^*\mathbf{E}_3)_l$ is defined by (A2.27). The second relation (A2.16) assumes the more complicated form

$$\mathcal{P}_1(\mathbf{r})_i=2\sum_k E_3(\mathbf{r})_k\Big[\sum_j d(0, \omega_3, -\omega_3)_{jl}E_2(\mathbf{r})_j{}^*\Big],$$
$$l=l(ik) \tag{A2.34}$$

and (A2.15) becomes

$$\mathcal{P}_3(\mathbf{r})=2\sum_k E_1(\mathbf{r})_k\Big[\sum_j d(0, \omega_3, -\omega_3)_{jl}E_2(\mathbf{r})_j\Big]. \tag{A2.35}$$

Thus the parametric interaction of three fields is completely described by the optical rectification tensor

[45] J. F. Nye, *Physical Properties of Crystals* (Oxford University Press, London, 1960) Chap. VII.

[46] M. Bass, P. A. Franken, and J. F. Ward, Phys. Rev. **138**, A534 (1965).

[47] J. F. Ward, Phys. Rev. **143**, 569 (1966).

when ω_2 (or ω_1) is sufficiently small (compared to the dispersion frequencies of the crystal) to be considered zero.

The linear electrooptic (Pockels) effect arises from a polarization $\mathcal{P}_1(\mathbf{r})$ due to the mixing of a field at zero frequency $\mathbf{E}_0(\mathbf{r})$ with the field $\mathbf{E}_1(\mathbf{r})$. We write

$$\mathbf{E}(\mathbf{r},\omega')=\mathbf{E}_1(\mathbf{r},\omega)+\mathbf{E}_0(\mathbf{r}) \tag{A2.36}$$

and obtain from (A2.10)

$$\mathcal{P}_1(\mathbf{r})=2\chi(-\omega_1,\omega_1,0):\mathbf{E}_1(\mathbf{r})\mathbf{E}_0(\mathbf{r}). \tag{A2.37}$$

It follows from (A2.11) that this can be written

$$\mathcal{P}_1(\mathbf{r})_i=4\sum_{jk} d(0,\omega_1,-\omega_1)_{kji}E_1(\mathbf{r})_jE_{0k}, \tag{A2.38}$$

where $\mathbf{d}(0,\omega,-\omega)$ is the optical rectification tensor introduced in (A2.30). This polarization can be regarded as arising from a term in the dielectric constant tensor $\boldsymbol{\varepsilon}$ linear in the applied field $\mathbf{E}_0$. The electrooptic tensor r_{ijk} is defined by the expansion

$$a_{ij}=a_{ij}^{(0)}+\sum_k r_{ijk}E_{0k}+\cdots, \tag{A2.39}$$

where

$$\mathbf{a}=\boldsymbol{\varepsilon}^{-1} \tag{A2.40}$$

is the inverse dielectric constant. It follows from this definition and from (A2.37) that

$$r(\omega)_{ijk}=-8\pi\sum_{nm} a_{in}^{(0)}\chi(-\omega,\omega,0)_{nmk}a_{mj}^{(0)}. \tag{A2.41}$$

Only the real symmetric part of $a_{ij}^{(0)}$ need be retained, and it can be assumed that the coordinate axes have been chosen to be principal axes of $\mathbf{a}^{(0)}$, so (A2.41) can be reduced to

$$r(\omega)_{ijk}=-8\pi a_i^{(0)}(\omega)a_j^{(0)}(\omega)\chi(-\omega,\omega,0)_{ijk}. \tag{A2.42}$$

This may be written in the condensed notation

$$r(\omega)_{lk}=-16\pi A(\omega)_l d(0,\omega,-\omega)_{kl}, \tag{A2.43}$$

where

$$\begin{aligned} d(0,\omega,-\omega)_{kl}&=\tfrac{1}{2}\chi(0,\omega,-\omega)_{kji}\\ r(\omega)_{lk}&=r(\omega)_{ijk}\\ A(\omega)_l&=a_i^{(0)}a_j^{(0)}\approx n^{-4}\qquad l=l(ij). \end{aligned} \tag{A2.44}$$

Here r_{lk} is the usual 6×3 electrooptic matrix, and n is the refractive index or an average over the (nearly equal) refractive indices of the crystal.

Arguments have been presented[48] that $\chi(-\omega_3,\omega_1,\omega_2)_{ijk}$ should have additional symmetry beyond (A2.17) and beyond the requirements of crystal symmetry. We should expect $\chi(-\omega_3,\omega_1,\omega_2)_{ijk}$ to be independent of ω_1, ω_2, $\omega_3=\omega_1+\omega_2$, providing ω_3 is much less than the frequencies of the virtual electronic transitions involved in the second-order polarization. It would then follow from (A2.17) that χ_{ijk} is real and invariant to any permutation of ijk: (proposed symmetry[48])

$$\chi_{ijk}=\chi_{jik}=\chi_{kji}=\chi_{ikj}. \tag{A2.45}$$

In condensed notation the SHG tensor becomes

$$\begin{matrix} d_{11} & d_{12} & d_{13} & d_{14} & d_{15} & d_{16}\\ d_{16} & d_{22} & d_{23} & d_{24} & d_{14} & d_{12}\\ d_{15} & d_{24} & d_{33} & d_{23} & d_{13} & d_{14} \end{matrix} \tag{A2.46}$$

with ten independent components. A number of SHG experiments[23] have verified (A2.46) in particular cases. For crystal classes $\bar{6}(C_{3h})$, $\bar{6}2m(D_{3h})$, $23(T)$, and $\bar{4}3m(T_d)$ the validity of (A2.46) is guaranteed by crystal symmetry alone regardless of the frequency dependence of χ. For classes $422(D_4)$ and $622(D_6)$, (A2.46) implies that $\mathbf{d}$ vanishes entirely. When $\mathbf{d}$ has the form (A2.46) the three relations (A2.26) and (A2.28) can all be written in condensed tensor notation

$$\begin{aligned} \mathcal{P}_1(\mathbf{r})&=2\mathbf{d}\cdot\mathbf{E}_2(\mathbf{r})^*\mathbf{E}_3(\mathbf{r})\\ \mathcal{P}_2(\mathbf{r})&=2\mathbf{d}\cdot\mathbf{E}_1(\mathbf{r})^*\mathbf{E}_3(\mathbf{r})\\ \mathcal{P}_3(\mathbf{r})&=2\mathbf{d}\cdot\mathbf{E}_1(\mathbf{r})\mathbf{E}_2(\mathbf{r})\\ \mathbf{d}&=\mathbf{d}(-\omega_3,\omega_0,\omega_0). \end{aligned} \tag{A2.47}$$

Measurements of the electro-optic coefficients indicate that $\mathbf{d}(0,\omega,-\omega)$ does not have the form (A2.46), so it is not possible to write (A2.34), (A2.35) in the form (A2.47).

We give for reference a formula for the *instantaneous* polarization in terms of the instantaneous field for the idealized special case of zero dispersion. We have already noted that this assumption fails for $\mathbf{d}(0,\omega,-\omega)$, and therefore we should not expect $\mathbf{d}(0,\omega,-\omega)$ and $\mathbf{d}(-2\omega,\omega,\omega)$ to be equal. Nevertheless, the idealized case may be helpful in interpreting our definitions of χ and $\mathbf{d}$. In the absence of any dispersion χ in (A2.10) is a constant. It then follows from (A2.1) and (A2.7) that (A2.10) may be written

$$\begin{aligned} \mathcal{P}(\mathbf{r},t)&=\chi:\mathbf{E}(\mathbf{r},t)\mathbf{E}(\mathbf{r},t)\\ &=2\mathbf{d}\cdot\mathbf{E}(\mathbf{r},t)\mathbf{E}(\mathbf{r},t). \end{aligned} \tag{A2.48}$$

Our assumptions imply that χ satisfies (A2.45) and $\mathbf{d}$ has the form (A2.46). Upon comparing with (A2.18) and (A2.30), we see that the instantaneous relation contains a factor 2 not present in the Fourier amplitude relations.

Let us compute the *average power* delivered to the field $\mathbf{E}(\mathbf{r},t)$ over some time interval $2T$

$$\begin{aligned} P&=-(2T)^{-1}\int_{-T}^{T}dt\int d\mathbf{r}\mathbf{E}(\mathbf{r},t)\cdot(\partial/\partial t)\mathcal{P}(\mathbf{r},t)\\ &=(i\pi/T)\int d\mathbf{r}\iint d\omega d\omega'\mathbf{E}(\mathbf{r},\omega)\cdot\mathcal{P}(\mathbf{r},\omega')\omega'\delta_T(\omega+\omega'), \end{aligned} \tag{A2.49}$$

[48] D. A. Kleinman, Phys. Rev. **126**, 1977 (1962).

where

$$\delta_T(\Omega)\equiv(\sin\Omega T)/\pi\Omega$$

$$\int_{-\infty}^{\infty}\delta_T(\Omega)\,d\Omega=1 \tag{A2.50}$$

is a representation of $\delta(\Omega)$ as $T\to\infty$. Thus, we obtain for sufficiently large T

$$P=(i\pi/T)\int d\mathbf{r}\int d\omega\mathbf{E}(\mathbf{r},\omega)^*\cdot\mathcal{P}(\mathbf{r},\omega)\omega$$

$$=(i\pi/T)\int d\mathbf{r}\iint_{-\infty}^{\infty}d\omega d\omega'\mathbf{E}(\mathbf{r},\omega)^*$$

$$\cdot\chi(-\omega,\omega',\omega-\omega'):\mathbf{E}(\mathbf{r},\omega')\mathbf{E}(\mathbf{r},\omega-\omega')\omega. \tag{A2.51}$$

Writing

$$\omega=\omega'+(\omega-\omega'),$$

and noting that the ω' and $(\omega-\omega')$ contributions to (A2.51) must be equal, we obtain

$$P=(2i\pi/T)\int d\mathbf{r}\iint_{-\infty}^{\infty}d\omega d\omega'\mathbf{E}(\mathbf{r},\omega)^*$$

$$\cdot\chi(-\omega,\omega',\omega-\omega'):\mathbf{E}(\mathbf{r},\omega')\mathbf{E}(\mathbf{r},\omega-\omega')\omega'. \tag{A2.52}$$

From the symmetry (A2.11) we can write

$$\mathbf{E}(\mathbf{r},\omega)^*\cdot\chi(-\omega,\omega',\omega-\omega'):\mathbf{E}(\mathbf{r},\omega')\mathbf{E}(\mathbf{r},\omega-\omega')$$
$$=\mathbf{E}(r,\omega')\cdot\chi(\omega',-\omega,\omega-\omega'):\mathbf{E}(\mathbf{r},\omega)^*\mathbf{E}(\mathbf{r},\omega-\omega'). \tag{A2.53}$$

Now upon making the interchange of variables in (A2.52)

$$\omega\to-\omega',\qquad\omega'\to-\omega,$$

which leaves $\omega-\omega'$ and $d\omega d\omega'$ invariant, we obtain

$$P=(2i\pi/T)\int d\mathbf{r}\iint_{-\infty}^{\infty}d\omega d\omega'\mathbf{E}(\mathbf{r},\omega)^*$$

$$\cdot\chi(-\omega,\omega',\omega-\omega'):\mathbf{E}(\mathbf{r},\omega')\mathbf{E}(\mathbf{r},\omega-\omega')(-\omega)=-2P. \tag{A2.54}$$

Thus, a direct consequence of the symmetry (A2.11) is the vanishing of the average power

$$P=0. \tag{A2.55}$$

Conversely, this condition can be required on physical grounds and the symmetry (A2.11) obtained as a consequence. Neither (A2.11) nor (A2.55) is valid when $\mathbf{E}(\mathbf{r},\omega)$ and $\mathcal{P}(\mathbf{r},\omega)$ are large in regions of ω where the crystal is strongly absorbing. (A2.55) expresses the conservation of energy in the conversion of power from one frequency domain to another through the nonlinear interaction.

We now calculate the average power P_3 delivered to a monochromatic field $\mathbf{E}_3(\mathbf{r},t)$ by the polarization $\mathcal{P}_3(\mathbf{r},t)$

$$P_3=-(2T)^{-1}\int_{-T}^{T}dt\int d\mathbf{r}\mathbf{E}_3(\mathbf{r},t)\cdot(\partial/\partial t)\mathcal{P}_3(\mathbf{r},t)$$

$$=(i\pi/T)\int d\mathbf{r}\iint_{-\infty}^{\infty}d\omega d\omega'\mathbf{E}_3(\mathbf{r},\omega)$$
$$\cdot\mathcal{P}_3(\mathbf{r},\omega')\omega'\delta_T(\omega+\omega')$$

$$=(i\pi/4T)\int d\mathbf{r}\int_{-\infty}^{\infty}d\omega[\mathbf{E}_3(\mathbf{r})\cdot\mathcal{P}_3(\mathbf{r})^*\delta(\omega_3+\omega)$$
$$+\mathbf{E}_3(\mathbf{r})^*\cdot\mathcal{P}_3(\mathbf{r})\delta(\omega_3-\omega)]\omega\delta_T(0)$$

$$=-\mathrm{Im}\left[\tfrac{1}{2}\omega_3\int d\mathbf{r}\mathbf{E}_3(\mathbf{r})^*\cdot\mathcal{P}_3(\mathbf{r})\right]. \tag{A2.56}$$

Similarly, we have

$$P_1=-\mathrm{Im}\left[\tfrac{1}{2}\omega_1\int d\mathbf{r}\mathbf{E}_1(\mathbf{r})^*\cdot\mathcal{P}_1(\mathbf{r})\right]$$

$$P_2=-\mathrm{Im}\left[\tfrac{1}{2}\omega_2\int d\mathbf{r}\mathbf{E}_2(\mathbf{r})^*\cdot\mathcal{P}_2(\mathbf{r})\right]. \tag{A2.57}$$

Using the symmetry (A2.17) it can easily be shown that

$$\mathbf{E}_1(\mathbf{r})^*\cdot\mathcal{P}_1(\mathbf{r})=\mathbf{E}_2(\mathbf{r})^*\cdot\mathcal{P}_2(\mathbf{r})=[\mathbf{E}_3(\mathbf{r})^*\cdot\mathcal{P}_3(\mathbf{r})]^*, \tag{A2.58}$$

and it follows immediately that

$$P_1+P_2+P_3=P=0 \tag{A2.59}$$

in agreement with (A2.55).

Obviously the discussion given here is not limited to strictly monochromatic fields. Relations (A2.15) and (A2.16) remain meaningful if all the amplitudes are slowly varying functions of time. To describe a *quasimonochromatic field* we can generalize (A2.2) to the form

$$\mathbf{E}_1(\mathbf{r},\omega)=\tfrac{1}{2}\mathbf{E}_1(\mathbf{r})g_1(\mathbf{r},\omega)+\tfrac{1}{2}\mathbf{E}_1(\mathbf{r})^*g_1(\mathbf{r},-\omega)^*, \tag{A2.60}$$

where the (complex) line shape $g_1(\mathbf{r},\omega)$ vanishes except when ω is near ω_1 and satisfies the normalization condition

$$\int_{-\infty}^{\infty}g_1(\omega)\,d\omega=1. \tag{A2.61}$$

Henceforth, for brevity we omit writing the argument $\mathbf{r}$. The mean square field over some time interval $-T<t<T$ is

$$\langle|\mathbf{E}(t)|^2\rangle_T\equiv(2T)^{-1}\int_{-T}^{T}|\mathbf{E}(t)|^2dt$$

$$=(\pi/T)\int_{-\infty}^{\infty}d\omega\mathbf{E}(\omega)$$

$$\cdot\int_{-\infty}^{\infty}\mathbf{E}(\omega')^*\delta_T(\omega-\omega')\,d\omega', \tag{A2.62}$$

where

$$\delta_T(\omega-\omega') \equiv [\sin(\omega-\omega')T/\pi(\omega-\omega')] \underset{T\to\infty}{\to} \delta(\omega-\omega'). \tag{A2.63}$$

What is ordinarily measured and called the line shape is the *power spectrum*

$$G_E(\omega) \equiv (\pi/T)\mathbf{E}(\omega)\cdot\int_{-\infty}^{\infty}\mathbf{E}(\omega')^*\delta_T(\omega-\omega')\,d\omega'$$

$$\int_{-\infty}^{\infty} G_E(\omega)\,d\omega = \langle|\,\mathbf{E}(t)\,|^2\rangle_T. \tag{A2.64}$$

The power spectrum is always defined with respect to a *resolution width* $\Delta\omega_T$ which may be defined

$$(\Delta\omega_T)^{-1} \equiv \int_{-\infty}^{\infty} |\,\delta_T(\omega-\omega')\,|^2 d\omega' = T/\pi. \tag{A2.65}$$

Similarly, the *linewidth* of the field may be defined

$$(\Delta\omega_1)^{-1} \equiv \int_{-\infty}^{\infty} |\,g_1(\omega')\,|^2 d\omega'. \tag{A2.66}$$

When $\mathbf{E}(\omega')$ varies negligibly as a function of ω' over the resolution width $\Delta\omega_T$ the power spectrum (A2.64) becomes

$$G_E(\omega) \underset{\Delta\omega_T \ll \Delta\omega_1}{\to} |\,\mathbf{E}(\omega)\,|^2\Delta\omega_T. \tag{A2.67}$$

For the quasimonochromatic field (A2.60) this gives

$$G_1(\omega) \underset{(\Delta\omega_T \ll \Delta\omega_1)}{=} \tfrac{1}{4}|\,\mathbf{E}_1(\mathbf{r})\,|^2[|\,g_1(\omega)\,|^2+|\,g_1(-\omega)\,|^2]\Delta\omega_T \tag{A2.68}$$

providing there is no overlap of the lineshapes $g_1(\pm\omega)$. The line shape and power spectrum of the polarization can be defined by relations analogous to (A2.60), (A2.61), (A2.64), and (A2.67).

We can now consider the mixing of two quasimonochromatic fields $\mathbf{E}_1(\omega)$ and $\mathbf{E}_2(\omega)$ of the form (A2.60) to produce a quasimonochromatic polarization $\mathcal{P}_3(\omega)$ at frequencies near $\omega_1+\omega_2$. The lineshape of the polarization is easily found from (A2.10) to be

$$g_{3P}(\omega) = \int_{-\infty}^{\infty} d\omega' g_1(\omega')\,g_2(\omega-\omega') \tag{A2.69}$$

and the amplitudes satisfy (A2.15), providing (a) none of the line-shape functions centered on different frequencies overlap, and (b) the dispersion of χ over the linewidth can be neglected. Similarly for difference mixing, the lineshapes corresponding to the amplitudes (A2.16) are

$$g_{2P}(\omega) = \int_{-\infty}^{\infty} d\omega' g_1(\omega')^* g_3(\omega-\omega')$$

$$g_{1P}(\omega) = \int_{-\infty}^{\infty} d\omega' g_2(\omega')^* g_3(\omega-\omega'). \tag{A2.70}$$

Here $g_3(\omega)$ is the line shape of the field at ω_3. The line shapes of the polarizations at ω_1, ω_2, ω_3 (distinguished by subscript P) are not necessarily the same as the line shapes of the fields at these frequencies. Thus, the line shape $g_3(\omega)$ for sum mixing is determined, not only by $g_{3P}(\omega)$, but also by phase-matching conditions in the crystal.

APPENDIX 3: EFFECTIVE NONLINEAR COEFFICIENTS

In (2.18), (3.18), and (4.9) the nonlinear properties of the medium are represented in the theory by a single quantity called an *effective nonlinear coefficient*. We shall now define precisely how this quantity is related to the second order polarization tensor χ defined in Appendix 2. We define the effective nonlinear coefficients d for SHG and χ for PG (or mixing) as follows:

$$d = \tfrac{1}{2}\mathbf{U}_2\cdot\chi(-\omega_2, \omega_1, \omega_1):\mathbf{U}_1\mathbf{U}_1 \qquad (\omega_2=2\omega_1) \tag{A3.1}$$

$$\chi = \mathbf{U}_3\cdot\chi(-\omega_3, \omega_1, \omega_2):\mathbf{U}_1\mathbf{U}_2 \qquad (\omega_3=\omega_1+\omega_2), \tag{A3.2}$$

where $\mathbf{U}_1$, $\mathbf{U}_2$, $\mathbf{U}_3$ are unit vectors denoting the directions of polarization of the electric fields at frequencies ω_1, ω_2, ω_3 respectively. In terms of the SHG tensor $d(-2\omega_1, \omega_1, \omega_1)_{ijk}$ defined in (A2.18) we have

$$d = \sum_{ijk} U_{2i}U_{1j}U_{1k}d(-2\omega_1, \omega_1, \omega_1)_{ijk}$$

$$= \sum_{il} U_{2i}(\mathbf{U}_1\mathbf{U}_1)_l d(-2\omega_1, \omega_1, \omega_1)_{il}, \tag{A3.3}$$

where d_{il} and $(\mathbf{U}_1\mathbf{U}_1)_l$ are in the condensed notation (A2.21), (A2.22). The χ of (A3.2) is relevant not only to PG with ω_3 the pump but also to sum-mixing of ω_1 and ω_2 to generate ω_3 according to (A2.15). In such an experiment $\mathbf{U}_3$ is determined by the crystal optics and the requirement of phase matching. Thus, the effective component of polarization at ω_3 is

$$\mathbf{U}_3\cdot\mathcal{P}_3(\mathbf{r}) = \chi E_1(\mathbf{r})E_2(\mathbf{r}), \tag{A3.4}$$

and the power (A2.56) delivered at ω_3 is

$$P_3 = -\chi\mathrm{Im}\left[\tfrac{1}{2}\omega_3\int d\mathbf{r}E_3(\mathbf{r})^*E_1(\mathbf{r})E_2(\mathbf{r})\right]. \tag{A3.5}$$

Furthermore, the symmetry (A2.17) insures that the same χ is also relevant to difference-mixing according to (A2.16). If χ is real, as is ordinarily the case, (A3.2) can be written in the alternative forms

$$\chi = \mathbf{U}_3\cdot\chi(-\omega_3, \omega_1, \omega_2):\mathbf{U}_1\mathbf{U}_2$$

$$= \mathbf{U}_1\cdot\chi(-\omega_1, -\omega_2, \omega_3):\mathbf{U}_2\mathbf{U}_3$$

$$= \mathbf{U}_2\cdot\chi(-\omega_2, -\omega_1, \omega_3):\mathbf{U}_1\mathbf{U}_3. \tag{A3.6}$$

We can limit our consideration to the SHG tensor under the assumption (A2.25) that dispersion in

ω_1, ω_2 can be neglected

$$\chi(-\omega_3, \omega_1, \omega_2)_{ijk} = 2d(-\omega_3, \omega_0, \omega_0)_{il} \qquad l = l(jk)$$
$$(2\omega_0 = \omega_3 = \omega_1 + \omega_2), \qquad \text{(A3.7)}$$

where $l(jk)$ is defined in (A2.20). To cover all the cases that might be of interest it is then necessary to generalize the definition (A3.3) to the form

$$d = \sum_{il} U_{3i}(\mathbf{U}_1\mathbf{U}_2)_l d(-\omega_3, \omega_0, \omega_0)_{il}, \qquad \text{(A3.8)}$$

where $(\mathbf{U}_1\mathbf{U}_2)_l$ is the symmetrized column vector (A2.27), and $i=1, 2, 3$ refers to the crystallographic coordinates X, Y, Z.

We assume the fields ω_1, ω_2, ω_3 are light waves propagating in the crystal along the z direction normal to the crystal face. The *laboratory coordinates* x, y, $\mathbf{z}$ and *crystallographic coordinates* X, Y, Z are defined in Fig. 1. The origin of x, y, z is taken to be on the beam axis at the incident surface of the crystal. Let $\mathbf{x}$, $\mathbf{y}$, $\mathbf{z}$ and $\mathbf{X}$, $\mathbf{Y}$, $\mathbf{Z}$ be unit vectors as shown in Fig. 1 at the laboratory crystal and natural crystal, respectively. Let $\mathbf{Z}$ lie in the x, z plane. Then the orientation of the crystal is specified by two angles θ_r and θ_m (the matching angle). The angle $\theta_r = \angle(\mathbf{y}, \mathbf{X})$ specifies a definite angle of rotation of the uniaxial crystal about its optic axis $\mathbf{Z}$. The vectors $\mathbf{U}_1$, $\mathbf{U}_2$, $\mathbf{U}_3$ will be referred to the laboratory coordinates

$$\mathbf{U} = \mathbf{x}U_x + \mathbf{y}U_y + \mathbf{z}U_z. \qquad \text{(A3.9)}$$

Since light waves in crystals are very nearly transverse we shall set

$$U_{1z} = U_{2z} = U_{3z} = 0. \qquad \text{(A3.10)}$$

In the experimental arrangements of interest $\mathbf{U}_1$, $\mathbf{U}_2$, $\mathbf{U}_3$ have only one component different from zero. Thus, the polarizations are completely specified by the notation $(1y, 2y, 3x)$, which means $\mathbf{U}_1 = \mathbf{y}$, $\mathbf{U}_2 = \mathbf{y}$, $\mathbf{U}_3 = \mathbf{x}$ as we assumed in Chap. 3 for phase matching in a negative uniaxial crystal. The phase-matching arrangement in a positive uniaxial crystal is $(1x, 2x, 3y)$. In addition, there are two possible phase-matching arrangements with $\mathbf{U}_1 \neq \mathbf{U}_2$ which we shall not consider here.

By means of the transformation relations between $\mathbf{x}$, $\mathbf{y}$, $\mathbf{z}$ and $\mathbf{X}$, $\mathbf{Y}$, $\mathbf{Z}$ d in (A3.8) can be written down as a function $d(\theta_r, \theta_m)^{\pm}$ where $(+)$ refers to positive birefringence $(n^e > n^o)$ with polarizations $(1x, 2x, 3y)$ and $(-)$ to negative birefringence $(n^e < n^o)$ and polarizations $(1y, 2y, 3x)$. These functions are given in the third column of Table I for all of the crystal classes which are optically nonlinear and uniaxial except $3(C_3)$. We omit $3(C_3)$ because the number of d_{il} is so large that it would be too cumbersome to put in the table. The nonvanishing d_{il} and the equalities required by symmetry are given in the second column. In some cases equalities are enclosed in parentheses; if the approximate symmetry (A2.46) holds, these equalities would require the enclosed coefficients to vanish. For a suitable choice of θ_r, $[d(\theta_r, \theta_m)^{\pm}]^2$ takes on its maximum value which we write $(d_m^{\pm})^2$ and list in the fourth column. For class $32(D_3)$ we have assumed $|d_{14}| \ll |d_{11}|$. When θ_m, is small it may be necessary to include the neglected components (A3.10). This is done simply by replacing θ_m in the table by $\theta_m + \rho$ for negative or $\theta_m - \rho$ for positive uniaxial crystals.

APPENDIX 4: COMPUTATIONS

Most of the computations presented in this paper were done with the aid of a package of routines (called DEPAC) which carried out the numerical integration of a system of simultaneous first-order differential equations of the form

$$\dot{y}_1 = f_1(x, y_1, \cdots)$$
$$\dot{y}_2 = f_2(x, y_1, y_2, \cdots), \qquad \text{(A4.1)}$$

where $\dot{y} = dy/dx$ and the $f_j(x, y_1, \cdots)$ are calculable real functions of the independent variable x and all the dependent variables. Integration begins at some arbitrary initial condition x_0, $y_1(0)$, $\cdots$ and proceeds by Hamming's predictor–corrector method[49] to some selected final value of x. Let us denote the real and imaginary parts of $2\pi H(\sigma, \kappa, \xi, \mu)$ defined in (2.16) by R and I:

$$2\pi H(\sigma', \kappa, \xi, \mu) = R + iI. \qquad \text{(A4.2)}$$

The differential equations satisfied by R and I have been given in KAB (A3). (In the equation for R, an erroneous τ appears on the right which should be σ.) For the case of no absorption $(\kappa = 0)$ these equations become

$$(\partial R/\partial\sigma') + R = [\sin\sigma'\xi(1-\mu) + \sin\sigma'\xi(1+\mu)]\sigma'^{-1}$$
$$(\partial I/\partial\sigma') + I = [\cos\sigma'\xi(1-\mu) - \cos\sigma'\xi(1+\mu)]\sigma'^{-1} \qquad \text{(A4.3)}$$

in the notation of (2.17).

Let us define the following variables:

$$x = \sigma' = \sigma + 4\beta s$$
$$y_1 = R$$
$$y_2 = I$$
$$y_3 = |H|^2 = (y_1^2 + y_2^2)(4\pi^2)^{-1}$$
$$y_4 = |H|^2 e^{-4s^2}$$
$$y_5 = (\pi^2/\xi)(2/\pi^{1/2}) \int_{x_0}^{x} (dx/4\beta) e^{-4s^2} |H|^2. \qquad \text{(A4.4)}$$

It follows from (2.23), (2.24), and (A4.4) that

$$h(\sigma, \beta, 0, \xi, \mu) = y_5(\infty) - y_5(-\infty), \qquad \text{(A4.5)}$$

where for brevity we do not explicitly indicate that

[49] R. W. Hamming, J. Assoc. Computing Machinery **6**, 37 (1959).

$y_5(x)$ depends upon the parameters σ, β, ξ, μ as well as the variable x. The appropriate equations (A4.1) become

$$\dot{y}_1=-y_1+[\sin x\xi(1-\mu)+\sin x\xi(1+\mu)]x^{-1}$$
$$\dot{y}_2=-y_2+[\cos x\xi(1-\mu)-\cos x\xi(1-\mu)]x^{-1}$$
$$\dot{y}_3=(y_1\dot{y}_1+y_2\dot{y}_2)(2\pi^2)^{-1}$$
$$\dot{y}_4=(\dot{y}_3-2y_3s\beta^{-1})e^{-4s^2}$$
$$\dot{y}_5=(\pi^{3/2}/2\beta\xi)y_4. \qquad \text{(A4.6)}$$

Integration can be stated at the initial condition [see KAB (A5)]

$$x_0=0$$
$$y_1(0)=\tan^{-1}\xi(1+\mu)+\tan^{-1}\xi(1-\mu)$$
$$y_2(0)=\tfrac{1}{2}\ln\{[1+\xi^2(1-\mu)^2]/[1+\xi^2(1+\mu)^2]\}$$
$$y_5(0)=0. \qquad \text{(A4.7)}$$

A more convenient procedure, especially when $\mu=0$, is to start at some point $x_0<0$ such that $y_5(-\infty)$ can be neglected in (A4.5) and $R(x_0)$, $I(x_0)$ can be easily computed from asymptotic formulas. With the exception of Fig. 5, all the computations in this paper have $\mu=0$ (focus in center of crystal); for this case

$$y_2(x)\equiv 0$$
$$y_3(x)\underset{(\mu=0)}{=}H(\sigma,\xi)^2=y_2^2/4\pi^2, \qquad \text{(A4.8)}$$

where $H(\sigma,\xi)$ has been defined in (2.70). If x is large and negative it follows from the asymptotic approximation (2.82) that

$$y_3(x)=(1+\cos 2x\xi)/(2\pi^2x^2\xi^2)+\cdots$$
$$(\mu=0,\ x<0,\ |x\xi|\gg 1). \qquad \text{(A4.9)}$$

Therefore we choose x_0 such that

$$1+\cos 2x_0\xi=0 \qquad |x_0\xi|\gg 1. \qquad \text{(A4.10)}$$

Most of the computations of $h(\sigma,\beta,0,\xi,0)$ carried out to construct Fig. 2 were started at $x_0\xi=-11\pi/2=-17.279$, and $y_5(-\infty)$ could be dropped in (A4.5). To obtain $y_5(\infty)$ the integration is carried in the positive x direction until $y_5(x)$ approaches a stable value.

We note in (A4.4) that the variables y_3 and y_4 could be obtained by a simple calculation from y_1 and y_2 without integrating the differential equations for y_3 and y_4 in (A4.6). It is advantageous, however, to obtain them by integration and costs very little in computing time. This provides a check on the accuracy of the integration; another valuable indication of loss of accuracy is the appearance of negative values for y_3 and y_4.

To compute Fig. 2 values were selected for σ, ξ, and B, β was calculated from (2.27), integration (with $\mu=0$) was started at $x_0=-17.279/\xi$ and carried forward until $4s^2>10$ which insured that $y_4<e^{-10}$. At this point, the value of y_5 was taken to be $h(\sigma, B, \xi)$ as defined in (2.28). Several trials were run with different σ and the optimum value of h determined by interpolation.

If we identify

$$x=\sigma$$
$$y_1=R=2\pi H$$
$$y_2\equiv 0$$
$$y_3=|H|^2, \qquad \text{(A4.11)}$$

we can use the above method to compute the function $|H(\sigma,\xi)|^2$ plotted in Figs. 6–10. In this case, the integration was started at

$$x_0=0, \qquad y_1=2\tan^{-1}\xi \qquad \text{(A4.12)}$$

and proceeded in the positive x direction. A different method to be described later was used for the region $\sigma<0$. The integration of (A4.6) or (A4.11) by Hamming's method is stable when x is increasing but unstable when x is decreasing. For this reason it is impossible when starting at $x_0=0$ to proceed in the decreasing direction much beyond $x=-3$.

If necessary the entire program just described could be carried out with $\kappa\neq 0$. The differential equations (A4.6) would have to be generalized to include κ, but the correct forms have been given previously in KAB (A.3). The only difficulty in including absorption is that the starting values $y_1(x_0)$, $y_2(x_0)$ would have to be obtained from a separate preliminary calculation which integrates from $\kappa=0$ to the desired κ.

The computation of $|H(\sigma,0,\xi,\mu)|^2$ as a function of μ using differential equations with μ as the independent variable has been described by Kleinman and Miller.[13] It is convenient to start such integrations at $\mu=0$ where $y_2=0$ and then choose σ such that y_1 is also zero. In Fig. 5 the curve $B=2$, $\xi=1.7$ was computed in this way by starting at $\mu_0=0$, $\sigma_0=-17.279/\xi=-10.164$, $y_1=y_2=0$. Integration was carried out over μ using (26) and (27) of Ref. 13 to the selected value of μ. The values of y_1 and y_2 so obtained were entered as starting values, along with $x_0=-10.164$, in the integration of (A4.6). The parameters of the latter integration were $\xi=1.7$, $\beta=1.534$, $\sigma=0.86$, and selected values of μ. The value of σ was found previously to be the optimum value at $B=2$, $\xi=1.7$, $\mu=0$. It was verified that a separate optimization of σ at each μ was unnecessary. The curve $B=0$, $\xi=2.8$ of Fig. 5 was computed by use of the relation

$$h(\sigma,0,0,\xi,\mu)=(\pi^2/\xi)\,|H(\sigma,0,\xi,\mu)|^2, \qquad \text{(A4.13)}$$

which follows immediately from (2.23) and (2.24), and is a simple generalization of (2.69). Using as

variables

$$x=\sigma$$
$$y_1=R$$
$$y_2=I$$
$$y_3=|H|^2, \tag{A4.14}$$

$y_3(x)$ was computed starting at the initial condition (A4.7) for selected values of μ. In each case the maximum of $y_3(x)$ was taken, which corresponds to optimizing σ.

To calculate the function $\bar{h}(\sigma, \beta, \xi)$ defined in (3.32) and plotted (after σ optimization) in Fig. 12 we define the variables

$$x=\sigma'$$
$$y_1=H(x, \xi)$$
$$y_2=y_1 e^{-4s^2}$$
$$y_3=(2\beta\pi^{1/2})^{-1}\int_{x_0}^{x} y_2 dx$$
$$y_4=(\pi^2/\xi)y_3^2, \tag{A4.15}$$

where $s=(\sigma'-\sigma)/4\beta$ and $H(x, \xi)$ is defined in (2.70). It follows from (3.42) that

$$\bar{H}(\sigma, \beta, \xi)=y_3(\infty)-y_3(-\infty). \tag{A4.16}$$

We choose the initial value x_0 such that $y_1(x_0)\approx 0$ and $y_3(-\infty)$ can be neglected; the value used was $x_0\xi=-17.279$. It then follows that

$$\bar{h}(\sigma, \beta, \xi)=y_4(\infty). \tag{A4.17}$$

The differential equations are

$$\dot{y}_1=-y_1+(\pi x)^{-1}\sin x\xi$$
$$\dot{y}_2=(\dot{y}_1-2s\beta^{-1}y_1)e^{-4s^2}$$
$$\dot{y}_3=(2\beta\sqrt{\pi})^{-1}y_2$$
$$\dot{y}_4=(2\pi^2/\xi)y_3\dot{y}_3, \tag{A4.18}$$

and the initial conditions are

$$x_0=-17.279/\xi$$
$$y_1(x_0)=0$$
$$y_3(x_0)=0$$
$$y_4(x_0)=0. \tag{A4.19}$$

To compute Fig. 12 values were selected for σ, ξ, and B, β was calculated from (2.27) and integration was carried forward from x_0 until $4s^2>10$, which insured that y_4 had reached its limiting value $y_4(\infty)$. Several trials were taken with different σ and the optimum value of $\bar{h}$ determined by interpolation.

The computations for $\sigma<0$ in Figs. 6–10 were done using a completely different method based on a Chebyshev polynominal approximation.[50] We describe this method in some detail because it is appropriate specifically to the region $\sigma<0$ which presents instability problems when the differential equation method is used. If integration is started at the exact initial condition (A4.7) the results are meaningless for $x<-3$. If the integration is started at (A4.10) and carried forward in x, one is relying on the accuracy of the asymptotic expression (A4.9). To insure sufficient accuracy one must use a large value of $|x_0\xi|$, which for moderate or small ξ may mean that the integration has to be carried a long way in x to reach the region of interest. For these reasons it is very desirable to have an accurate analytical approximation for the function $H(\sigma, \xi)$ in the region $\sigma<0$.

The exponential integral function is defined by[50]

$$E_1(z)=\int_z^\infty (e^{-t}/t)dt$$
$$|\arg z|<\pi. \tag{A4.20}$$

It follows that

$$\int_{z_1}^{z_2}(e^{-t}/t)dt=E_1(z_1)-E_1(z_2), \tag{A4.21}$$

providing the path of integration does not cross the negative real axis. Upon making the substitution $t=-\sigma(1+i\tau)$ in (2.70) we immediately obtain

$$H(\sigma, \xi)\underset{(\sigma<0)}{=}\pi^{-1}e^{-\sigma}\mathrm{Im}[E_1(-\sigma+i\xi\sigma)], \tag{A4.22}$$

where the condition $\sigma<0$ insures that the path of integration does not cross the negative real axis as required in (A4.21). We now define a second function $p(z)$

$$E_1(z)=e^{-z}p(z), \tag{A4.23}$$

and write (A4.22) in the form

$$H(\sigma, \xi)\underset{(\sigma<0)}{=}\pi^{-1}\mathrm{Im}[e^{-i\xi\sigma}p(-\sigma+i\xi\sigma)]. \tag{A4.24}$$

From (A4.20) and (A4.23), it can easily be shown that $p(z)$ satisfies the differential equation

$$p-(dp/dz)=1/z, \tag{A4.25}$$

and the boundary condition

$$p(z)\to 0$$
$$z\to\infty, |\arg z|<\pi. \tag{A4.26}$$

The general solution of (A4.25) is $p(z)+ae^z$, where a is an arbitrary constant. When

$$\mathrm{Re}(z)>0 \tag{A4.27}$$

the two relations (A4.25) and (A4.26) require $a=0$ and therefore uniquely determine $p(z)$. However,

[50] *Tables of Chebyshev Polynominals* [U.S. Department of Commerce, Washington D.C. (1952)].

when (A4.27) is not satisfied we have no way of determining a, and $p(z)$ is not uniquely determined by (A4.25) and (A4.26). Therefore (A4.27) is required for the validity of the results we shall obtain.

In view of (A4.26), we may attempt to expand $p(z)$ in inverse powers of z. The expansion which formally satisfies (A4.25) is

$$p(z)=z^{-1}\sum_0^\infty(-z)^n n!. \tag{A4.28}$$

For $|z|\gg 1$ the leading terms of this series may give a useful asymptotic approximation, but for all $z\neq 0$ the series eventually diverges. We can, however, obtain approximations of arbitrarily high precision in the form of polynomials in z^{-1},

$$p_n(z)=b_1z^{-1}+\cdots+b_nz^{-n}, \tag{A4.29}$$

which satisfy an equation very closely related to (A4.25)

$$p_n-(dp_n/dz)=(1/z)[1+\tau_nT_n(w/z)]. \tag{A4.30}$$

Here w and τ_n are parameters to be specified later and

$$T_n(x)=\sum_{j=0}^n T_n^{(j)}x^j \tag{A4.31}$$

is a suitable polynomial of degree n. The coefficients b_j in (A4.29) must satisfy the recurrence relations

$$b_{j+1}+jb_j=\tau_nT_n^{(j)}w^j \qquad (j=1, 2, \cdots, n) \tag{A4.32}$$

and the special relation

$$b_1=1+\tau_nT_n^{(0)}. \tag{A4.33}$$

The solution of (A4.32) is

$$b_j=(j-1)!(-)^j\sum_{k=j}^n(\tau_nT_n^{(k)}/k!)(-w)^k \qquad (j=1, \cdots, n). \tag{A4.34}$$

For $j=1$ this is consistent with (A4.33) only if

$$-\tau_n^{-1}=T_n^{(0)}+\sum_{k=1}^n[T_n^{(k)}/k!](-w)^k. \tag{A4.35}$$

We may now eliminate the parameter w by setting $w=z$ in (A4.34) and (A4.35), which gives (A4.29) the form of a rational function instead of a simple polynominal. Our final result is

$$p_n(z)=\{[F_{n-1}(z)]/G_n(z)\} \qquad n=1, 2, \cdots \tag{A4.36}$$

where

$$F_{n-1}(z)=\sum_{k=0}^{n-1}(-z)^k\sum_{j=k+1}^n[(j-k-1)!/j!]T_n^{(j)}$$

$$G_n(z)=-\sum_{k=0}^n(-z)^kT_n^{(k)}/k!. \tag{A4.37}$$

We can integrate (A4.30) by means of the integrating factor e^{-z} and obtain

$$p_n(z)-p(z)=\tau_ne^z\int_z^\infty(e^{-t}/t)T_n(z/t)\,dt \tag{A4.38}$$

after setting $w=z$ on the right. In view of (A4.27), the path of integration over t can be taken along the ray through z, which insures that (z/t) is real and in the range $0\leq z/t\leq 1$. We choose $T_n(x)$ to be the Chebyshev polynominals[50]

$$T_n(x)\equiv\cos[n\cos^{-1}(2x-1)] \qquad 0\leq x\leq 1$$

$$T_n(0)=(-)^n, \qquad T_n(1)=1. \tag{A4.39}$$

Since $T_n(z/t)$ in (A4.38) oscillates between ± 1 we may estimate the error $|p_n-p|$ very simply

$$|p_n(z)-p(z)|\approx|\tau_n(z)p(z)|, \tag{A4.40}$$

showing that τ_n is a measure of the fractional error. As $z\to 0$ we have $|\tau_n|\to 1$ indicating a breakdown in the approximation for any value of n.

Our computations were carried out with $n=7$ for which (A4.37) become[51]

$$315F_6(z)=2022+77328z+285120z^2+271328z^3+91968z^4+12032z^5+512z^6$$

$$315G_7(z)=315+30870z+246960z^2+493920z^3+352800z^4+103488z^5+12544z^6+512z^7. \tag{A4.41}$$

With $z=-\sigma+i\xi\sigma$ computations were performed for selected values of σ starting at $\sigma_1=-\pi/24\xi$. The accuracy at this point was poorest for the largest ξ used which was $\xi=50$. The maximum fractional error in the computations was determined by

$$\tau_7(z_1)^{-1}=G_7(0.00262+0.131i)$$

$$=-133-17.3i$$

$$|\tau_7(z_i)|=0.0074. \tag{A4.42}$$

Denoting the real and imaginary parts of F and G in (A4.41) by F_r, F_i, G_r, G_i, we can write (A4.24) in the form

$$H(\sigma,\xi)\underset{(\sigma<0)}{=}\frac{(F_iG_r-F_rG_i)\cos\xi\sigma-(F_rG_r+F_iG_i)\sin\xi\sigma}{\pi(G_r^2+G_i^2)}. \tag{A4.43}$$

The real and imaginary parts of polynominals for complex arguments can be computed very conveniently using standard routines which do arithmetic with complex numbers.

[51] Ref. 50, p. XXIV.